AD-A062 989 PENNSYLVANIA STATE UNIV UNIVERSITY PARK APPLIED RESE--ETC F/G 20/1
AXISYMMETRIC SCATTERING OF A SPHERICAL WAVE BY A PROLATE SPHERO--ETC(U)
MAY 78 A GERMON N00017-73-C-1418

UNCLASSIFIED ARL/PSU/TM-78-174 NL

1 OF 2
AD A062989

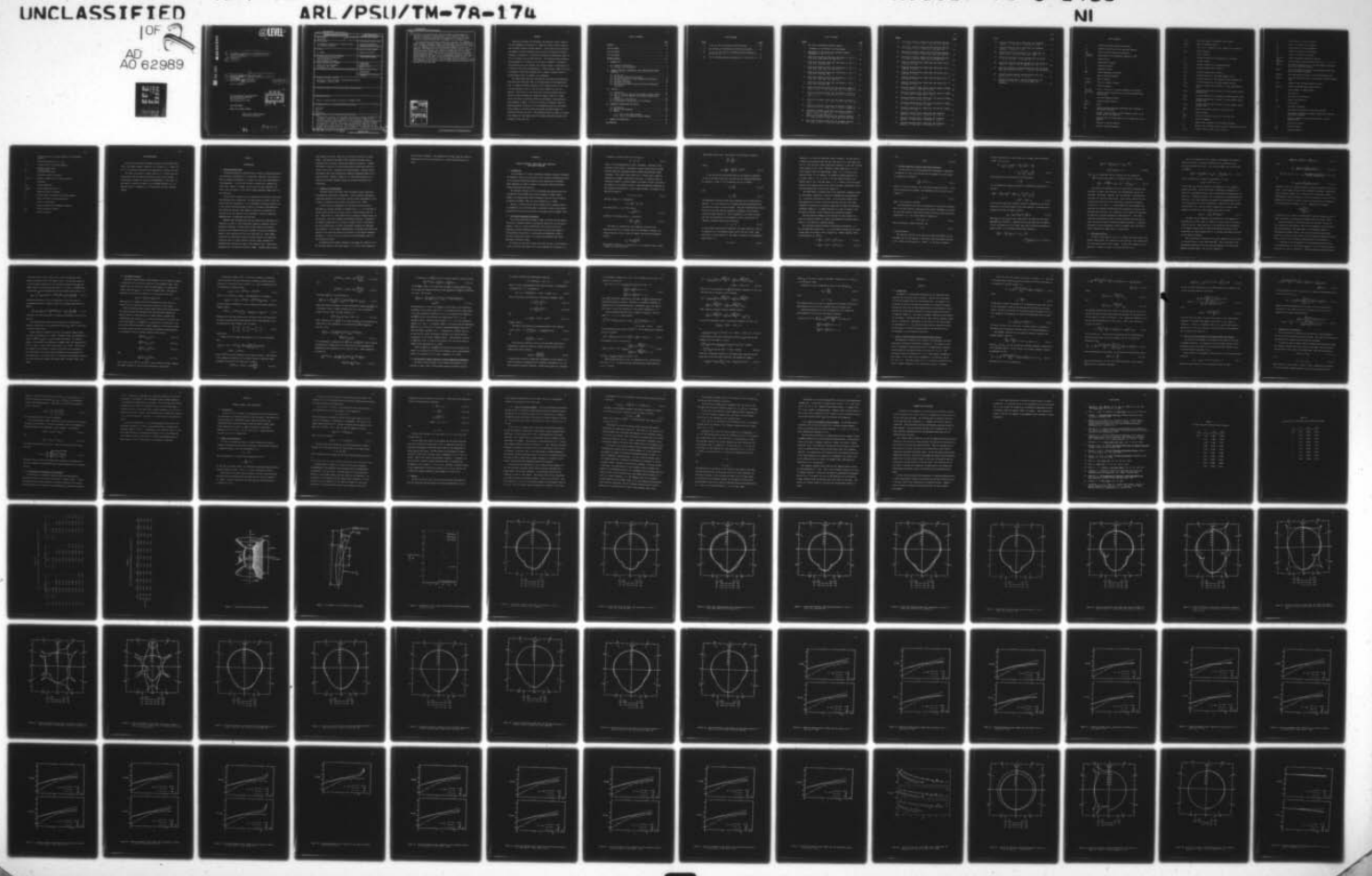

(12) LEVEL II

5C

(6) AXISYMMETRIC SCATTERING OF A SPHERICAL WAVE BY A PROLATE SPHEROID.

(10) A./Germon

(9) Technical Memorandum (14) ARL/PSU/TM-78-174

File No. TM 78-174

(11) 15 May 1978

Contract No. N00017-73-C-1418

Copy No. 49 (15)

(12) 100 P.

The Pennsylvania State University
APPLIED RESEARCH LABORATORY
Post Office Box 30
State College, PA 16801

NAVY DEPARTMENT

NAVAL SEA SYSTEMS COMMAND

Approved for Public Release
Distribution Unlimited

UNCLASSIFIED

SECURITY CLASSIFICATION OF THIS PAGE *(When Data Entered)*

REPORT DOCUMENTATION PAGE		READ INSTRUCTIONS BEFORE COMPLETING FORM
1. REPORT NUMBER TM 78-174 ✓	2. GOVT ACCESSION NO.	3. RECIPIENT'S CATALOG NUMBER
4. TITLE *(and Subtitle)* Axisymmetric Scattering of a Spherical Wave by a Prolate Spheroid		5. TYPE OF REPORT & PERIOD COVERED Technical Memorandum 6. PERFORMING ORG. REPORT NUMBER
7. AUTHOR(s) A. Germon		8. CONTRACT OR GRANT NUMBER(s) N00017-73-C-1418 ✓
9. PERFORMING ORGANIZATION NAME AND ADDRESS Applied Research Laboratory ✓ Post Office Box 30 State College, PA 16801		10. PROGRAM ELEMENT, PROJECT, TASK AREA & WORK UNIT NUMBERS
11. CONTROLLING OFFICE NAME AND ADDRESS Naval Sea Systems Command Washington, DC 20362		12. REPORT DATE 15 May 1978 13. NUMBER OF PAGES 92
14. MONITORING AGENCY NAME & ADDRESS *(if different from Controlling Office)*		15. SECURITY CLASS. *(of this report)* UNCLASSIFIED 15a. DECLASSIFICATION/DOWNGRADING SCHEDULE

16. DISTRIBUTION STATEMENT *(of this Report)*

Approved for Public Release - Distribution Unlimited
Per NAVSEA - June 28, 1978

17. DISTRIBUTION STATEMENT *(of the abstract entered in Block 20, if different from Report)*

18. SUPPLEMENTARY NOTES

Master of Science Thesis in Acoustics, November 1978.

19. KEY WORDS *(Continue on reverse side if necessary and identify by block number)*

scattering
spheroid
wave
reflection

20. ABSTRACT *(Continue on reverse side if necessary and identify by block number)*

Theoretical analyses are performed, and numerical results obtained for the axisymmetric scattering of a spherical wave by either a rigid or soft (pressure release) prolate spheroid. In the numerical calculations, the complex far-field reflection factor (ratio of scattered-to-incident pressure) is computed as a function of frequency and observation angle for a 7-to-1 fineness ratio prolate spheroid. Ten different source locations are considered, all of which lie on the axis of symmetry. In addition, the super-

→ next Page

DD FORM 1 JAN 73 1473 EDITION OF 1 NOV 65 IS OBSOLETE

UNCLASSIFIED

SECURITY CLASSIFICATION OF THIS PAGE *(When Data Entered)*

20. position of the incident and scattered fields is investigated for a variety of two-source configurations. In one instance, these two sources are assumed to have equal strengths and to vibrate in phase, while in a second instance they are assumed to be incoherent.

The computations have been performed for relatively low frequencies, where the exact tabulated forms of the spheroidal wave functions may be used. A reduced frequency, defined by kd/2 ranged from 0.1 to 40, where k is the wavenumber, and d is the interfocal distance of the 7-to-1 spheroid. The results for the directivity functions indicate that the reflection factor depends only slightly on aspect angle for a single source, but when two in-phase sources are considered, the scattering is very dependent on angle. If the two sources are incoherent, then the patterns approach the shape of the corresponding pattern for the single source closest to the pole, particularly when the second source is relatively far from the first. The reflection factor is shown to increase with frequency in the rigid case and to remain essentially constant with frequency in the soft case.

ABSTRACT

Theoretical analyses are performed, and numerical results obtained for the axisymmetric scattering of a spherical wave by either a rigid or soft (pressure release) prolate spheroid. In the numerical calculations, the complex far-field reflection factor (ratio of scattered-to-incident pressure) is computed as a function of frequency and observation angle for a 7-to-1 fineness ratio prolate spheroid. Ten different source locations are considered, all of which lie on the axis of symmetry. In addition, the superposition of the incident and scattered fields is investigated for a variety of two-source configurations. In one instance, these two sources are assumed to have equal strengths and to vibrate in phase, while in a second instance they are assumed to be incoherent.

The computations have been performed for relatively low frequencies, where the exact tabulated forms of the spheroidal wave functions may be used. A reduced frequency, defined by $kd/2$ ranges from 0.1 to 40, where k is the wavenumber, and d is the interfocal distance of the 7-to-1 spheroid. The results for the directivity functions indicate that the reflection factor depends only slightly on aspect angle for a single source, but when two in-phase sources are considered, the scattering is very dependent on angle. If the two sources are incoherent, then the patterns approach the shape of the corresponding pattern for the single source closest to the pole, particularly when the second source is relatively far from the first. The reflection factor is shown to increase with frequency in the rigid case and to remain essentially constant with frequency in the soft case.

TABLE OF CONTENTS

LIST OF TABLES

LIST OF FIGURES

Figure | Page

LIST OF SYMBOLS

a	separation distance between two sources
A_n	expansion coefficient of the scattered pressure
A_{mn}	Green's function expansion coefficient
A_r^m, B_r^m, C_r^m	coefficients in the difference equation in dr^{mn}
c	sound velocity
C	normalization constant
d	interfocal distance
$d\tau'$	elementary volume
d_r^{mn}	prolate expansion coefficient
e	base of natural logarithm
$G(\underline{r}/\underline{r}')$	Green's function
$G_o(\underline{r}/\underline{r}')$	free space Green's function
h	reduced frequency
h_η, h_ζ, h_ϕ	metric coefficients in prolate spheroidal coordinates
$h_m^{(1),(2)}(\xi)$	spherical Hankel functions of the first and second kind, respectively
i	unit pure imaginary number
$j_n(\xi)$	spherical Bessel function
$K_m(\eta,\xi)$	Kernel
K_{mn}	Green's function expansion coefficient after inclusion of the angular functions
ℓ'	distance from the single, or the innermost, source to the closest pole of the spheroid
ℓ''	distance from the second source to the closest pole of the spheroid
L	length of a prolate spheroid
L_o	length of the given spheroid

m,n	order and degree of spheroidal wave function
$n_n(\xi)$	spherical Neumann function
N	upper limit of summation in the computation of pressures
N_{mn}	norm of $S_{mn}(h,\eta)$
p	positive integer
p_o	constant pressure factor defined by $p_o = k^2\rho cQ/2\pi$
$\bar{p}_i$	incident pressure
$\bar{p}_{i,o}$	incident pressure on the spheroid surface
$\bar{p}_{i,1}$	incident pressure due to Source 1
$\bar{p}_{i,2}$	incident pressure due to Source 2
$\bar{p}_{s1}$	scattered pressure in the rigid boundary case
$\bar{p}_{s2}$	scattered pressure in the pressure release boundary case
$\bar{p}_{s1,o}$	scattered pressure on the rigid spheroid surface
$\bar{p}_{s1,1}$	scattered pressure due to Source 1 in the rigid boundary case
$\bar{p}_{s1,2}$	scattered pressure due to Source 1 in the pressure release boundary case
$\bar{p}_{s2,o}$	scattered pressure on the pressure release spheroid surface
$\bar{p}_{s2,1}$	scattered pressure due to Source 1 in the pressure release boundary case
$\bar{p}_{s2,2}$	scattered pressure due to Source 2 in the pressure release boundary case
$P_n^m(\eta)$	associated Legendre function of the first kind
Q	source strength
$Q_n^m(\eta)$	associated Legendre function of the second kind
r	index of summation
$\underline{r}$	general space coordinate in the Green's function
$\underline{r}'$	general space coordinate of the source in the Green's function
r_1,r_2	distances from a given point to the foci

R	minor radius of a prolate spheroid
R_k	radius of curvature of a spheroid
R_o	minor radius of the given spheroid
R_1	radius of curvature at the equator
R_2	radius of curvature at the pole
$R_{mn}(h,\xi)$	prolate spheroidal radial wave function
$R_{mn}^{(j)}(h,\xi)$	prolate radial function of the jth kind (j = 1, 2, 3 or 4)
$R(h,\eta)$	far-field reflection factor, for both boundary conditions due to two incoherent sources
$\overline{R}(h,\eta)$	far-field reflection factor, for both boundary conditions due to two sources in phase
$\overline{R}_1(h,\eta)$	far-field reflection factor in the rigid boundary case
$\overline{R}_2(h,\eta)$	far-field reflection factor in the pressure release boundary case
$\lvert\overline{R}\rvert$	modulus of the far-field reflection factor
$S_{mn}(h,\eta)$	prolate spheroidal angular wave function
t	time variable, or dummy variable
T	time function
T_o	amplitude of time function
u_{mn}	general field function
V	total volume
x,y,z	Cartesian coordinates
x	also general coordinate in Dirac delta function
z	also general coordinate in general expression of the wave differential equation
x'	general coordinate of the source position, or first derivative of x
δ	Dirac delta function
δ_{op}	Kronecker symbol
∇^2	Laplacian operator

ε	fineness ratio of a prolate spheroid or infinitesimal quantity
ε_p	quantity defined by $\varepsilon_p = 2 - \delta_{op}$
ε_o	fineness ratio of the given spheroid
θ	spherical aspect angle
θ_c	critical angle
ϕ	rotational coordinate
η	spheroidal angular coordinate
η', ξ', ϕ'	prolate coordinates of the source position
λ	wavelength
λ_{mn}	prolate eigenvalue
$\lambda_{mn}(0)$	prolate eigenvalue when h = 0
ξ	spheroidal radial coordinate
ξ_o	prolate radial coordinate of the given spheroid
ξ''	radial coordinate of the second source
ρ	density of the medium
ψ	general variable in the Helmholtz equation
ψ_{mn}	prolate spheroidal harmonic
ω	angular frequency

ACKNOWLEDGEMENTS

This work was supported by NAVSEA, Code 037, SF 43-452-702, Task 19579. The author wishes to thank Dr. M. T. Pigott, Dr. J. Tichy, and Dr. G. C. Lauchle who offered him the opportunity to pursue this work.

The author also wishes to deeply thank Dr. G. C. Lauchle for the useful advice and experience he provided, as well as the friendly relationship he showed all along the accomplishment of this task. He also wants to express his thanks to his esteemed teachers, Dr. E. J. Skudrzyk and Dr. W. Thompson, Jr. for their help and their valuable remarks.

CHAPTER I

INTRODUCTION

1.1 General Considerations

The problems related to spheroids are of various types like diffraction and scattering, perturbation in a steady flow, radiation, and cavitation. They are commonly encountered in acoustics, as well as in hydrodynamics or electromagnetics. The very wide variety of shapes that a spheroid may take, from a sphere to a needle, in the case of prolate spheroids, and from a disk to a sphere, in the case of oblate spheroids, makes their use very practical.

In the field of acoustics, we are interested in radiation, scattering, and diffraction due to spheroids. For that purpose, we have to solve the equation for wave propagation. As the spheroidal coordinate system is one of the eleven coordinate systems in which, for harmonic time dependence, the reduced wave equation (the Helmholtz equation) is separable, the solution to the wave equation can be expressed in terms of spheroidal eigenfunctions, or spheroidal wave functions.

Mathematicians and physicists have investigated the spheroidal wave equations, in order to find expressions leading to numerical values or asymptotic expansions. Between 1830 and 1860, Lamé first developed solutions to the Helmholtz equation in general ellipsoidal coordinates. However, their complexity did not allow efficient use. Niven (1880), noting that the spheroidal coordinate systems reduced to the spherical coordinate system at large distances from the origin, expanded the spheroidal wave functions in terms of the spherical ones. Power series expansions were introduced by MacLaurin (1898). Abraham (1899) obtained

some integral solutions; those were treated more extensively by Poole (1923). Then Meixner and Shäfke (1954) performed extensive work on spheroidal wave functions, introducing asymptotic expansions. Flammer (1957) made a collection of the preceding works and provided tables for various coefficients, eigenvalues and eigenfunctions. Silbiger (1961) and Slepian (1965) have investigated asymptotic expansions which are of great use today. Recently, Hanish et al. (1970) and Van Buren et al. (1975) have provided extensive tables for the wave functions at low frequencies.

1.2 Problem to be Investigated

Different efforts have taken place concerning acoustic radiation, scattering and diffraction by spheroids. A very extensive bibliography concerning spheroidal wave functions, and the various advancements on the acoustics of spheroids can be found in Van Buren et al. (1975).

In this study, we investigate the far-field reflection factor generated by a prolate spheroid of fineness ratio, $\varepsilon = 7.1$, insonified by a point source located on its major axis at a short distance from the pole. Both cases of a rigid surface and of a pressure release surface are investigated. The source assumes ten different positions. Furthermore, we consider combinations of two sources in phase as well as incoherent, one source being fixed, the other successively occupying the remaining nine positions. For all these configurations, we determine the directivity pattern of the reflection factor for the values of the reduced frequency parameter: $h = kd/2 = 20, 35, 40$, where k is the wavenumber, and d is the interfocal distance.

We determine the frequency response in the range of h from 0.1 to 20 for the three values of the aspect angle: $\theta = 0°, 90°, 180°$ as measured

from the axis of symmetry. The computations are made using the tables of spheroidal wave functions by Hanish et al. (1970) and Van Buren et al. (1975).

CHAPTER II

PROLATE SPHEROIDAL COORDINATES, WAVE FUNCTIONS, AND GREEN'S FUNCTION

2.1 Introduction

In this chapter the prolate spheroidal coordinate system is discussed. The Helmholtz equation is expressed in that coordinate system and is reduced to two ordinary differential equations after separation of variables. These equations are solved, leading to the prolate radial and prolate angular spheroidal wave functions.

The approach followed to solve the differential equations was first introduced by Niven (1880) and has been extended by Flammer (1957). However, the normalization scheme followed is that one first introduced by Meixner and Shäfke (1954) and used by Kanish et al. (1970).

Further, the derivation of the free-space Green's function, which is of fundamental use in field problems, is derived in terms of the prolate spheroidal wave functions according to the scheme given by Flammer (1957).

2.2 The Prolate Spheroidal Coordinates

The prolate spheroidal coordinate system is derived from the general ellipsoidal coordinate system by choosing the major axis to be an axis of symmetry. That is, it may be generated by the rotation of the two-dimensional elliptic coordinate system about its major axis (Figure 1). The alternative possibility of rotating the two-dimensional elliptic coordinate system wtih respect to its minor axis generates the oblate spheroidal coordinate system.

An ellipse is the locus of points such that the sum of the distances r_1 and r_2 from two fixed points (the foci), separated by a distance d, is

a constant, a property which can be written as

$$r_1 + r_2 = \xi d \quad , \tag{2.2.1}$$

where ξ is the nondimensional elliptic coordinate. Therefore, after rotation of the ellipse, ξ represents a given ellipsoid and by analogy with the spherical coordinate system is called the spheroidal radial coordinate. For a given finite value of d, ξ varies from 1, where it represents the segment connecting the two foci, to infinity, where it represents a sphere of infinite radius, the center of which is located at the origin of the coordinate system.* Some characteristic dimensions of the ellipsoid represented by ξ can be easily derived: the length of the spheroid is given by

$$L = r_1 + r_2 = \xi d \quad , \tag{2.2.2}$$

the minor radius, R, is obtained by

$$R^2 + \left(\frac{d}{2}\right)^2 = r_1^2 + r_2^2$$

and noting that $r_1 = r_2 = \xi d/2$, we get

$$R = \frac{d}{2}\sqrt{\xi^2 - 1} \quad ; \tag{2.2.3}$$

therefore, the fineness ratio, ε, is given by

$$\varepsilon = \frac{L}{2R} = \frac{\xi}{\sqrt{\xi^2 - 1}} \tag{2.2.4}$$

The radius of curvature R_k of the spheroid varies with the observation point on its surface and can be obtained by looking at an elliptic section in the x-z plane of Figure 1 and writing the general relation

$$R_k = \frac{(1 + x'^2)^{3/2}}{|x''|} \quad ,$$

*If we let $\xi \to \infty$ while $d \to 0$, keeping $\xi d = D$, the spheroid tends towards a sphere of finite radius D/2.

where primes denote d/dz. The equation of the ellipse is given by

$$\frac{x^2}{R^2} + \frac{z^2}{(\frac{L}{2})^2} = 1 \quad .$$

Hence,

$$R_k = \frac{L^2}{4R}[1 - \frac{16z^2}{L^4}(\frac{L^2}{4} - R^2)]^{3/2} \quad . \tag{2.2.5}$$

In the mid-section the extreme values of the radius of curvature are R_1 at the equator and R_2 at the pole, and are obtained respectively by letting z = 0 and z = L/2 in Equation (2.2.5); we obtain

$$R_1 = \frac{L^2}{4R} \tag{2.2.6}$$

and

$$R_2 = \frac{2R^2}{L} \quad . \tag{2.2.7}$$

The spheroidal coordinate system being orthogonal has a second family of surfaces. It is the double set of conjugate hyperboloids obtained from the same focal points as the ellipsoids. They can be generated by rotating about the z axis the nonfocal hyperbolas, orthogonal to the previous confocal ellipses (Figure 1). Such a hyperbola is the locus of points such that the difference of the distances r_1 and r_2 from the foci is constant, a property which can be written as

$$r_1 - r_2 = \eta d \quad . \tag{2.2.8}$$

It can be easily seen that this hyperbola, for large values of r_1 and r_2, is asymptotic to a line making an angle $\cos^{-1}\eta$ with the z axis. That means that for large values of ξ this angle is identical to the spherical aspect angle, i.e.,

$$\theta = \cos^{-1}\eta \quad . \tag{2.2.9}$$

Therefore, η is called the spheroidal angle coordinate. As each value of η defines one hyperboloid and only one, each value of θ in the range from zero to π also defines a unique hyperboloid asymptotic to the cone of angle θ with respect to the z axis. Therefore, η must range from 1 to -1 to cover the whole family of hyperboloids. When $\eta = 0$, it refers to the equatorial plane of the spheroid, the hyperbola degenerating into the x-y plane. When $\eta = +1$, it refers to the pole region located on the positive side of the z axis and, when $\eta = -1$, it refers to the pole region located on the negative side of the z-axis, the angle θ being here defined from the positive side of the z-axis (Figure 1).

The third family of surfaces used in the spheroidal coordinate system are the surfaces orthogonal to both the ellipsoids and the hyperboloids, i.e., the planes containing the z-axis. As the previous surfaces have been generated by rotation of plane curves about this axis, the third coordinate ϕ represents the rotational angle and is called the rotational coordinate (Figure 1). It ranges from zero to 2π and is similar to the rotational coordinate in both spherical and cylindrical systems.

From the previous remarks, we can see that for large values of ξ, where the spheroid reduces to a sphere, the spheroidal coordinate system reduces to the spherical coordinate system.

The following relations between the Cartesian coordinates x, y, z and the spheroidal coordinates ξ, η, ϕ can be easily derived and are given in many works like Flammer (1957), Hanish et al. (1970), Skudrzyk (1971), and Van Buren et al. (1975):

$$x = \frac{d}{2}[(1 - \eta^2)(\xi^2 - 1)]^{1/2} \cdot \cos \phi \ , \qquad (2.2.10)$$

$$y = \frac{d}{2}[(1 - \eta^2)(\xi^2 - 1)]^{1/2} \cdot \sin \phi \ , \qquad (2.2.11)$$

and

$$z = \frac{d}{2}\eta\xi \quad . \tag{2.2.12}$$

2.3 The Wave Equation in Prolate Spheroidal Coordinates

As our interest is in investigating wave propagation in spheroidal coordinates, we first solve the equation of propagation in that system by separation of variables,

$$\frac{\partial^2\psi}{\partial t^2} - c^2\nabla^2\psi = 0 \quad , \tag{2.3.1}$$

where t is the time variable, and c the wave propagation velocity. As we will be concerned with harmonic time dependence, the function of time T reduces to

$$T = T_o e^{-i\omega t} \tag{2.3.2}$$

where ω is the angular frequency.

Our investigation will then be concentrated on solving the remaining part of the wave equation, representing the spatial dependence of pressure (or any chosen quantity like particle velocity, density, velocity potential, temperature), i.e., the classic Helmholtz equation is:

$$(\nabla^2 + k^2)\psi = 0 \quad , \tag{2.3.3}$$

where ψ represents a general variable, and

$$k = \frac{\omega}{c} \tag{2.3.4}$$

is the wave number.

The Laplacian operator can be derived by using the formulas for the divergence and for the gradient in spheroidal coordinates given in Hanish et al. (1970), and Van Buren et al. (1975). It can also be computed

directly from the metric coefficients as in Flammer (1957) and Lauchle (1970). This leads to:

$$\nabla^2 = \frac{4}{d^2(\xi^2 - \eta^2)}\left[\frac{\partial}{\partial\eta}(1 - \eta^2)\frac{\partial}{\partial\eta} + \frac{\partial}{\partial\xi}(\xi^2 - 1)\frac{\partial}{\partial\xi} + \frac{\xi^2 - \eta^2}{(\xi^2 - 1)(1 - \eta^2)}\frac{\partial^2}{\partial\phi^2}\right] \quad . \tag{2.3.5}$$

After substitution into Equation (2.3.3) and using

$$h = \frac{kd}{2} \tag{2.3.6}$$

as a nondimensional frequency parameter, the Helmholtz equation can be written:

$$\left[\frac{\partial}{\partial\eta}(1 - \eta^2)\frac{\partial}{\partial\eta} + \frac{\partial}{\partial\xi}(\xi^2 - 1)\frac{\partial}{\partial\xi} + \frac{\xi^2 - \eta^2}{(\xi^2 - 1)(1 - \eta^2)}\frac{\partial^2}{\partial\phi^2} + h^2(\xi^2 - \eta^2)\right]\psi = 0 \quad . \tag{2.3.7}$$

As the prolate spheroidal coordinate system is orthogonal we can use the separation of variables method to solve that equation. Solutions can be obtained in the form of Lamé's products:

$$\psi_{mn} = S_{mn}(h,\eta)R_{mn}(h,\xi)\cdot\begin{matrix}\cos\\ \sin\end{matrix} m\phi \quad , \tag{2.3.8}$$

where $S_{mn}(h,\eta)$ and $R_{mn}(h,\xi)$ are, respectively, the angle and the radial spheroidal wave functions. Substituting the right-hand side of Equation (2.3.8) into Equation (2.3.7) leads, after some calculations presented in Lauchle (1970), to two ordinary differential equations:

$$\frac{d}{d\eta}\left[(1 - \eta^2)\frac{d}{d\eta}S_{mn}(h,\eta)\right] + \left[\lambda_{mn} - h^2\eta^2 - \frac{m^2}{1 - \eta^2}\right]S_{mn}(h,\eta) = 0 \tag{2.3.8.a}$$

and

$$\frac{d}{d\xi}[(\xi^2 - 1)\frac{d}{d\xi} R_{mn}(h,\xi)] - [\lambda_{mn} - h^2\xi^2 + \frac{m^2}{\xi^2 - 1}]R_{mn}(h,\xi) = 0 \quad , \qquad (2.3.8.b)$$

where λ_{mn} are eigenvalues and are identical for both equations.

These two equations appear to be similar and are of the type:

$$\frac{d}{dz}[(1 - z^2)\frac{du_{mn}}{dz}] + [\lambda_{mn} - h^2z^2 - \frac{m^2}{1 - z^2}]u_{mn} = 0 \quad . \qquad (2.3.9)$$

The solution of Equations (2.3.8) are particular ellipsoidal wave functions, or Lamé's wave functions, for the degenerate case of the spheroidal coordinates. However, they are difficult to determine and not useful for practical applications. Power series solutions are not of great use either, due to the singularities presented by Equation (2.3.9) for $z = \pm 1$ and $z \to \infty$. Niven (1880) first investigated these equations and expressed the spheroidal wave functions as series of the spherical wave functions, as a consequence of the identity of spheroidal and spherical coordinate systems for large values of ξ. The radial functions are expressed in terms of spherical Bessel functions and the angle functions in terms of associated Legendre functions. A detailed derivation of those expressions is given in Flammer (1957) and Lauchle (1970); therefore, we simply give an outline here.

2.4 The Angle Functions

We have to solve Equation (2.3.8.a). We must first note that in most physical applications, the continuity of the field on a line closed around the z-axis imposes that m be an integer. We will also, without loss of generality, consider m as zero or positive and that $n \geq m$.

For h = 0, Equation (2.3.8.a) reduces to the angular differential equation obtained in spherical coordinates and is satisfied by the associated Legendre functions of the first kind $P_n^m(\eta)$ and of the second kind $Q_n^m(\eta)$:

$$\frac{d}{d\eta}[(1 - \eta^2)\frac{d}{d\eta} P_n^m(\eta)] + [\lambda_{mn}(0) - \frac{m^2}{1 - \eta^2}]P_n^m(\eta) = 0 \quad , \qquad (2.4.1)$$

where the eigenvalues, denoted by $\lambda_{mn}(0)$ when h = 0, are:

$$\lambda_{mn}(0) = n(n + 1), \; n \geq m \quad .$$

In that case, λ_{mn} does not depend on the frequency or on m, yielding a simple calculation. On the other hand, in spheroidal coordinates, i.e., when $h \neq 0$, λ_{mn} depends on both h and m, which makes the computations more difficult. In physical problems, we are interested in solutions which are finite at $\eta = \pm 1$; these solutions are known as the eigenfunctions of the first kind $S_{mn}(h,\eta)$ of order m and degree n. Equation (2.3.8.a) differs from Equation (2.4.1) only by having a singularity at infinity; this suggests an expression of the eigenfunctions under the form:

$$S_{mn}(h,\eta) = \sum_{r=0,1}^{\infty'} d_r^{mn}(h) P_{m+r}^m(\eta) \quad . \qquad (2.4.2)$$

The prime over the summation sign indicates that the summation is performed only on even values of r when n-m is even, and on odd values of r when n-m is odd. Angle functions of the second kind may be expressed in an identical manner from the associated Legendre functions of the second kind, but their singularities at $\eta = \pm 1$ give them little usefulness in most physical problems.

Then, substitution of Equation (2.4.2) into Equation (2.3.8.a) yields a recursion formula for the coefficients d_r^{mn}. Use is then made of the orthogonality property and of the recursion formula for the associated Legendre functions $p_n^m(\mu)$. The relation obtained is

$$A_r^m d_{r+2}^{mn}(h) + B_r^m d_r^{mn}(h) + C_r^m d_{r-2}^{mn}(h) = 0 \qquad (2.4.3)$$

with

$$A_r^m = \frac{(2m + r + 1)(2m + r + 2)}{(2m + 2r + 3)(2m + 2r + 5)} h^2 \quad , \qquad (2.4.4.a)$$

$$B_r^m = (m + r)(m + r + 1) - \lambda_{mn} + \frac{2(m+r)(m+r+1) - 2m^2 - 1}{(2m+2r-1)(2m+2r+3)} h^2 \quad , (2.4.4.b)$$

and

$$C_r^m = \frac{r(r - 1)}{(2m + 2r + 3)(2m + 2r + 5)} h^2 \quad . \qquad (2.4.4.c)$$

Equation (2.4.3) is a linear homogeneous difference equation of the second order. It must admit two non-trivial independent solutions. Examination of the recursion formula (2.4.3) shows that as r approaches infinity $d_r^{mn}(h)/d_{r-2}^{mn}(h)$ either increases as $-4r^2/h^2$ or decreases to zero as $-h^2/4r^2$. Therefore, the latter is chosen in order to insure absolute convergence of the series defined in Equation (2.4.2). Expressing the condition

$$\lim_{r \to \infty} \frac{d_r^{mn}(h)}{d_{r-2}^{mn}(h)} = 0$$

in Equation (2.4.3) leads to a transcendental equation between λ_{mn} and h^2. These calculations are discussed in Flammer (1957) and Lauchle (1970).

Different methods of calculation have been developed to solve the very complicated transcendental equation last obtained, such as the power series developments of the eigenvalues, or the Bowkamp's method of approximation (Flammer (1975)]. The latter has been utilized by Van Buren et al. (1975) in their tables of prolate spheroidal angular functions which we used in the calculations reported later in this document.

A last step in the determination of the spheroidal wave functions is the normalization of the functions $S_{mn}(h,\eta)$. The fact that S_{mn} reduces to P_n^m when h is zero is considered. Different methods have been introduced

by Chu and Stratton (1941), Page (1944), Morse and Feshbach (1953), Meixner and Shäfke (1954), and Flammer (1957). For the same reason as in the preceding paragraph, we will consider the method of Meixner and Shäfke, which has been used by Van Buren et al. (1975). The $d_r^{mn}(h)$ must be such that $S_{mn}(h,\eta)$ and $P_n^m(\eta)$ have the same normalization factor, i.e.:

$$N_{mn} = \int_{-1}^{+1} [S_{mn}(h,\eta)]^2 d\eta = \int_{-1}^{+1} [P_n^m(\eta)]^2 d\eta = \frac{2}{2n+1} \frac{(n+m)!}{(n-m)!} \quad . \quad (2.4.5)$$

Substituting Equation (2.4.2) into Equation (2.4.5), and using the orthogonality property of $P_n^m(\eta)$, yields the following normalization for $d_r^{mn}(h)$:

$$\sum_{r=o,1}^{\infty'} \frac{2}{2(m+r)+1} \frac{(r+2m)!}{r!} [d_r^{mn}(h)]^2 = \frac{2}{2n+1} \frac{(n+m)!}{(n-m)!} \quad . \quad (2.4.6)$$

Therefore, the coefficients d_r^{mn} are completely determined, as well as the $S_{mn}(h,\eta)$.

This normalization scheme has the advantage of eliminating the numerical integration of the normalization factor N_{mn} which is often used in physical applications.

Graphs showing the behavior of some of the angular eigenfucntions are shown in Van Buren et al. (1975). Different tables are available for values of $d_r^{mn}(h)$, $S_{mn}(h,\eta)$, λ_{mn} and other coefficients. An extensive number of coefficients are tabulated in Flammer (1957) and eigenfunctions for $m = 0$ and $h \leq 40$ are given in Van Buren et al. (1975). These tables are limited to low values of h because of the very slow convergence of the calculations and the very large intermediate values encountered in the computations. For large values of h, different approximation formulas have been developed by Meixner and Shäfke (1954), Silbiger (1961), and others.

2.5 The Radial Functions

The radial functions must satisfy Equation (2.3.8.b) which is similar to Equation (2.3.8.a) with the exception of the parameter range. This suggests that we express the radial functions $R_{mn}(h,\xi)$ in terms of the angular functions $S_{mn}(h,\eta)$. As shown in Flammer (1957), solutions of Equations (2.3.8.b) for all values of ξ can be given in the form

$$R_{mn}(h,\xi) = \int_a^b K_{mn}(\eta,\xi) S_{mn}(h,\eta) d\eta \quad , \tag{2.5.1}$$

where $K_m(\eta,\xi)$ is a Kernel function, discussed below, and a and b are chosen so that the bilinear concomittant vanishes at those limits.

Physical problems usually require radial functions for both standing-wave type solutions and progressive wave type solutions, whereas the angular functions, being solutions on closed contours, require only standing-wave type solutions. So, we will use functions of the first and second kind, $R_{mn}^{(1)}(h,\xi)$ and $R_{mn}^{(2)}(h,\xi)$, respectively, and functions of the third and fourth kind obtained by complex summation of the first two kinds. As we have already noticed, the spheroidal coordinate system degenerates to the spherical one as ξ becomes infinite, which implies:

$$R_{mn}^{(1)}(h,\xi) \underset{\xi\to\infty}{\to} j_n(\xi) \quad , \tag{2.5.2.a}$$

$$R_{mn}^{(2)}(h,\xi) \underset{\xi\to\infty}{\to} n_n(\xi) \quad , \tag{2.5.2.b}$$

$$R_{mn}^{(3)}(h,\xi) \underset{\xi\to\infty}{\to} h_n^{(1)}(\xi) \quad , \tag{2.5.2.c}$$

and

$$R_{mn}^{(4)}(h,\xi) \underset{\xi\to\infty}{\to} h_n^{(2)}(\xi) \quad , \tag{2.5.2.d}$$

where $j_n(\xi)$, $n_n(\xi)$, $h_n^{(1)}(\xi)$, and $h_n^{(2)}(\xi)$ are the spherical Bessel, Neumann and Hankel functions of the first and second kind, respectively.

According to Flammer (1957), the Kernel in spherical coordinates can be calculated, and only the solution yielding the Bessel functions expansion is considered for our problem, i.e., after transformation into the spheroidal coordinate system:

$$K_m(\eta,\xi) = C(1 - \eta^2)^{m/2}(\xi^2 - 1)^{m/2}e^{ih\eta\xi} \quad , \tag{2.5.3}$$

where C is an arbitrary constant. Then Equation (2.5.1) becomes:

$$R_{mn}(h,\xi) = C \int_a^b (1 - \eta^2)^{m/2}(\xi^2 - 1)^{m/2}e^{ih\eta\xi}S_{mn}(h,\eta)d\eta \quad , \tag{2.5.4}$$

and the bilinear concomittant is given by [Morse and Feshbach (1953) and Flammer (1957)]:

$$e^{ih\eta\xi}(1 - \eta^2)^{1+m/2}\left[\left(\frac{m\eta}{1 - \eta^2} - ih\xi\right)S_{mn}(h,\eta) + S'_{mn}(h,\eta)\right] \quad . \tag{2.5.5}$$

Expansions for the radial functions of the first, third, and fourth kind are then evaluated by substituting Equation (2.4.2) into Equation (2.5.4) and applying the three different sets of limits:

$$\left\{\begin{matrix} a = -1 \\ b = +1 \end{matrix}\right\} \quad , \quad \left\{\begin{matrix} a = i\infty \\ b = +1 \end{matrix}\right\} \quad \text{and} \quad \left\{\begin{matrix} a = -1 \\ b = i\infty \end{matrix}\right\} \quad , \tag{2.5.6}$$

respectively.

Flammer (1957) has shown that Equation (2.5.4) can be transformed into:

$$R_{mn}(h,\xi) = C(\xi^2 - 1)^{m/2} \sum_{r=o,1}^{\infty'} d_r^{mn}(h)\frac{i^r(2m + r)!}{2^{m+r}r!(m + r)!}(h\xi)^r \int_a^b \cdot e^{ih\xi t}(1 - t^2)^{m+r}dt \quad , \tag{2.5.7}$$

where the d_r^{mn} are those calculated for the angle functions. The evaluation of the integral in Equation (2.5.7) yields a series of spherical Bessel and Hankel functions for the three sets of limits:

$$\int_{-1}^{+1} e^{ih\xi t}(1 - t^2)^k dt = 2.2^k k!\frac{j_k(h\xi)}{(h\xi)^k} \quad , \tag{2.5.8.a}$$

$$\int_{i\infty}^{+1} e^{ih\xi t}(1 - t^2)^k dt = 2^k k! \frac{h_k^{(1)}(h\xi)}{(h\xi)^k} \quad , \qquad (2.5.8.b)$$

and

$$\int_{-1}^{i\infty} e^{ih\xi t}(1 - t^2)^k dt = 2^k k! \frac{h_k^{(2)}(h\xi)}{(h\xi)^k} \quad . \qquad (2.5.8.c)$$

Therefore, $R_{mn}^{(1)}(h,\xi)$ can be written as:

$$R_{mn}^{(1)}(h,\xi) = C\frac{(\xi^2 - 1)^{m/2}}{(h\xi)^m} \sum_{r=o,1}^{\infty'} d_r^{mn}(h)\frac{i^r(2m + r)!}{r!} j_{m+r}(h\xi) \quad , \qquad (2.5.9)$$

where the arbitrary constant C is then determined by normalizing $R_{mn}^{(1)}(h,\xi)$. A convenient choice is based on Equation (2.5.2.a) and the asymptotic formula for $j_n(\xi)$ when ξ becomes infinite, i.e.:

$$R_{mn}^{(1)}(h,\xi) \underset{\xi\to\infty}{\to} \frac{1}{h\xi} \cos[h\xi - \frac{\pi}{2}(n + 1)] \quad . \qquad (2.5.10)$$

After computation of C, $R_{mn}^{(1)}(h,\xi)$ is found, according to the normalization method used in the computation of the coefficients $d_r^{mn}(h)$ [Equation (2.4.6.)] to be:

$$R_{mn}^{(1)}(h,\xi) = \frac{(n - m)!}{(n + m)!}(\frac{\xi^2 - 1}{\xi^2})^{m/2} \sum_{r=o,1}^{\infty'} i^{r+m-n} d_r^{mn}(h) \cdot$$

$$\cdot \frac{(2m + r)!}{r!} j_{m+r}(h\xi) \quad . \qquad (2.5.11)$$

In the same manner, expressions for $R_{mn}^{(3)}(h,\xi)$ and $R_{mn}^{(4)}(h,\xi)$ can be obtained by application of Equations (2.5.8.b) and (2.5.8.c) and performing the normalization with Equations (2.5.2.c) and (2.5.2.d). These expressions are given by:

$$R_{mn}^{(3),(4)}(h,\xi) = \frac{(n - m)!}{(n + m)!}(\frac{\xi^2 - 1}{\xi^2})^{m/2} \sum_{r=o,1}^{\infty'} i^{r+m-n} d_r^{mn}(h) \cdot$$

$$\cdot \frac{(2m + r)!}{r!} h_{m+r}^{(1),(2)}(h\xi) \quad . \qquad (2.5.12)$$

An expression for $R_{mn}^{(2)}(h,\xi)$ may be derived using the classic relation:

$$R_{mn}^{(3),(4)}(h,\xi) = R_{mn}^{(1)}(h,\xi) \pm iR_{mn}^{(2)}(h,\xi) \quad , \tag{2.5.13}$$

as in Flammer (1957), or by replacing the spherical Bessel function j_{m+r} by the spherical Neumann functions in the expression of $R_{mn}^{(1)}(h,\xi)$ [Equation (2.5.11)]. This yields:

$$R_{mn}^{(2)}(h,\xi) = \frac{(n-m)!}{(n+m)!}\left(\frac{\xi^2-1}{\xi^2}\right)^{m/2} \sum_{r=0,1}^{\infty'} i^{r+m-n} d_r^{mn}(h) \frac{(2m+r)!}{r!} \cdot$$

$$n_{m+r}(h\xi) \quad . \tag{2.5.14}$$

This expansion is, in fact, an asymptotic series which is not absolutely convergent for any finite value of $h\xi$. It converges only for large values of $h\xi$, and consequently [Equation (2.5.13)], the expression for $R_{mn}^{(3)}(h,\xi)$ and $R_{mn}^{(4)}(h,\xi)$ are also only valid for large values of $h\xi$, i.e., as asymptotic forms. Large $h\xi$ does not imply $h \gg 1$, $\xi \approx 1$, but necessarily implies $h \approx 1$, and $\xi \gg 1$ [Silbiger (1961)]. An alternate way of expressing $R_{mn}^{(2)}(h,\xi)$ is to write it as a series of associated Legendre functions of both kinds $P_n^m(\xi)$ and $Q_n^m(\xi)$, for $\xi > 1$ [Hanish et al. (1970)], that is, writing that the radial and angular functions of the second kind are proportional to one another [Flammer (1957)]. This provides a solution for $R_{mn}^{(2)}(h,\xi)$ which is valid for low values of $h\xi$, and can be found in Flammer (1957) and Hanish et al. (1970).

Tables of $R_{mn}^{(1)}(h,\xi)$ and $R_{mn}^{(2)}(h,\xi)$ and their first derivatives with respect to ξ are given in the last two references, with a more extensive range of the parameters m, n, h and ξ in Hanish et al. (1970).

2.6 The Free-Space Green's Function in Prolate Spheroidal Coordinates

The Green's function $G(\underline{r}|\underline{r}')$ of the scalar wave equation is the solution at point $\underline{r}$ when a unit-strength source is placed at point $\underline{r}'$.

So, $G(\underline{r}|\underline{r}')$ satisfies the inhomogeneous equation:

$$(\nabla^2 + k^2)G(\underline{r}/\underline{r}') = \delta(\underline{r} - \underline{r}') \quad , \tag{2.6.1}$$

where δ is the three-dimensional Dirac delta function. In spheroidal coordinates $\delta(\underline{r} - \underline{r}')$ is defined by:

$$\delta(\underline{r} - \underline{r}') = h_\eta^{-1} h_\xi^{-1} h_\phi^{-1} \delta(\eta - \eta')\delta(\xi - \xi')\delta(\phi - \phi') \quad , \tag{2.6.2}$$

where h_η, h_ξ and h_ϕ are the metrical coefficients (Flammer, 1957):

$$h_\eta = \frac{d}{2}\left(\frac{\xi^2 - \eta^2}{1 - \eta^2}\right)^{1/2} \quad , \tag{2.6.3.a}$$

$$h_\xi = \frac{d}{2}\left(\frac{\xi^2 - \eta^2}{\xi^2 - 1}\right)^{1/2} \quad , \tag{2.6.3.b}$$

and

$$h_\phi = \frac{d}{2}[(1 - \eta^2)(\xi^2 - 1)]^{1/2} \tag{2.6.3.c}$$

[Flammer (1957)].

The metric coefficients are introduced because δ must satisfy:

$$\int_V \delta(\underline{r} - \underline{r}')dz' = 1 = \int_0^{2\pi}\int_{-1}^{+1}\int_{o,1}^{\infty} [\delta(\underline{r} - \underline{r}')h_\eta' h_\xi' h_\phi']d\eta' d\xi' d\phi' \tag{2.6.4}$$

with

$$\int_{x'=x-\varepsilon}^{x'=x+\varepsilon} \delta(x - x')dx' = 1 \quad . \tag{2.6.5}$$

The solution of Equation (2.6.1) in the case when there are no boundaries is called the free-space Green's function $G_o(\underline{r}/\underline{r}')$ and is given by the classic formula:

$$G_o(\underline{r}/\underline{r}') = \frac{e^{ik|\underline{r}-\underline{r}'|}}{4\pi|\underline{r} - \underline{r}'|} \quad . \tag{2.6.6}$$

To express this function in spheroidal coordinates, we will expand it in terms of the natural eigenfunctions in spheroidal coordinates, i.e., the wave functions previously described. Noting that $G_o(\underline{r}/\underline{r}')$ is a solution

of the Helmholtz equation for $\underline{r} \neq \underline{r}'$, and is symmetrical in $\underline{r}$ and $\underline{r}'$, we express it in the form:

$$G_o(\eta,\xi,\phi/\eta',\xi',\phi') = \sum_{m,n} A_{mn} S_{mn}(h,\eta) S_{mn}(h,\eta') \cos m(\phi - \phi') \cdot \begin{cases} R_{mn}^{(1)}(h,\xi) R_{mn}^{(3)}(h,\xi'), & \xi < \xi' \\ R_{mn}^{(1)}(h,\xi') R_{mn}^{(3)}(h,\xi), & \xi > \xi' \end{cases} \quad (2.6.7)$$

where $R_{mn}^{(1)}$ represents standing-wave solutions, and $R_{mn}^{(3)}$ progressive-wave solutions diverging at infinity. Therefore, the radiation condition is respected for all observed situations. Furthermore, A_{mn} is the same in both cases to insure the continuity of the Green's function at $\xi = \xi'$.

We now integrate Equation (2.6.1), applied on $G_o(\underline{r}/\underline{r}')$, over the range $[\xi' - \varepsilon, \xi' + \varepsilon]$, which yields:

$$\int_{\xi'-\varepsilon}^{\xi'+\varepsilon} (\nabla^2 + k^2) G_o(\eta,\xi,\phi/\eta',\xi',\phi') d\xi = -\int_{\xi'-\varepsilon}^{\xi'+\varepsilon} h_\eta^{-1} h_\xi^{-1} h_\phi^{-1} \delta(\eta - \eta') \cdot \delta(\xi - \xi') \delta(\phi - \phi') d\xi \,. \quad (2.6.8)$$

After multiplying both sides by $(\frac{1}{2} d)^2 (\xi^2 - \eta^2)$ and making use of Equation (2.6.5), we obtain:

$$[(\xi^2 - 1) \frac{\partial}{\partial \xi} G_o(\eta,\xi,\phi/\eta',\xi',\phi')]_{\xi'-\varepsilon}^{\xi'+\varepsilon} = -\frac{2}{d} \delta(\eta - \eta') \delta(\phi - \phi') \,. \quad (2.6.9)$$

From Equation (2.6.7) we can write:

$$\frac{\partial}{\partial \xi} G_o(\eta,\xi,\phi/\eta',\xi',\phi') = \sum_{m,n} K_{mn} \cdot \begin{cases} R_{mn}^{(3)}(h,\xi') \dfrac{\partial R_{mn}^{(1)}(h,\xi)}{\partial \xi}, & \xi < \xi' \\ R_{mn}^{(1)}(h,\xi') \dfrac{\partial R_{mn}^{(3)}(h,\xi)}{\partial \xi}, & \xi > \xi' \end{cases} \quad (2.6.10)$$

with $K_{mn} = A_{mn} S_{mn}(h,\eta) S_{mn}(h,\eta') \cos m(\phi - \phi')$.

Substituting Equation (2.6.10) into Equation (2.6.9), and passing to the limit $\xi = \xi'$, the radial functions and derivatives being continuous at $\xi = \xi'$ we get:

$$\{(\xi^2 - 1)\sum_{m,n} K_{mn}[R^{(1)}_{mn}(h,\xi)\frac{\partial R^{(3)}_{mn}(h,\xi)}{\partial \xi} - R^{(3)}_{mn}(h,\xi)\frac{\partial R^{(1)}_{mn}(h,\xi)}{\partial \xi}]\}_{\xi=\xi'} =$$

$$= -\frac{2}{d}\delta(\eta - \eta')\delta(\phi - \phi') \quad . \qquad (2.6.11)$$

After use of the expression for $R^{(3)}_{mn}(h,\xi)$ given in Equation (2.5.13), the left-hand side of Equation (2.6.11) becomes:

$$\{(\xi^2 - 1)\sum_{m,n} K_{mn}[R^{(1)}_{mn}(h,\xi)\frac{\partial R^{(1)}_{mn}(h,\xi)}{\partial \xi} + iR^{(1)}_{mn}(h,\xi)\frac{\partial R^{(2)}_{mn}(h,\xi)}{\partial \xi}$$

$$- R^{(1)}_{mn}(h,\xi)\frac{\partial R^{(1)}_{mn}(h,\xi)}{\partial \xi} - iR^{(2)}_{mn}(h,\xi)\frac{\partial R^{(1)}_{mn}(h,\xi)}{\partial \xi}]\}_{\xi=\xi'} \quad .$$

Then, using the Wronskian relation [Flammer (1957)]:

$$R^{(1)}_{mn}(h,\xi)\frac{\partial R^{(2)}_{mn}(h,\xi)}{\partial \xi} - R^{(2)}_{mn}(h,\xi)\frac{\partial R^{(1)}_{mn}(h,\xi)}{\partial \xi} = \frac{1}{h(\xi^2 - 1)}$$

in this last expression yields a new form for Equation (2.6.11), i.e.:

$$\frac{i}{h}\sum_{m,n} K_{mn} = -\frac{2}{d}\delta(\eta - \eta')\delta(\phi - \phi')$$

or

$$\sum_{m,n} A_{mn} S_{mn}(h,\eta) S_{mn}(h,\eta')\cos m(\phi - \phi') = ik\delta(\eta - \eta')\delta(\phi - \phi') \quad . \qquad (2.6.12)$$

We now multiply both sides of Equation (2.6.12) by $S_{pq}(h,\eta)\cos p\phi$, and integrate over the range of η and ϕ:

$$\int_{-1}^{+1}\int_{o}^{2\pi} S_{pq}(h,\eta)\cos p\phi \sum_{m,n} A_{mn} S_{mn}(h,\eta) S_{mn}(h,\eta')\cos m(\phi - \phi')\,d\phi\,d\eta =$$

$$= \int_{-1}^{+1}\int_{o}^{2\pi} S_{pq}(h,\eta)\cos p\phi\; ik\delta(\eta - \eta')\delta(\phi - \phi')\,d\phi\,d\eta \quad . \qquad (2.6.13)$$

Using the orthogonality property of the angular wave functions and the properties of the Dirac delta functions, the integration yields:

$$A_{pq} S_{pq}(h,\eta') N_{pq} \frac{2\pi}{2 - \delta_{op}} \cos p\phi' = ikS_{pq}(h,\eta')\cos p\phi' \quad , \qquad (2.6.14)$$

where N_{pq} is the norm of $S_{pq}(h,\eta')$ defined in Equation (2.4.5), and δ_{op} is the Kronecker symbol.

Therefore, we have determined the value of the constant A_{pq}:

$$A_{pq} = \frac{ik\varepsilon_p}{2\pi N_{pq}} \tag{2.6.15}$$

with

$$\varepsilon_p = 2 - \delta_{op} \quad . \tag{2.6.16}$$

The arbitrary choice of p and q in Equation (2.6.13) makes it possible to apply Equation (2.6.15) for all possible values of the set (p,q).

Substituting Equation (2.6.15) into Equation (2.6.7) yields the final expression for the free space Green's function:

$$G_o(\eta,\xi,\phi/\eta',\xi',\phi') = \frac{ik}{2\pi} \sum_{m=o}^{\infty} \varepsilon_m \sum_{n=m}^{\infty} \frac{S_{mn}(h,\eta)S_{mn}(h,\eta')}{N_{mn}} \cos m(\phi - \phi') \cdot \begin{cases} R_{mn}^{(1)}(h,\xi)R_{mn}^{(3)}(h,\xi') \ , & \xi < \xi' \\ R_{mn}^{(1)}(h,\xi')R_{mn}^{(3)}(h,\xi) \ , & \xi > \xi' \end{cases} \quad . \tag{2.6.17}$$

CHAPTER III

ANALYSIS

3.1 Introduction

In Chapter II, we developed expressions for the spheroidal wave functions and free-space Green's function. They are the tools needed to solve the problems that will be presented here. Our purpose is to calculate the ratio of the scattered pressure to the directly incident pressure far away from a prolate spheroid which is insonified at a given frequency by a point source located at a finite distance on the axis of the spheroid (Figure 2). Two types of boundary conditions on the spheroid are considered: a perfectly rigid surface, and a perfect pressure release surface. Furthermore, combinations of two sources of the same strength are investigated, i.e., two sources in phase and two incoherent sources. In this section, we derive the expressions for the reflection factor corresponding to those different situations.

3.2 Case of a Prolate Spheroid with Perfectly Rigid Surface

The spheroid is centered at the origin of the spheroidal coordinate system and is defined by the radial coordinate ξ_o. We consider a point source of strength Q emitting sound waves at a nondimensional frequency h, and located on the positive z-axis at a point $(\xi', +1, \phi')$. The observation point has coordinates (ξ, η, ϕ). The problem is symmetrical with respect to the z-axis, so the coordinate ϕ' is arbitrary, and we will let $\phi = \phi'$. This also results in $m = 0$. The entire problem will be solved by simply looking at a cross section in a plane ϕ = constant.

As we will treat the problem of infinite ξ we have $\xi > \xi'$. Using the free space Green's function given by Equation (2.6.17) for this limit, we can express the incident pressure by

$$\bar{p}_i = p_o \sum_{n=o}^{\infty} \frac{S_{on}(h,\eta)S_{on}(h,1)}{N_{on}} R_{on}^{(1)}(h,\xi')R_{on}^{(3)}(h,\xi) \qquad (3.2.1)$$

with

$$p_o = \frac{k^2 \rho c Q}{2\pi} \quad . \qquad (3.2.2)$$

We now want to express the pressure at the observation point, which is due to the scattering of sound by the spheroid when insonified by the point source. We call this pressure the scattered pressure and denote it by $\bar{p}_{s1}$. It is expedient to express $\bar{p}_{s1}$ in terms of the spheroidal wave functions, i.e.:

$$\bar{p}_{s1} = \sum_{n=o}^{\infty} A_n S_{on}(h,\eta)R_{on}^{(3)}(h,\xi) \quad . \qquad (3.2.3)$$

The radial function of the third kind is chosen because it represents a progressive wave diverging at infinity, which is the required behavior.

The boundary condition for the rigid-type surface is given by the Neumann boundary condition:

$$\frac{\partial \bar{p}_{i,o}}{\partial \xi} + \frac{\partial \bar{p}_{s1,o}}{\partial \xi} = 0 \text{ at } \xi = \xi_o \text{ and } \xi_o < \xi' \quad , \qquad (3.2.4)$$

where $\bar{p}_{i,o}$ and $\bar{p}_{s1,o}$ are the incident and scattered pressures, respectively, on the boundary surface. On the surface, the incident pressure is written as [Equation 2.6.17)]:

$$\bar{p}_{i,o} = p_o \sum_{n=o}^{\infty} \frac{S_{on}(h,\eta)S_{on}(h,\eta')}{N_{on}} R_{on}^{(1)}(h,\xi)R_{on}^{(3)}(h,\xi') \text{ at } \xi = \xi_o \quad , \qquad (3.2.5)$$

and Equation (3.2.4) can be written as:

$$p_o \sum_{n=o}^{\infty} \frac{S_{on}(h,\eta)S_{on}(h,\eta')}{N_{on}} R_{on}^{(1)'}(h,\xi_o)R_{on}^{(3)}(h,\xi') = - \sum_{n=o}^{\infty} A_n S_{on}(h,\eta) \cdot R_{on}^{(3)'}(h,\xi_o) \quad , \quad (3.2.6)$$

where

$$R_{on}^{(1)'}(h,\xi_o) = \left.\frac{\partial R_{on}^{(1)}(h,\xi)}{\partial \xi}\right|_{\xi=\xi_o} \quad (3.2.7.a)$$

and

$$R_{on}^{(3)'}(h,\xi_o) = \left.\frac{\partial R_{on}^{(3)}(h,\xi)}{\partial \xi}\right|_{\xi=\xi_o} \quad . \quad (3.2.7.b)$$

The boundary condition must be respected on the whole surface of the body and for any source location which means that Equation (3.2.6) must be true for all values of η and ξ' (provided $\xi' > \xi_o$). Therefore, Equation (3.2.6) must be verified separately for each order n. Hence, after division by $-S_{on}(h,\eta)$ we obtain:

$$-p_o \frac{S_{on}(h,1)}{N_{on}} R_{on}^{(1)'}(h,\xi_o)R_{on}^{(3)}(h,\xi') = A_n R_{on}^{(3)'}(h,\xi_o) \quad (3.2.8)$$

for all values of n. This gives the expression for the coefficients A_n. After substituting this value into Equation (3.2.3), we obtain the expression of $\bar{p}_{sl}$:

$$\bar{p}_{sl} = -p_o \sum_{n=o}^{\infty} \frac{S_{on}(h,\eta)S_{on}(h,1)}{N_{on}} \frac{R_{on}^{(1)'}(h,\xi_o)}{R_{on}^{(3)'}(h,\xi_o)} R_{on}^{(3)}(h,\xi')R_{on}^{(3)}(h,\xi) \quad . \quad (3.2.9)$$

From the expression for $\bar{p}_i$ and $\bar{p}_{sl}$, we can now write the reflection factor

$$\bar{R}_1(h,\xi,\eta) = \frac{\bar{p}_{sl}}{\bar{p}_i} \quad . \quad (3.2.10)$$

As we are interested in the far-field reflection factor, we will replace $R_{on}^{(3)}(h,\xi)$ by its asymptotic expansion:

$$R_{on}^{(3)}(h,\xi) \underset{\xi\to\infty}{\to} \frac{1}{h\xi} e^{ih\xi} e^{-i\frac{\pi}{2}(n+1)} = \frac{e^{ih\xi}}{h\xi}(-i)^{n+1} \qquad (3.2.11)$$

so that the final expression for the reflection factor at infinity in the case of the rigid spheroid is given by:

$$\bar{R}_1(h,\eta) = -\frac{\sum_{n=o}^{\infty} A_n^o(h,\eta)\frac{R_{on}^{(1)'}(h,\xi_o)}{R_{on}^{(3)'}(h,\xi_o)} R_{on}^{(3)}(h,\xi')(-i)^n}{\sum_{n=o}^{\infty} A_n^o(h,\eta) R_{on}^{(1)}(h,\xi')(-i)^n} \qquad (3.2.12)$$

with

$$A_n^o(h,\eta) = \frac{S_{on}(h,\xi)S_{on}(h,1)}{N_{on}} \quad . \qquad (3.2.13)$$

We notice that this result is valid for any value of the source angular coordinate η' provided that symmetry with respect to the z-axis is conserved. A value of η' different from +1 or -1 would then describe a problem with a ring source defined by the intersection of the spheorid ξ' and the hyperboloid defined by η'.

3.3 Case of a Prolate Spheroid with Pressure Release Type Surface

The situation is analogous to the previous one except for the type of boundary condition. The expression for the incident pressure remains unchanged, and we still express the scattered pressure (denoted by $\bar{p}_{s2}$) in the form given in Equation (3.2.3).

Then, we write a new boundary condition, which is a Dirichlet boundary condition:

$$\bar{p}_{i,o} + \bar{p}_{s2,o} = 0 \text{ at } \xi = \xi_o \text{ and } \xi_o < \xi' \quad . \qquad (3.3.1)$$

Keeping the same notation as in the previous section, we find:

$$p_o \sum_{n=o}^{\infty} \frac{S_{on}(h,\eta)S_{on}(h,1)}{N_{on}} R_{on}^{(1)}(h,\xi_o)R_{on}^{(3)}(h,\xi') = -\sum_{n=o}^{\infty} A_n S_{on}(h,\eta) \cdot R_{on}^{(3)}(h,\xi_o) \qquad (3.3.2)$$

which determines the value of A_n for all n. Hence, the expression for the scattered pressure $\bar{p}_{s2}$ is

$$\bar{p}_{s2} = -p_o \sum_{n=o}^{\infty} A_o^n(h,\eta) \frac{R_{on}^{(1)}(h,\xi_o)}{R_{on}^{(3)}(h,\xi_o)} R_{on}^{(3)}(h,\xi')R_{on}^{(3)}(h,\xi) \; . \qquad (3.3.3)$$

Making the same approximation as in Equation (3.2.11) we obtain the expression for the reflection factor at infinity for the case of the spehroid with pressure release surface:

$$\bar{R}_2(h,\eta) = \frac{\bar{p}_{s2}}{\bar{p}_i} = - \frac{\sum_{n=o}^{\infty} A_n^o(h,\eta) \frac{R_{on}^{(1)}(h,\xi_o)}{R_{on}^{(3)}(h,\xi_o)} R_{on}^{(3)}(h,\xi')(-i)^n}{\sum_{n=o}^{\infty} A_n^o(h,\eta) R_{on}^{(1)}(h,\xi')(-i)^n} \; . \qquad (3.3.4)$$

3.4 Combination of Two Sources

We now consider the combination of two sources of equal strength on the axis, at finite distances from the spheroid. Two cases are investigated: the sources are in phase, and the sources are incoherent.

In the first case, we simply apply the superposition theorem by adding the incident pressures due to each source on one hand, and the scattered pressures due to each source on the other hand. This can be written as:

$$\bar{p}_i = \bar{p}_{i,1} + \bar{p}_{i,2} \qquad (3.4.1.a)$$

and

$$\bar{p}_s = \bar{p}_{s,1} + \bar{p}_{s,2} \; , \qquad (3.4.1.b)$$

where subscript 1 and 2 refer to Sources 1 and 2, respectively, and where $\bar{p}_i$ is the resulting incident pressure, and $\bar{p}_s$ the resulting scattered

pressure. We will denote scattered pressures $\bar{p}_{s1}$, $\bar{p}_{s1,1}$, and $\bar{p}_{s1,2}$ in the rigid type boundary problem, and $\bar{p}_{s2}$, $\bar{p}_{s2,1}$, and $\bar{p}_{s2,2}$ in the pressure release type boundary problem. Generally, we can write the reflection factor in the form:

$$\bar{R}(h,\eta) = \frac{\bar{p}_s}{\bar{p}_i} = \frac{\bar{p}_{s,1} + \bar{p}_{s,2}}{\bar{p}_{i,1} + \bar{p}_{i,2}} \tag{3.4.2}$$

and the computation will be made accordingly.

For the incoherent sources, statistical theory shows that the energies add and not the pressures. In terms of pressure, this can be expressed by adding the square of the magnitude of the pressures. So we obtain:

$$|\bar{p}_i|^2 = |\bar{p}_{i,1}|^2 + |\bar{p}_{i,2}|^2 \tag{3.4.3.a}$$

and

$$|\bar{p}_s|^2 = |\bar{p}_{s,1}|^2 + |\bar{p}_{s,2}|^2 \tag{3.4.3.b}$$

following the same notation as above. Then, the reflection factor takes the form:

$$R(h,\eta) = \frac{|\bar{p}_s|}{|\bar{p}_i|} = \sqrt{\frac{|\bar{p}_{s,1}|^2 + |\bar{p}_{s,2}|^2}{|\bar{p}_{i,1}|^2 + |\bar{p}_{i,2}|^2}} \quad . \tag{3.4.4}$$

Obviously, $R(h,\eta)$ is now a real number and no phase can be defined for it, due to the constantly varying difference of phase between the two incoherent sources.

3.5 An Alternative Interpretation of the Problem

The solution of the boundary condition could have been directly obtained by working on the Green's function as in Flammer (1957). In fact, the incident and scattered pressures are exactly identical to the Green's functions except for the constant of proportionality p_o defined in Equation

(3.2.2). Therefore, we can apply the reciprocity property of the Green's functions to our problem, in the same manner as Morse (1968) applied it to the problem of diffraction by a cylinder. We can say that the incident pressure $\bar{p}_i$ at the point of coordinates $(+\infty,\eta)$, due to a point source located at (ξ',η'), is the same as the pressure created at (ξ',η') by the same source located at $(+\infty,\eta)$. The same reciprocity theorem can be applied to the scattered pressure. Therefore, it is also true for the reflection factor.

As we have considered $\xi \to \infty$, the wave impinging on the body in the reciprocal situation is, in fact, a plane wave which is incident under the aspect angle $\theta = \cos^{-1} \eta$. Consequently, our reflection factor is also the reflection factor at the observation point on the z axis defined by $(\xi',+1)$ when the body is insonified by a plane wave impinging under the aspect angle $\theta = \cos^{-1} \eta$ with respect to the positive z semi-axis.

CHAPTER IV

NUMERICAL COMPUTATIONS AND RESULTS

4.1 Introduction

In this section, we present the calculations which have been carried out according to the formulas derived in the last chapter. The computations have been made on an IBM 370/167 digital computer located at The Pennsylvania State University campus, using the WATFIV compiler which allows computations directly in complex variables as expressed in Equations (3.2.12), (3.3.4), (3.4.2), and (3.4.4). Single precision was used in all of the computations.

4.2 Range of the Parameters

As seen in the previous chapter, we have considered two types of boundary conditions and three source situations. The body radial coordinate ξ_o remained constant in all the calculations, i.e.:

$$\xi_o = 1.01$$

which corresponds to a fineness ratio [Equation (2.2.4)]:

$$\varepsilon_o = \frac{L_o}{2R_o} = 7.1 \quad .$$

In the case of a single source, ten different locations have been considered along the positive z axis: $1.02 \leq \xi' \leq 1.20$ in increments of 0.02.

The values of the radial wave functions of the first and second kind and their first derivatives have been taken from the tables by Hanish et al. (1970). Then the function of the third kind was written according to Equation (2.5.13).

In the case of two sources, we considered one source fixed at the position $\xi' = 1.02$, the second source successively taking the nine remaining positions denoted in the range above.

For all source locations, we determined the directivity pattern of the reflection factor for three values of the parameter h:

$$h = 20,\ 35,\ 40 \quad .$$

Those calculations were made for values of the aspect angle $\theta = \cos^{-1}\eta$ from 0 to 180 degrees, in increments of two degrees. The values of the angular wave functions for $\theta \leq 90°$ were obtained from the tables of Van Buren et al. (1975). For $\theta > 90°$, we used the symmetry relation:

$$S_{on}(h,-\eta) = (-1)^n S_{on}(h,\eta) \qquad (4.2.1)$$

which can also be written:

$$S_{on}(h,\pi - \theta) = (-1)^n S_{on}(h,\theta) \quad . \qquad (4.2.2)$$

For all of the source locations, we also determined the frequency response of the reflection factor for three values of the aspect angle:

$$\theta = 0,\ 90,\ 180° \quad .$$

Those calculations were carried out for the following thirteen values of h:

h = 0.1, 0.4, 0.6, 1.0, 2.0, 4.0, 6.0, 10.0, 12.0, 14.0, 16.0, 18.0, 20.0.

We have listed in Tables I, II, and III the various parameters corresponding to the different source locations and the nondimensional frequencies h = 20, 35, and 40. In those tables, d is the interfocal distance, L_o the length, and R_o the minor radius of the spheroid, λ the wavelength, ℓ' the distance from the single source located at ξ' to the closest pole of the spheroid, ξ'' the radial coordinate of the second source and ℓ'' its distance from the pole of the spheroid, and a the

separation distance between the two sources. Those values were determined from the following simple relations:

$$\ell' = \frac{d}{2}(\xi' - \xi_o) \quad , \tag{4.2.3.a}$$

$$h = \frac{2\pi}{\lambda}\frac{d}{2} \quad , \tag{4.2.3.b}$$

$$R_o = \frac{d}{2}\sqrt{\xi_o^2 - 1} \quad , \tag{4.2.3.c}$$

$$a = \frac{d}{2}(\xi'' - \xi') = \ell'' - \ell' \tag{4.2.3.d}$$

and

$$L_o = \xi_o d \quad . \tag{4.2.3.e}$$

We note that, because ξ_o is very close to 1, $L_o = \xi_o d$ is not very different from d.

As the tables give values of the angular and the radial functions only for n covering the range from 0 to 49, an important point was to check the convergence of the three series used for the computation of $\bar{p}_i/p_o$, $\bar{p}_{s1}/p_o$, and $\bar{p}_{s2}/p_o$. We have checked the convergence of these series as a function of the upper limit of summation N, for h = 20, 35, and 40. Some of the results are presented in Figure 3. In general, it was found that a number of terms between h/2 and h is necessary for convergence, in the range ξ' = 1.02 to 1.20. Therefore, we used 50 terms in the computations of directivity patterns at h = 20, 35, and 40, and 25 terms for frequency response curves between h = 0 and h = 20.

4.3 Results

In spite of the fact that all the calculations have been made for both the rigid-type and the pressure release-type boundaries, the bulk

of the results presented are for the former case; only a few typical results are presented for the latter case.

4.3.1 Case of the rigid boundary. For the rigid spheroid insonified by both one and two sources, we have plotted directivity patterns showing the modulus of the reflection factor, $|\bar{R}|$ as a function of θ in Figure 4 through 20 and the variations of $|\bar{R}|$ with h are shown in Figure 21 through 35. In all directivity curves, the source(s) is (are) located on the θ = 0° axis.

In the case of a single source, the directivity patterns (Figures 4-9) are very similar to each other. They exhibit a nearly omnidirectional pattern for $\theta \leq 90°$, while for $\theta > 90°$, a lobe develops in the forward direction. For a given value of h, successive curves are similar to each other when ξ' is larger. In particular, curves obtained for $\xi' = 1.02$ are only slightly different from the curves for $\xi' > 1.02$. When the separation distance ℓ' increases, the overall level of the reflection factor is seen to decrease. This may be due to the lower amount of energy impinging on the spheroid (spherical spreading loss). But with ℓ'/λ remaining constant, the level of $|\bar{R}|$ is higher when a higher frequency in considered, which seems to imply diffraction phenomena becomes more important.

In the case of the combination of two in-phase sources (Figures 10-14), the directivity patterns differ from the patterns obtained with a single source, and are more irregular. Of particular interest is the formation of cusps at some angles. These cusps should not be interpreted as a sudden increase in scattered pressure as this is not the case. They result because of a null in the incident pressure field defined by Equation (3.4.1.2). The two in-phase sources separated by a distance a [see Table

II and Equation (4.2.3.d)] represent a doublet whose directivity function is given by

$$D_{doublet} = \cos(\frac{ka}{2} \cos\theta) = \cos(\frac{\pi a}{\lambda} \cos\theta) \quad . \tag{4.3.1}$$

The nulls in the incident pressure field (which correspond to cusps in the reflection factor), therefore, occur at angles for which

$$\frac{a}{\lambda} \cos\theta_c = \pm \frac{2p+1}{2} \quad , \tag{4.3.2}$$

where p is a positive integer. It further follows that cusps will not occur if $a/\lambda < \frac{1}{2}$.

The values of a/λ for the various source locations and reduced frequencies are tabulated in Table III. Also shown in this table are the critical angles (θ_c) calculated from Equation (4.3.2); obviously, angles ($\pi - \theta_c$) are also critical; they correspond to the minus sign in the right-hand side of Equation (4.3.2). Clearly, these angles correspond closely to the aspect angles of reflection factor where a cusp occurs (Figures 11-14).

In the case of two closely-spaced incoherent source (Figures 16-20), the directivity pattern for the incident pressure in the far field does not depend any longer on the phase relationship between the source, i.e., $|\overline{p_i}|$ is essentially omnidirectional. For the scattered pressure, there is a simple addition of energies and therefore an "averaging" of the two scattered fields. Because of the spherical spreading of the wave incident on the body, the sound wave due to the outermost source is weaker than that due to the innermost source. As a consequence, the resulting reflection factor is very close to that one due to the single source located at $\xi' = 1.02$, for a given frequency, i.e., $|\overline{R}|$ changes little as ξ'' increases. We could expect that for larger values of ξ'', the energy due to the outermost source would be negligible, and the resulting reflection factor would be identical to the reflection factor due to the innermost source alone.

The frequency response curves of $|\bar{R}|$ (Figures 21-35) also show the similarities and difference cited above.

In the case of a simple source (Figures 21-25), the level of $|\bar{R}|$ decreases over the entire frequency range ($0.1 \leq h \leq 20$) as ξ' increases.

In the case of two sources in phase (Figures 26-30), especially for $\xi'' > 1.10$, the frequency response curves are seen to be less regular. This is due to the complexity of the incident field.

In the case of two incoherent sources (Figures 31-35), all frequency response curves are similar to the frequency response curve of a single source at $\xi' = 1.02$.

A generality for all of the curves is that at low frequencies, i.e. $h < 1.5$, $|\bar{R}|$ increases with a slope of 6 dB/octave in the $\theta = 0°$ direction and 12 dB/octave in the $\theta = 90°$ direction. In the direction $\theta = 180°$, $|\bar{R}|$ increases linearly with a slope slightly less than 6 dB/octave over the frequency range of computation. We note that for $h < 1.5$, all the curves have the same behavior in a given direction ($\theta = 0°$, $\theta = 90°$ or $\theta = 180°$), but also that for $h < 1.5$ and ξ' not greater than 1.20 we have:

$$\lambda > 2d$$

and

$$\ell' < 0.2d \quad .$$

This means that all the points on the surface of the spheroid are almost in phase and the source is relatively close to its pole; therefore, the situation is similar to the case when the source is on the body itself. It is noted that the frequency response curves begin to deviate from a constant-slope character for reduced frequencies greater than approximately 1.5. This is to be expected because $d > \lambda/2$ for this range.

Using Table IV, we have expressed $|\bar{R}|$ as a function of the nondimensional parameter $k\ell'$, in the case of a single source and for: $\theta = 0°, 90°, 180°$, and $h = 16, 20, 35, 40$. Figure 36 shows these results. It appears that $k\ell'$ is not a perfect scaling parameter. However, based on these curves, it does appear that the magnitude of the reflection factor uniformly decreases as the source moves farther away from the pole of the spheroid.

4.3.2 Case of the pressure release boundary. As mentioned before, we present only a few of the results for a pressure release boundary. Curves are presented for two source locations: $\xi' = 1.02$, $\xi' = 1.12$, and their combinations (Figures 37 to 41).

The directivity patterns for a single source are very regular, having a slightly higher level in the forward-scattered direction. This regularity is due to the type of boundary condition. Indeed, the source is always relatively close to the body where we know that for the source on the body itself, an omnidirectional pattern always results with such a boundary condition. In comparing the calculations of the soft spheroid with those of the rigid boundary, for a common set of parameters, the overall level of the reflection factor is seen to be slightly less, indicating that diffraction is not as important.

The frequency response curves show that $|\bar{R}|$ remains almost constant for low frequencies ($h < 1.0$). This is to be expected because of the type of boundary condition. Because of the spherical spreading of the impinging wave as h or ξ' increases, the level of $|\bar{R}|$ decreases and the situation becomes different from the limiting case of the source on the body. This results in a shorter range of h for which the low-frequency behavior is linear.

CHAPTER V

SUMMARY AND CONCLUSIONS

A theoretical investigation of the scattering of sound by a prolate spheroid insonified by a point source or a combination of point sources on the axis has been performed. Two limiting types of boundary conditions on the body have been considered, i.e., Neumann and Dirichlet boundary conditions. Both directivity patterns and frequency response curves have been obtained. This work has been limited to low frequencies ($h \leq 40$) where numerical computations have been performed using tables of the spheroidal wave functions.

For a single source located on the axis of symmetry at various positions relative to the pole of the rigid spheroid, the directivity characteristics were found to be essentially omnidirectional. When two in-phase sources were placed on the axis, the directivity characteristics were found to contain much variation with aspect angle. If the two sources were assumed incoherently related, the patterns approached the shape of the corresponding pattern for the single source closest to the pole, particularly when the second source was relatively far from the first. The reflection factor was found to increase with frequency by 6 dB/octave for the forward and backscattered directions, and by 12 dB/octave for the broadside aspect angle.

As this work has been strictly theoretical, it would be of great interest to obtain experimental results, particularly for the source positions close to the body, and for the combinations of incoherent sources. Emphasis could be placed on frequency responses which have not been commonly investigated.

It also seems appropriate to extend the present results to higher frequencies. As tabulated values of the eigenfunctions are not available for $h > 40$, it would be necessary to use asymptotic expansions as given in Silbiger (1961) and Slepian (1965), for example. Those theoretical results could also be compared to experimental results obtained at higher frequencies.

BIBLIOGRAPHY

1. Abraham, M., Ann. Physik., Vol. 66, No. 435, 1898; Vol. 2, No. 132, 1900; Math. Ann., Vol. 52, No. 81, 1899.

2. Chu, L. J. and J. A. Stratton, J. Math. Phys., Vol. 20, No. 259, 1941.

3. Flammer, C., Spheroidal Wave Functions, Stanford University Press, Stanford, California, 1957.

4. Hanish, S., R. V. Baier, A. L. Van Buren, and B. J. King, "Tables of Radial Spheroidal Wave Functions, Vol. 1, Prolate, m = 0," Naval Research Laboratory Report No. 7088, Naval Research Laboratory, Washington, D.C., June 30, 1970.

5. Lauchle, G. C., "Acoustic Radiation from Vibrating Prolate Spheroids," M.S. Thesis in Aerospace Engineering, The Pennsylvania State University, University Park, Pennsylvania, 1970.

6. Lauchle, G. C., "Acoustic Diffraction by Spheroids," Ph.D. Thesis in Engineering Acoustics, The Pennsylvania State University, University Park, Pennsylvania, 1974; J. Acous. Soc. Am., Vol. 58, No. 3, 1975.

7. MacLaurin, R. C., Trans. Cambr. Phil. Soc., Vol. 17, No. 41, 1898.

8. Meixner, J. and F. W. Shäfke, Mathieusche Funktionen und Sphäroidfuktionen, Springer-Verlag, Berlin, Germany, 1954.

9. Morse, P. M. and H. Feshbach, Methods of Theoretical Physics, McGraw-Hill Book Company, Inc., New York, 1953.

10. Morse, P. M. and K. U. Ingard, Theoretical Acoustics, McGraw-Hill Book Company, Inc., New York, 1968.

11. Niven, C., Phi. Trans. Am., Vol. 171, No. 117, 1880.

12. Page, L., Phys. Rev., Vol. 65, No. 3 and 4, 1944.

13. Poole, E. G. C., Quart. J. Pure Appl. Math., Vol. 49, No. 309, 1923.

14. Silbiger, A., "Asymptotic Formulas for Spheroidal Wave Functions," Cambridge Acoustical Associates, Inc., Report U-123-48, 1961.

15. Skudrzyk, E., The Foundations of Acoustics: Basic Mathematics and Basic Acoustics, Springer-Verlag, New York, Wien, 1971.

16. Slepian, D. J., Math. Phys., Vol. 44, 1965.

17. Van Buren, A. L., B. J. King, R. V. Baier and S. Hanish, "Tables of Angular Spheroidal Wave Functions, Vol. 1, Prolate, m = 0," Naval Research Laboratory, Washington, D.C., June 30, 1975.

Table I

ℓ'/d and ℓ'/R_o for Different Source Locations

ξ_o	ξ'	ℓ'/d	ℓ'/R_o
1.01	1.02	0.005	0.035
-	1.04	0.015	0.106
-	1.06	0.025	0.176
-	1.08	0.035	0.247
-	1.10	0.045	0.317
-	1.12	0.055	0.388
-	1.14	0.065	0.458
-	1.16	0.075	0.529
-	1.18	0.085	0.600
-	1.20	0.095	0.670

Table II

a/d and a/R_o for Different Sets of Source Locations

ξ'	ξ''	a/d	a/R_o
1.02	1.04	0.010	0.071
-	1.06	0.020	0.141
-	1.08	0.030	0.212
-	1.10	0.040	0.282
-	1.12	0.050	0.353
-	1.14	0.060	0.423
-	1.16	0.070	0.494
-	1.18	0.080	0.564
-	1.20	0.090	0.634

Table III

L_o/λ, ℓ'/λ, a/λ, and θ_c for Different Source Locations at h = 20, 35, 40

ξ' or ξ''	h = 20				h = 34				h = 40			
	L_o/λ	ℓ'/λ or ℓ''/λ	a/λ	θ_c	L_o/λ	ℓ'/λ or ℓ''/λ	a/λ	θ_c	L_o/λ	ℓ'/λ ℓ''/λ	a/λ	θ_c
1.02	6.43	0.0318	-	-	11.25	0.0557	-	-	12.86	0.0637	-	-
1.04	-	0.0955	0.0637	-	-	0.167	0.111	-	-	0.191	0.127	-
1.06	-	0.159	0.127	-	-	0.279	0.223	-	-	0.318	0.255	-
1.08	-	0.223	0.191	-	-	0.390	0.334	-	-	0.446	0.382	-
1.10	-	0.286	0.255	-	-	0.501	0.446	-	-	0.573	0.509	10.8°
1.12	-	0.350	0.318	-	-	0.613	0.557	26.0°	-	0.700	0.637	38.3°
1.14	-	0.414	0.382	-	-	0.724	0.668	41.5°	-	0.828	0.764	49.1°
1.16	-	0.477	0.446	-	-	0.836	0.780	50.0°	-	0.955	0.891	55.9°
1.18	-	0.541	0.509	10.8°	-	0.947	0.891	55.9°	-	1.082	1.019	60.6°
1.20	-	0.605	0.573	29.0°	-	1.058	1.003	60.1°	-	1.210	1.146	64.1°

Table IV

$k\ell'$ for Different Source Locations for h = 16, 20, 35, 40

	ξ'	1.02	1.04	1.06	1.08	1.10	1.12	1.14	1.16	1.18	1.20
$k\ell'$ for	h = 16	0.16	0.48	0.80	1.12	1.44	1.76	2.08	2.40	2.72	3.04
	h = 20	0.20	0.60	1.00	1.40	1.80	2.20	2.60	3.00	3.40	3.80
	h = 35	0.35	1.05	1.75	2.45	3.15	3.85	4.55	5.25	5.95	6.65
	h = 40	0.40	1.20	2.00	2.80	3.60	4.40	5.20	6.00	6.80	7.60

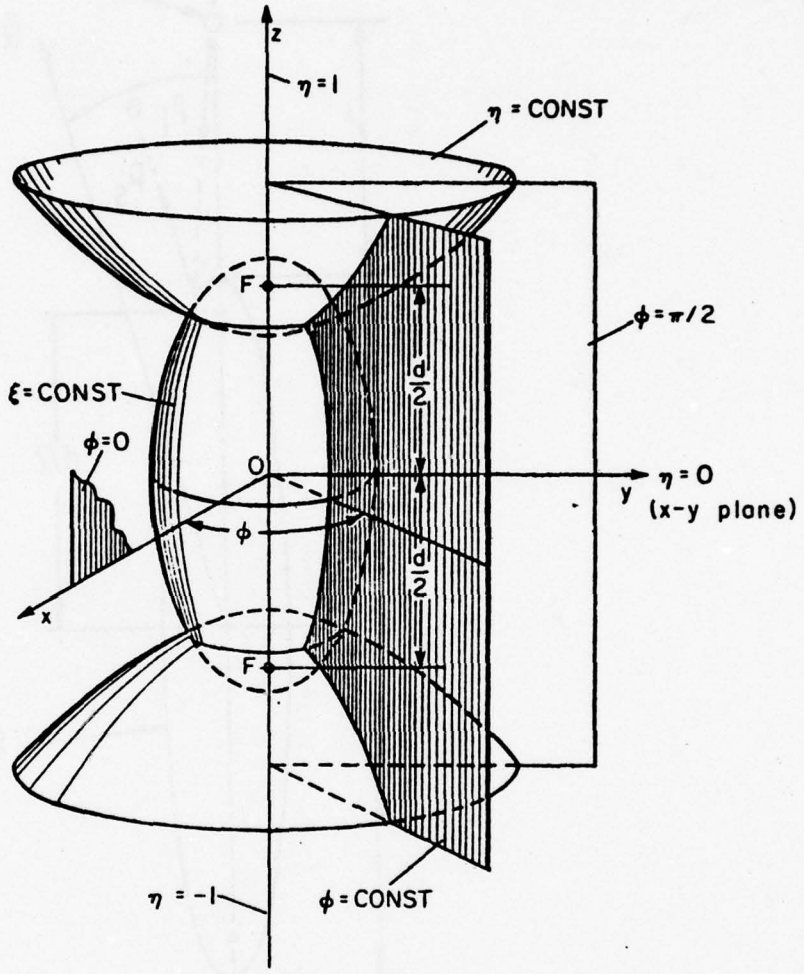

Figure 1. The Prolate Spheroidal Coordinate System

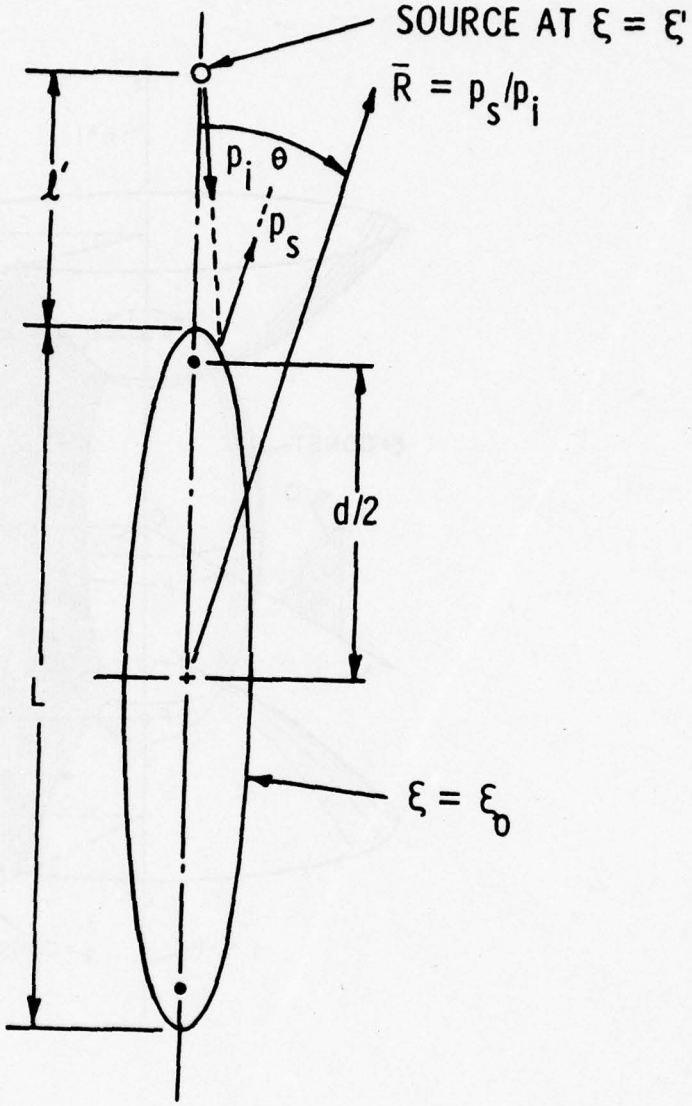

Figure 2. A Schematic of the Problem to be Investigated

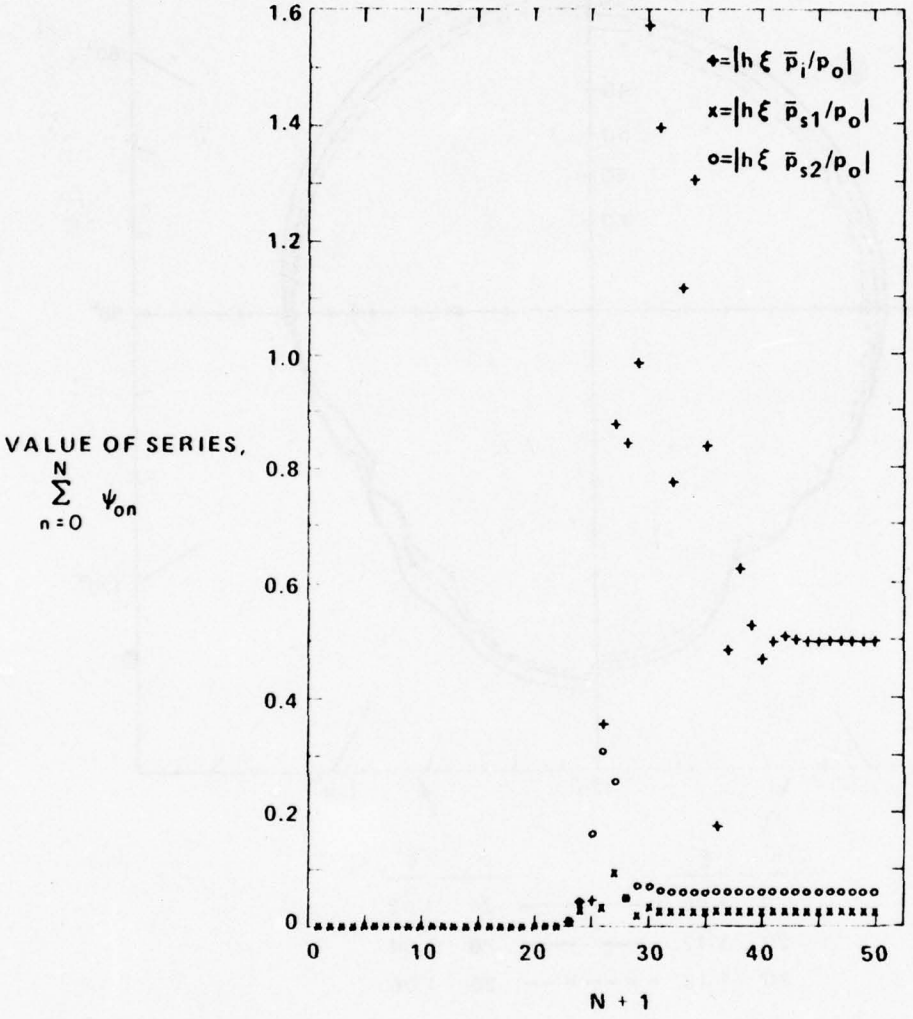

Figure 3. Convergence of the Incident and Scattered Pressure Expansions; h = 40; $\xi' = 1.12$

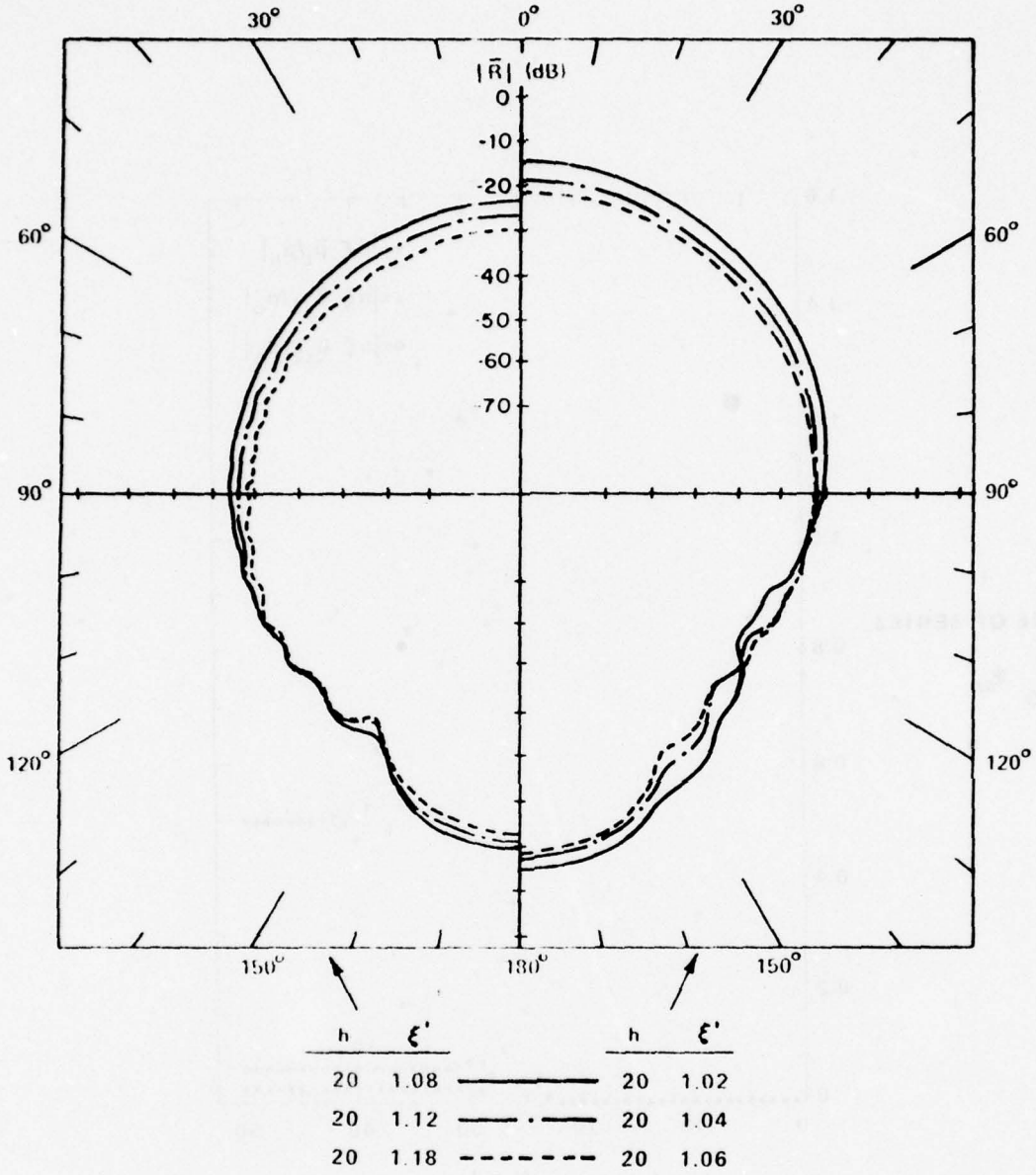

Figure 4. Directivity Patterns, Rigid Case, One Source; h = 20; ξ' = 1.02, 1.04, 1.06, 1.08, 1.12, and 1.18

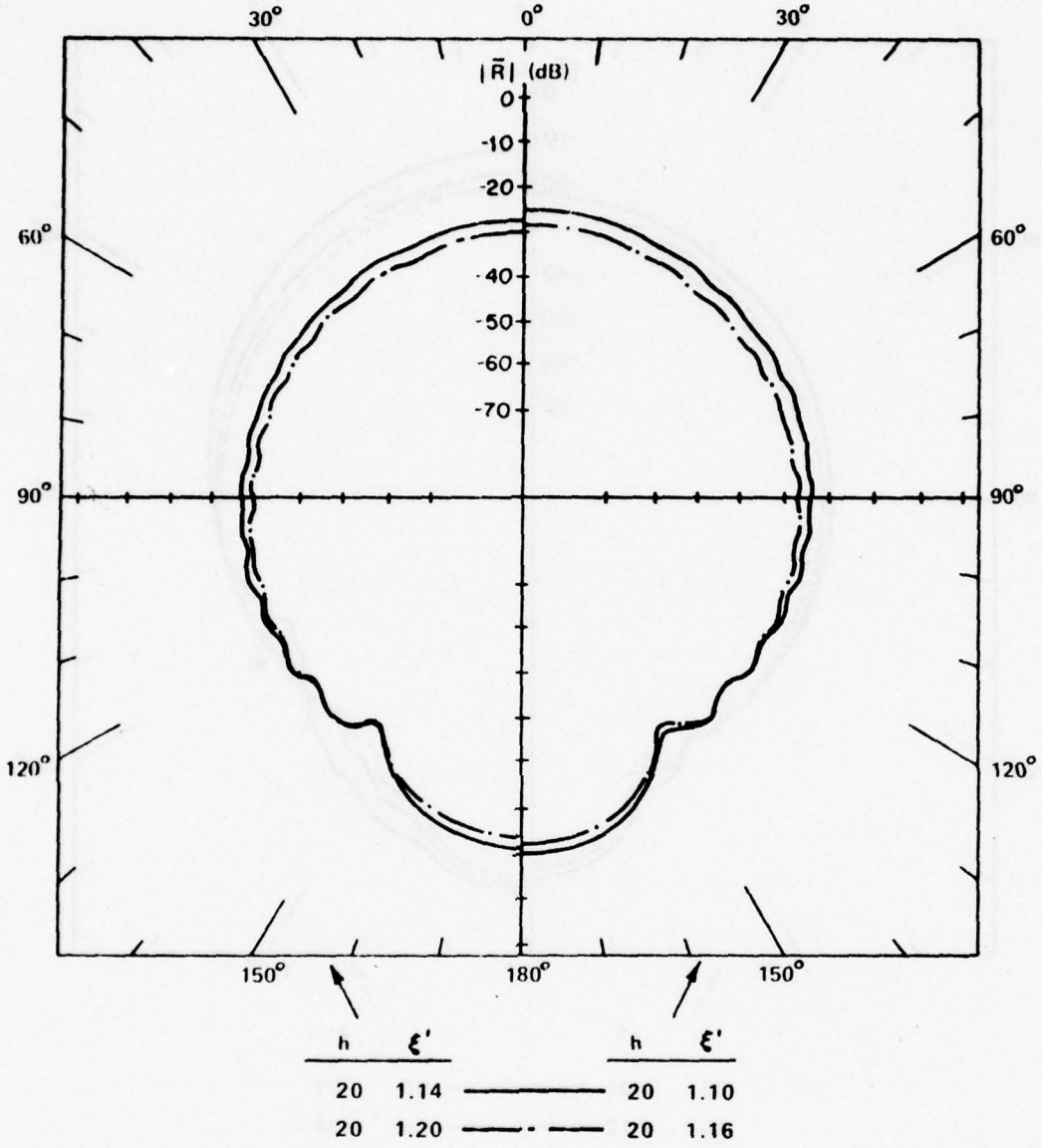

Figure 5. Directivity Patterns, Rigid Case, One Source; h = 20; ε' = 1.10, 1.14, 1.16, and 1.20

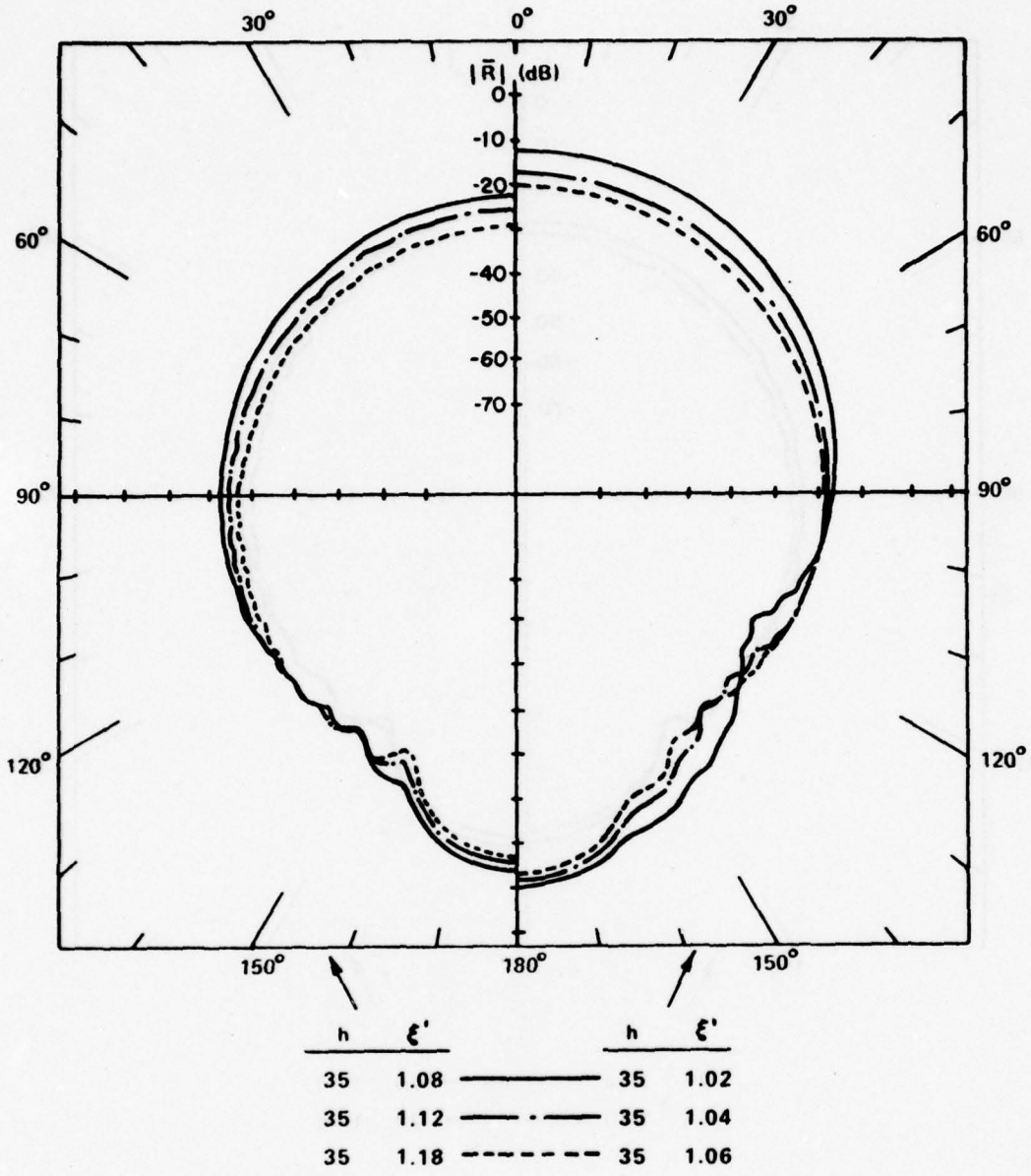

Figure 6. Directivity Patterns, Rigid Case, One Source; h = 35; ξ' = 1.02, 1.04, 1.06, 1.08, 1.12, and 1.18

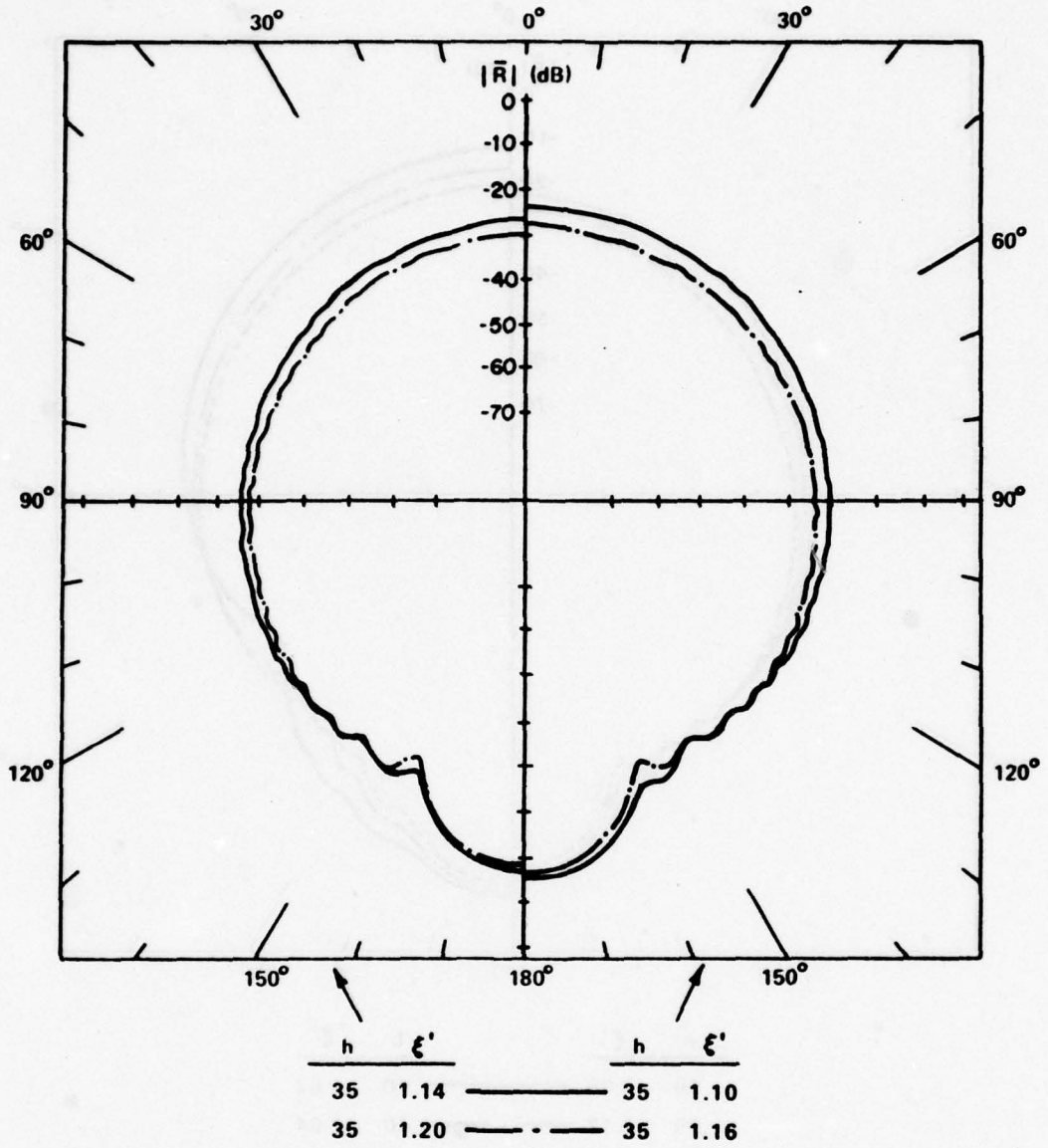

Figure 7. Directivity Patterns, Rigid Case, One Source; h = 35; ξ' = 1.10, 1.14, 1.16, and 1.20

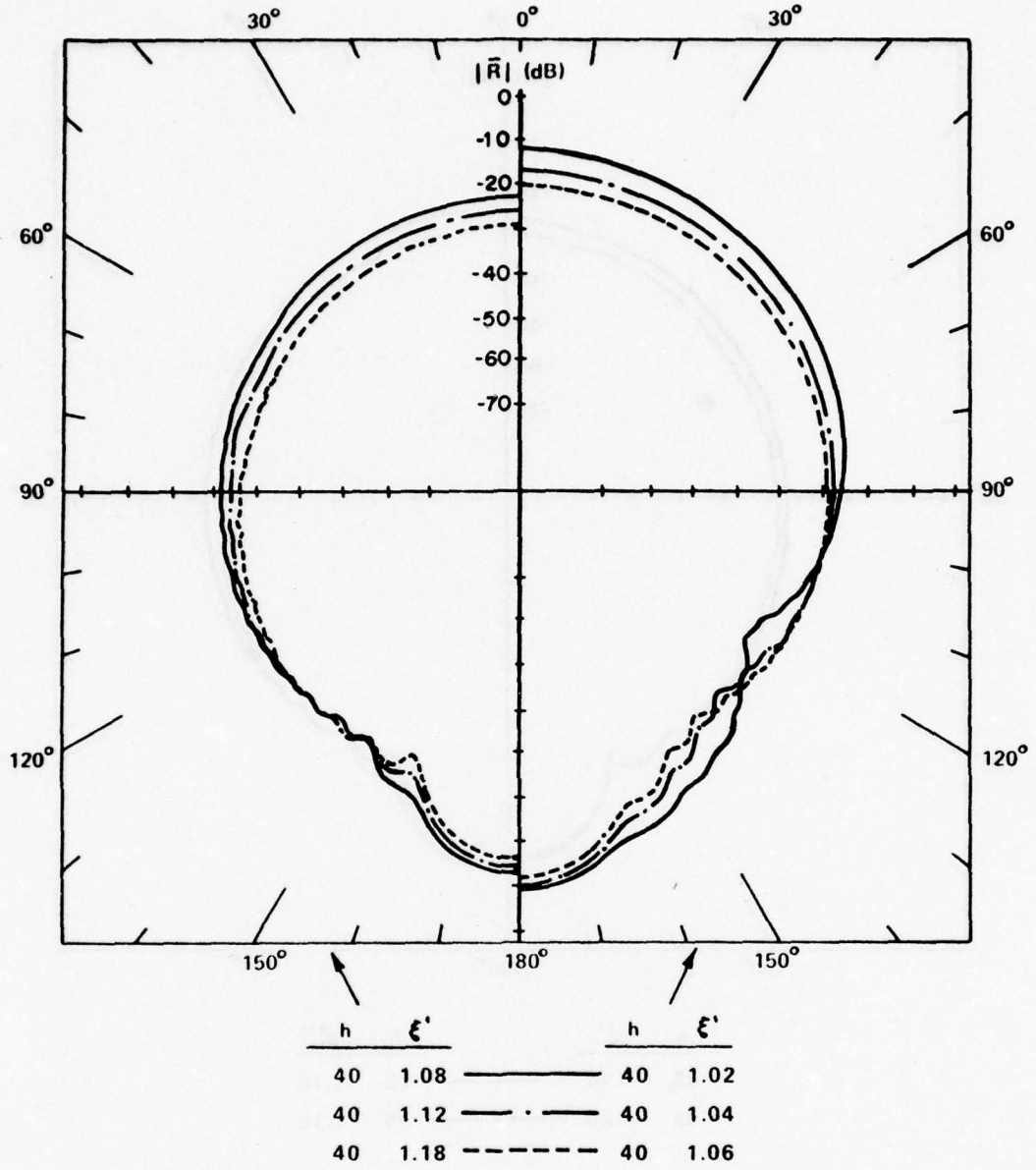

Figure 8. Directivity Patterns, Rigid Case, One Source; h = 40; ξ' = 1.02, 1.04, 1.06, 1.08, 1.12, and 1.18

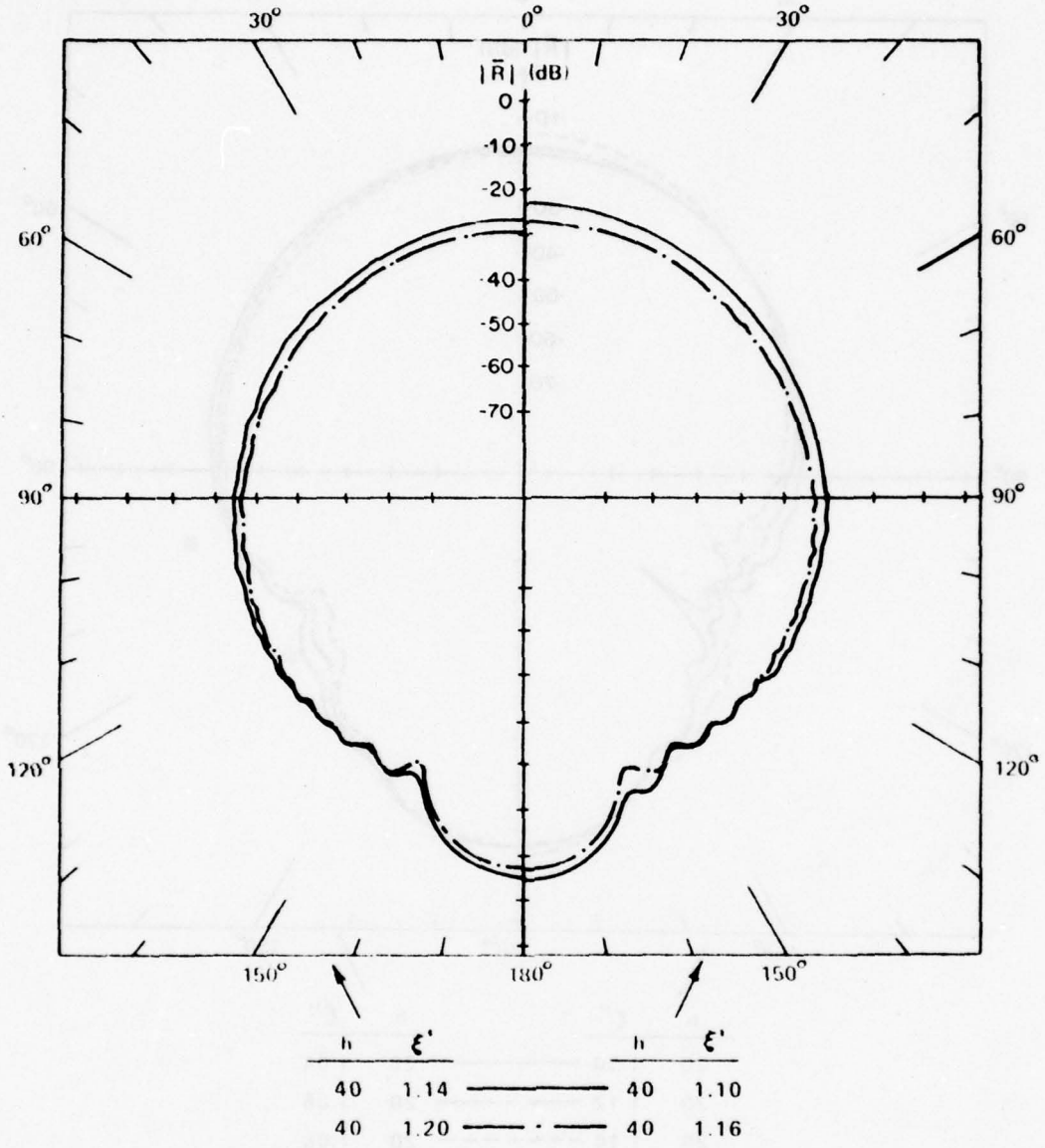

Figure 9. Directivity Patterns, Rigid Case, One Source; h = 40; ε' = 1.10, 1.14, 1.16, and 1.20

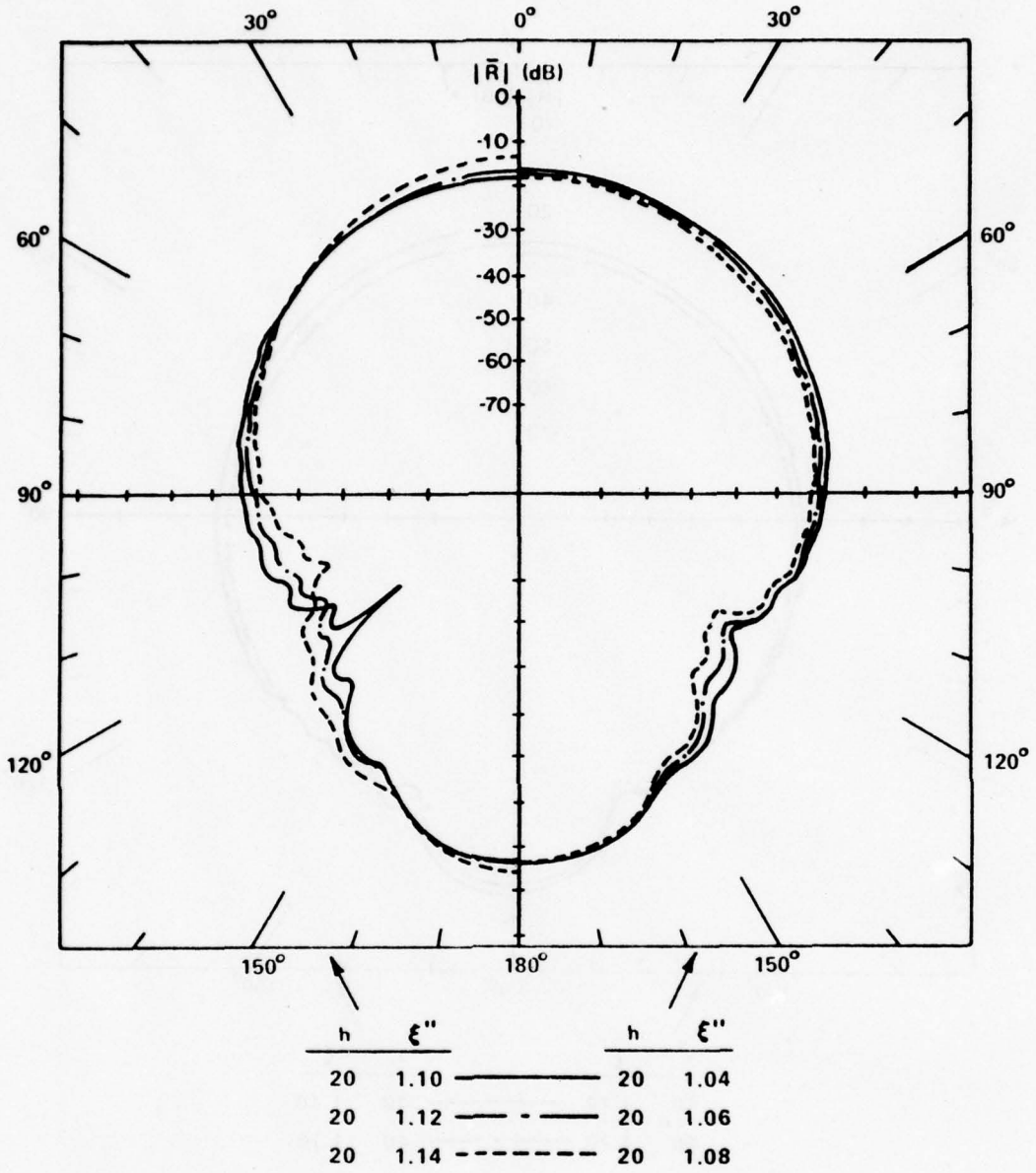

Figure 10. Directivity Patterns, Rigid Case, Two Sources in Phase; $\xi' = 1.02$; $h = 20$; $\xi'' = 1.04, 1.06, 1.08, 1.10, 1.12$, and 1.14

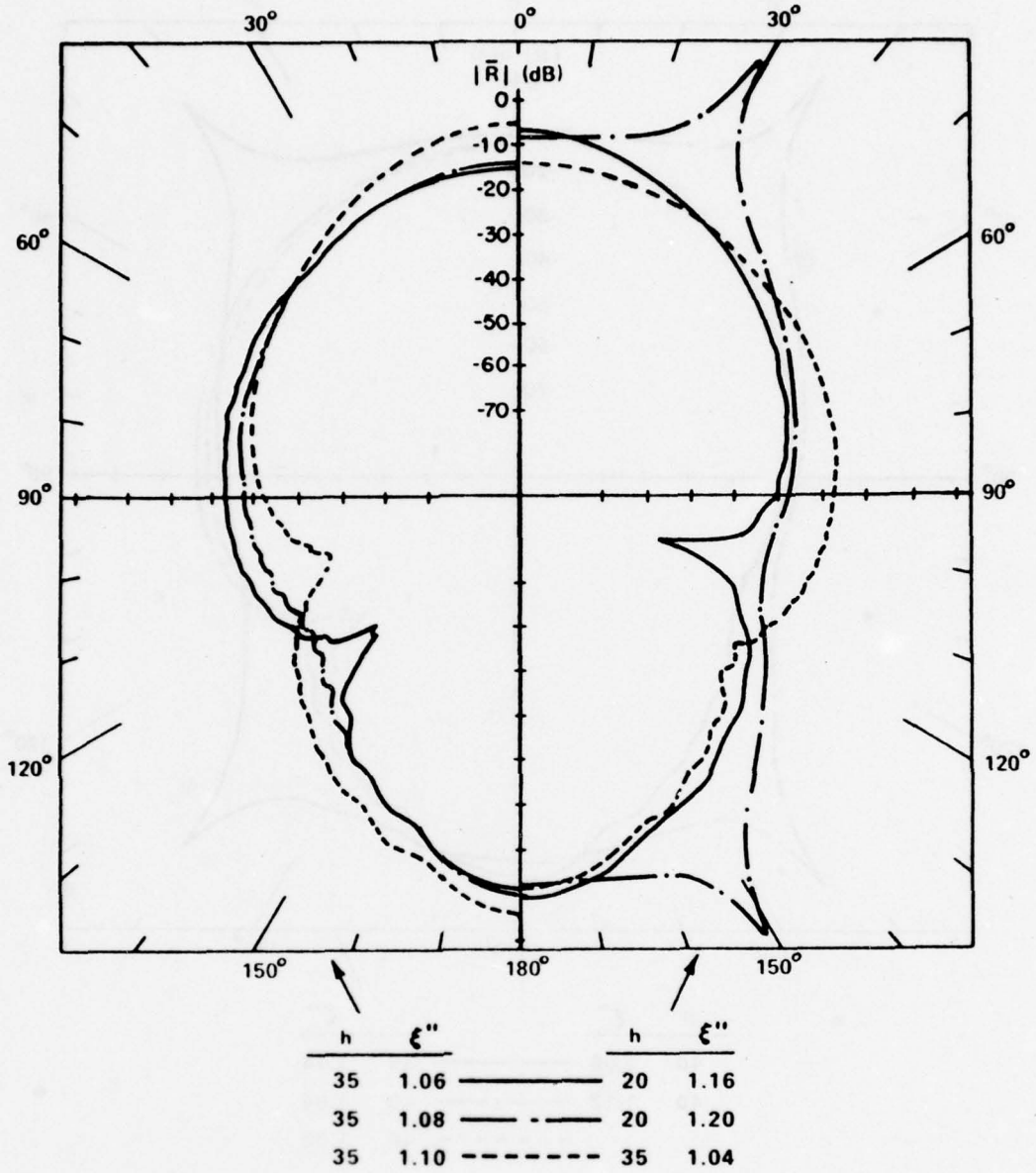

Figure 11. Directivity Patterns, Rigid Case, Two Sources in Phase; ξ" 1.02; h = 20; ξ" = 1.16 and 1.20; h = 35; ξ" = 1.04, 1.06, 1.08, and 1.10

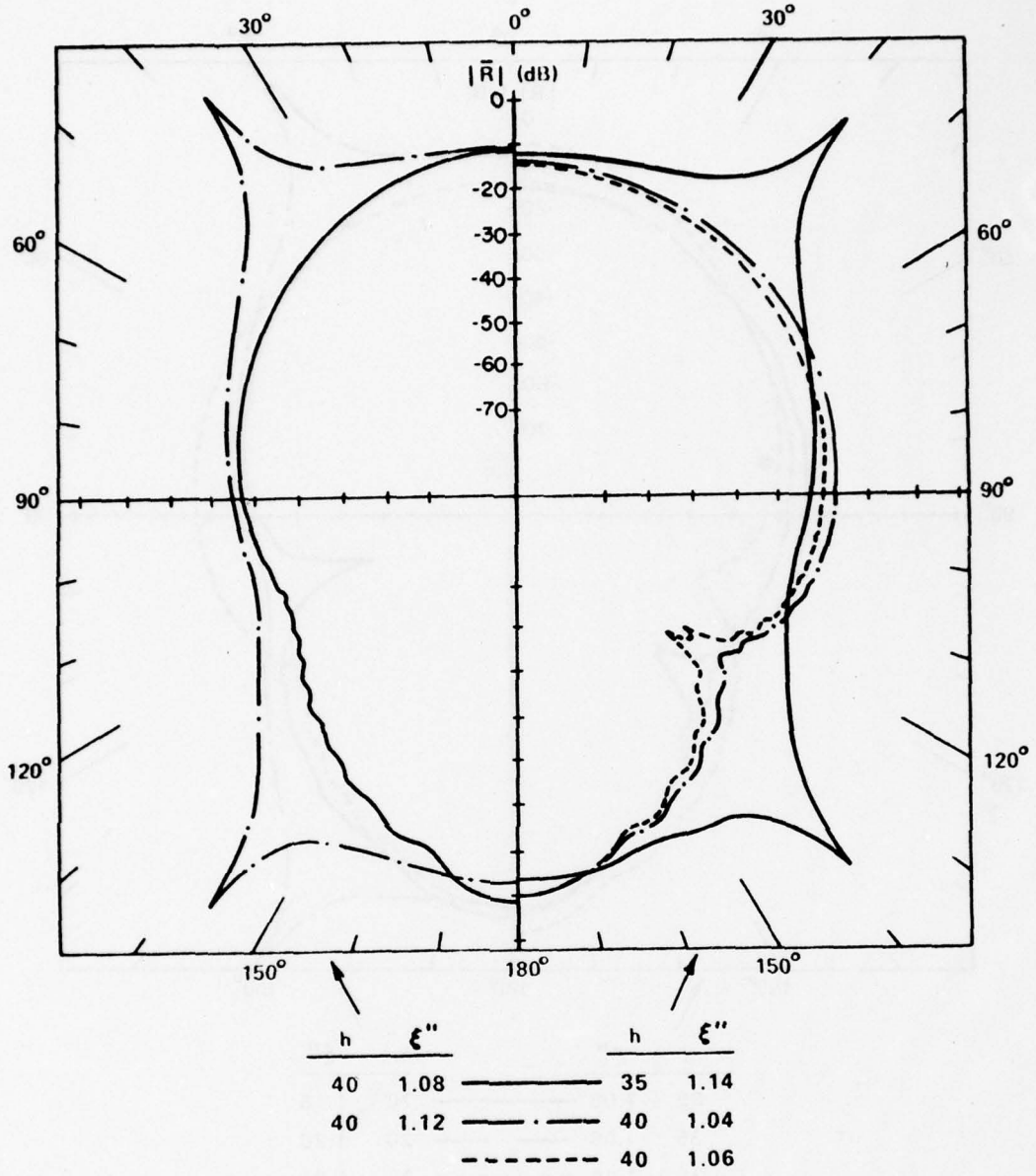

Figure 12. Directivity Patterns, Rigid Case, Two Sources in Phase; $\xi' = 1.02$; h = 35; $\xi'' = 1.14$; h = 40; $\xi'' = 1.04$, 1.06, 1.08 and 1.12

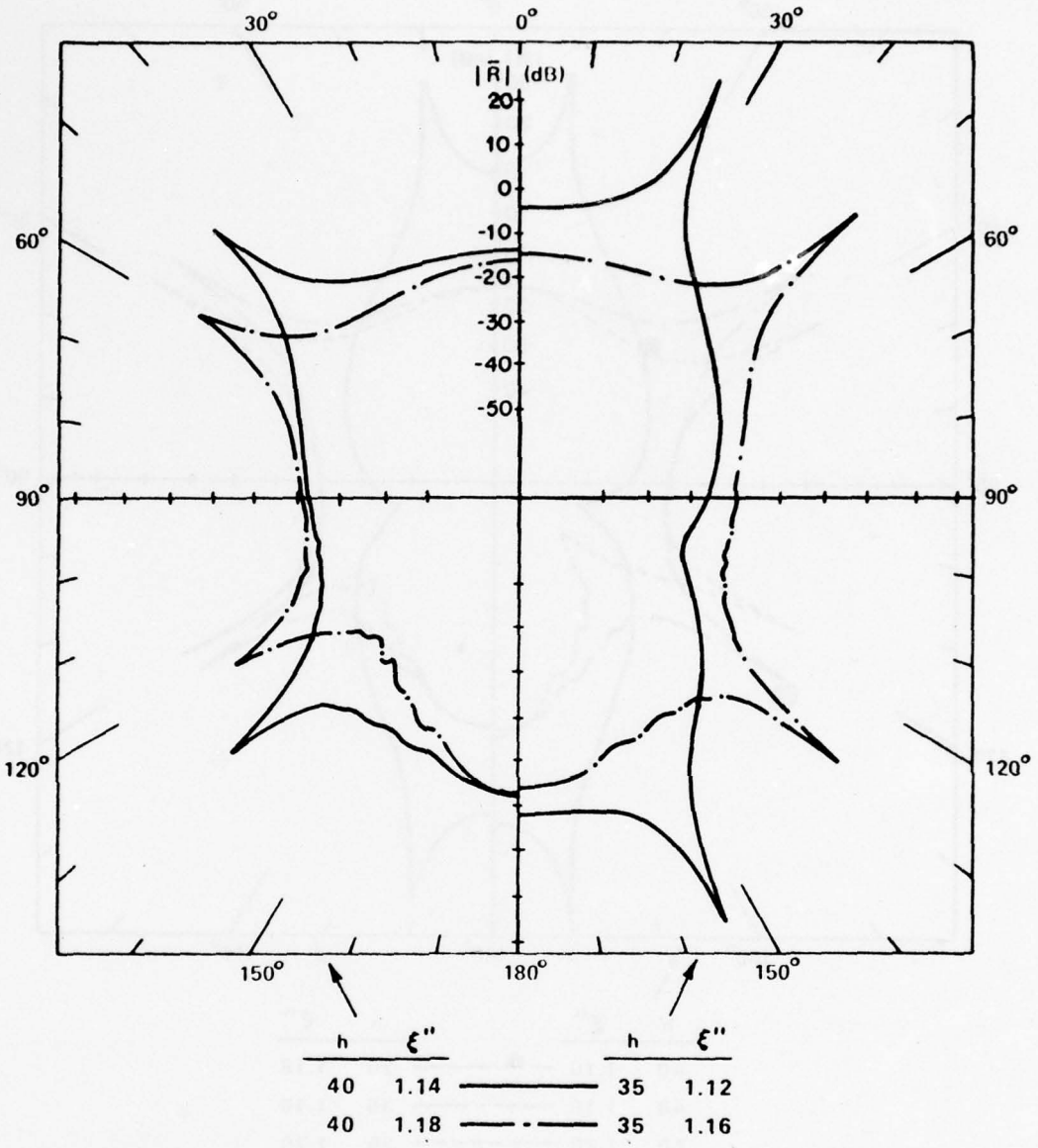

Figure 13. Directivity Patterns, Rigid Case, Two Sources in Phase; $\xi' = 1.02$; h = 35, $\xi'' = 1.12$ and 1.16; h = 40; $\xi'' = 1.14$ and 1.18

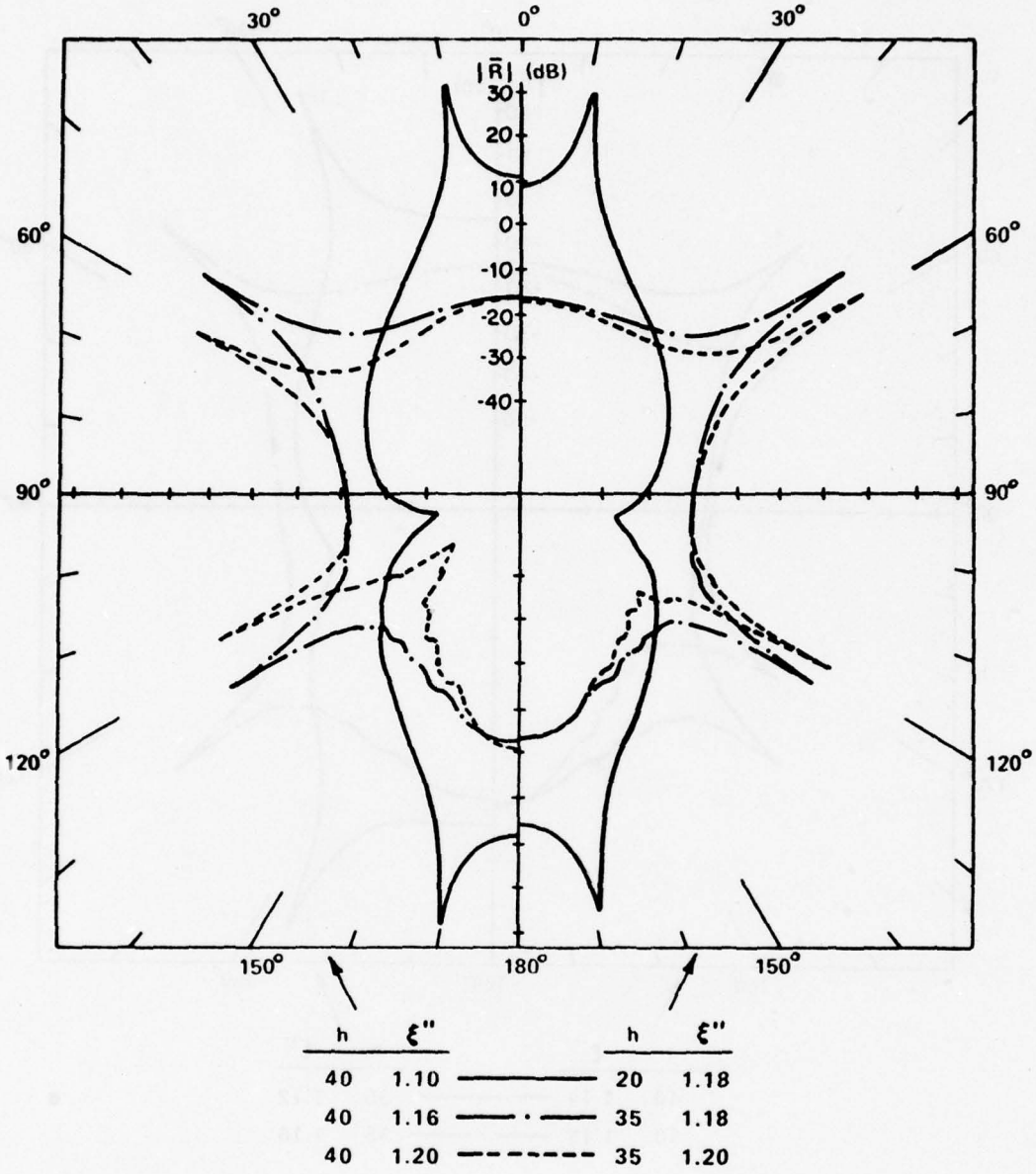

Figure 14. Directivity Patterns, Rigid Case, Two Sources in Phase; $\xi'' = 1.02$; h = 20; $\xi'' = 1.18$; h = 35; $\xi'' = 1.18$ and 1.20; h = 40; $\xi'' = 1.10$, 1.16, and 1.20

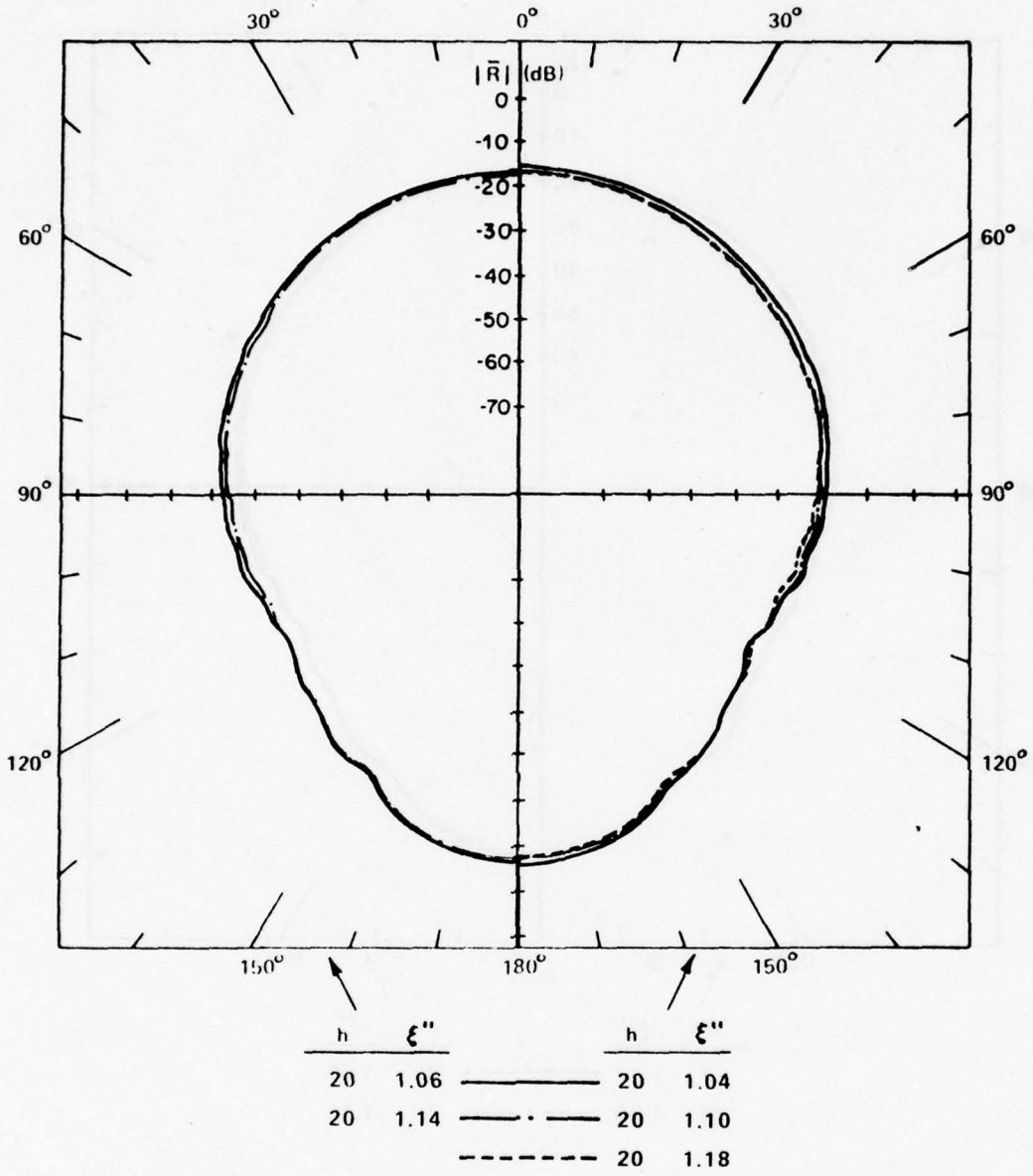

Figure 15. Directivity Patterns, Rigid Case, Two Incoherent Sources; $\xi' = 1.02$; $h = 20$; $\xi'' = 1.04, 1.06, 1.10, 1.14$, and 1.18

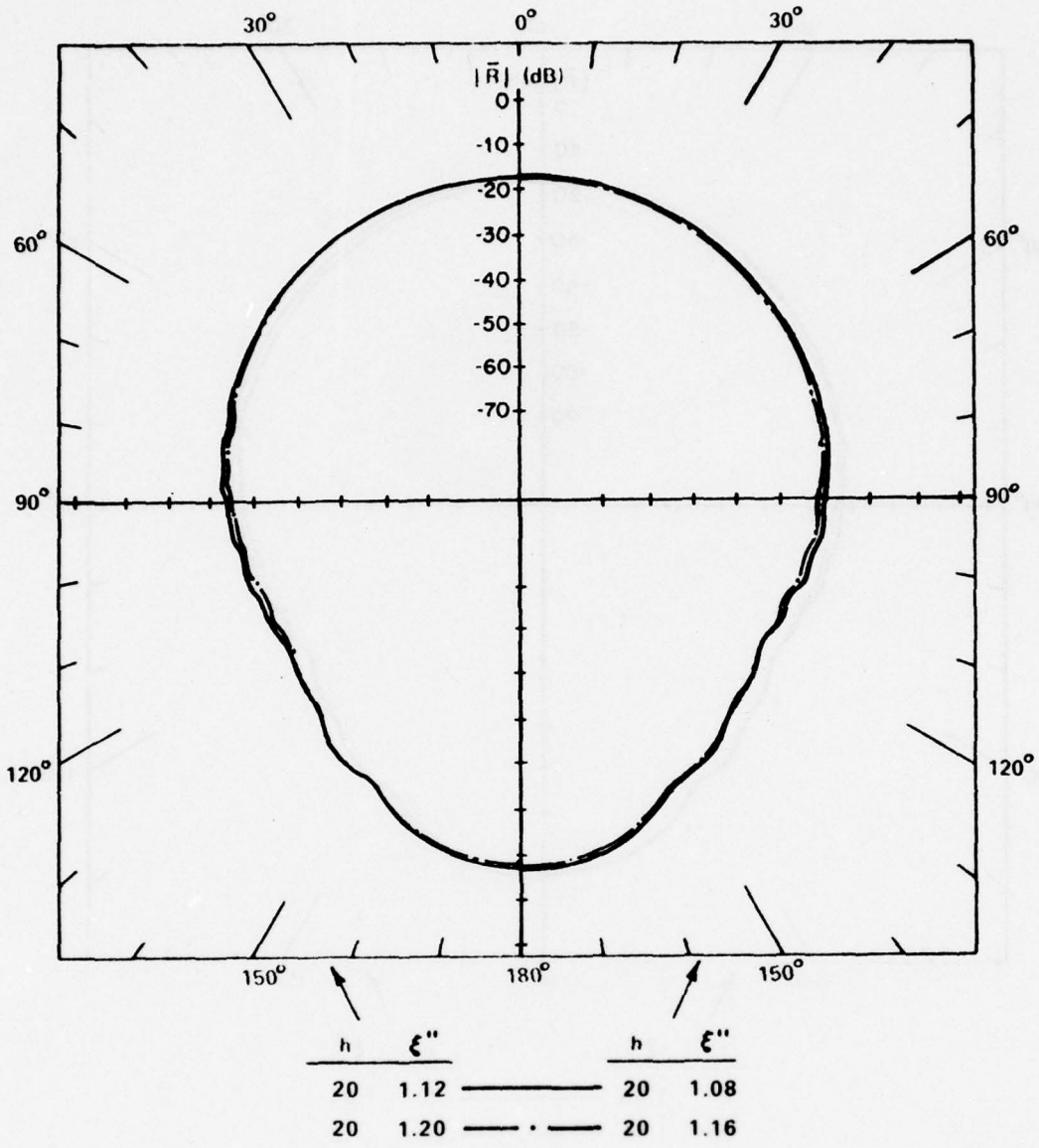

Figure 16. Directivity Patterns, Rigid Case, Two Incoherent Sources; $\xi' = 1.02$; $h = 20$; $\xi'' = 1.08$, 1.12, 1.16, and 1.20

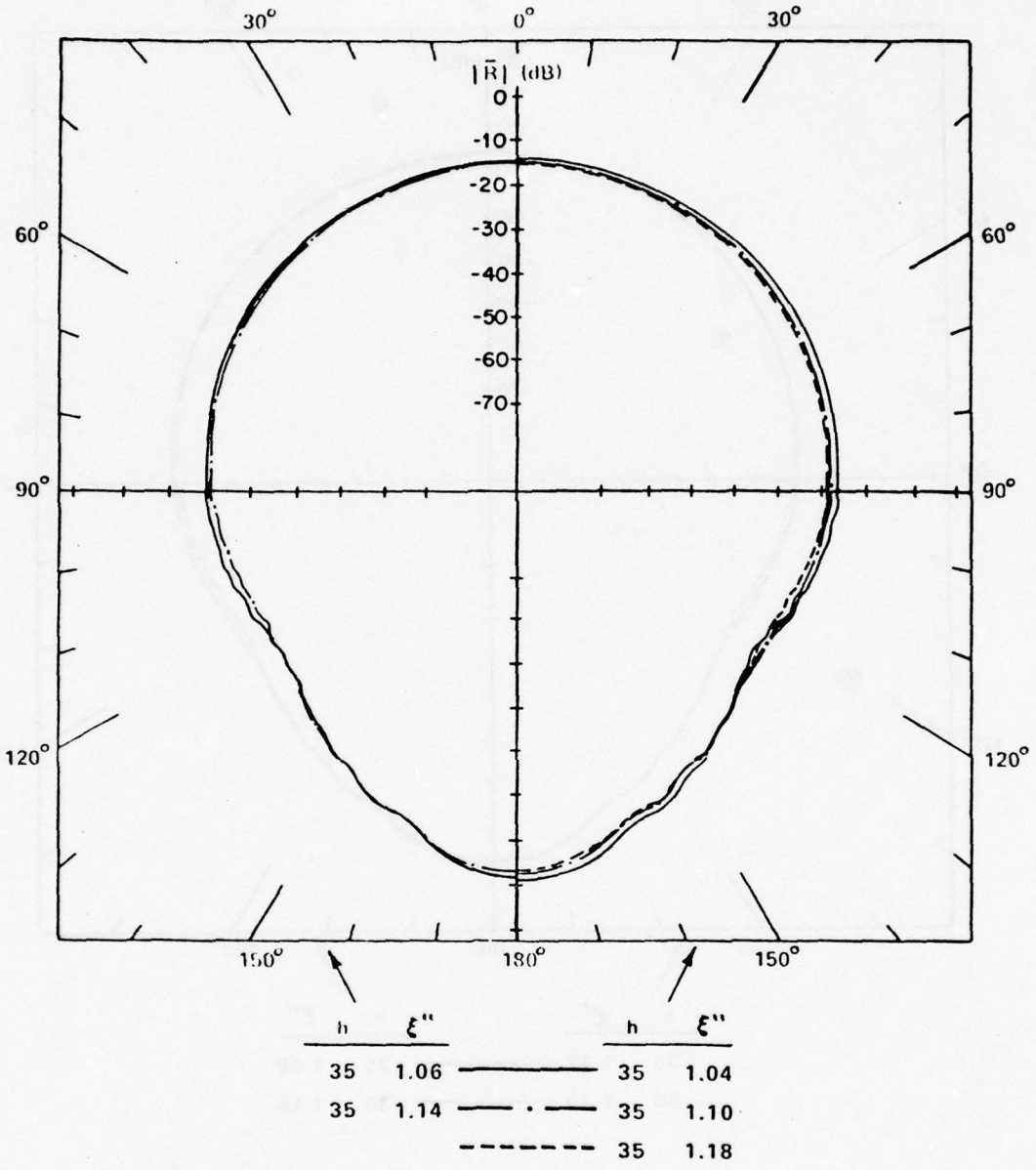

Figure 17. Directivity Patterns, Rigid Case, Two Incoherent Sources; $\xi' = 1.02$; $h = 35$; $\xi'' = 1.04$, 1.06, 1.10, 1.14, and 1.18

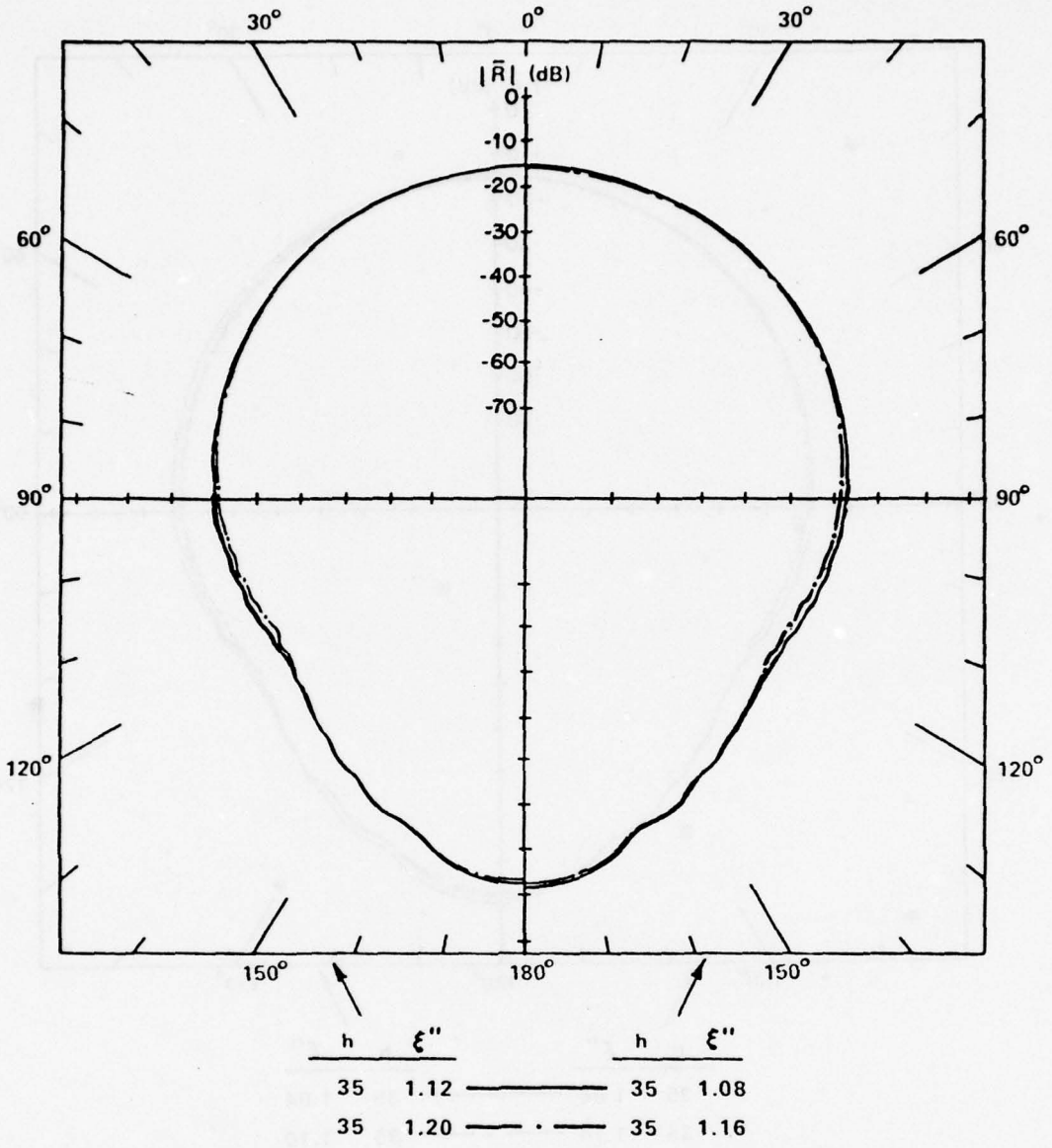

Figure 18. Directivity Patterns, Rigid Case, Two Incoherent Sources; $\xi' = 1.02$; $h = 35$; $\xi'' = 1.08$, 1.12, 1.16, and 1.20

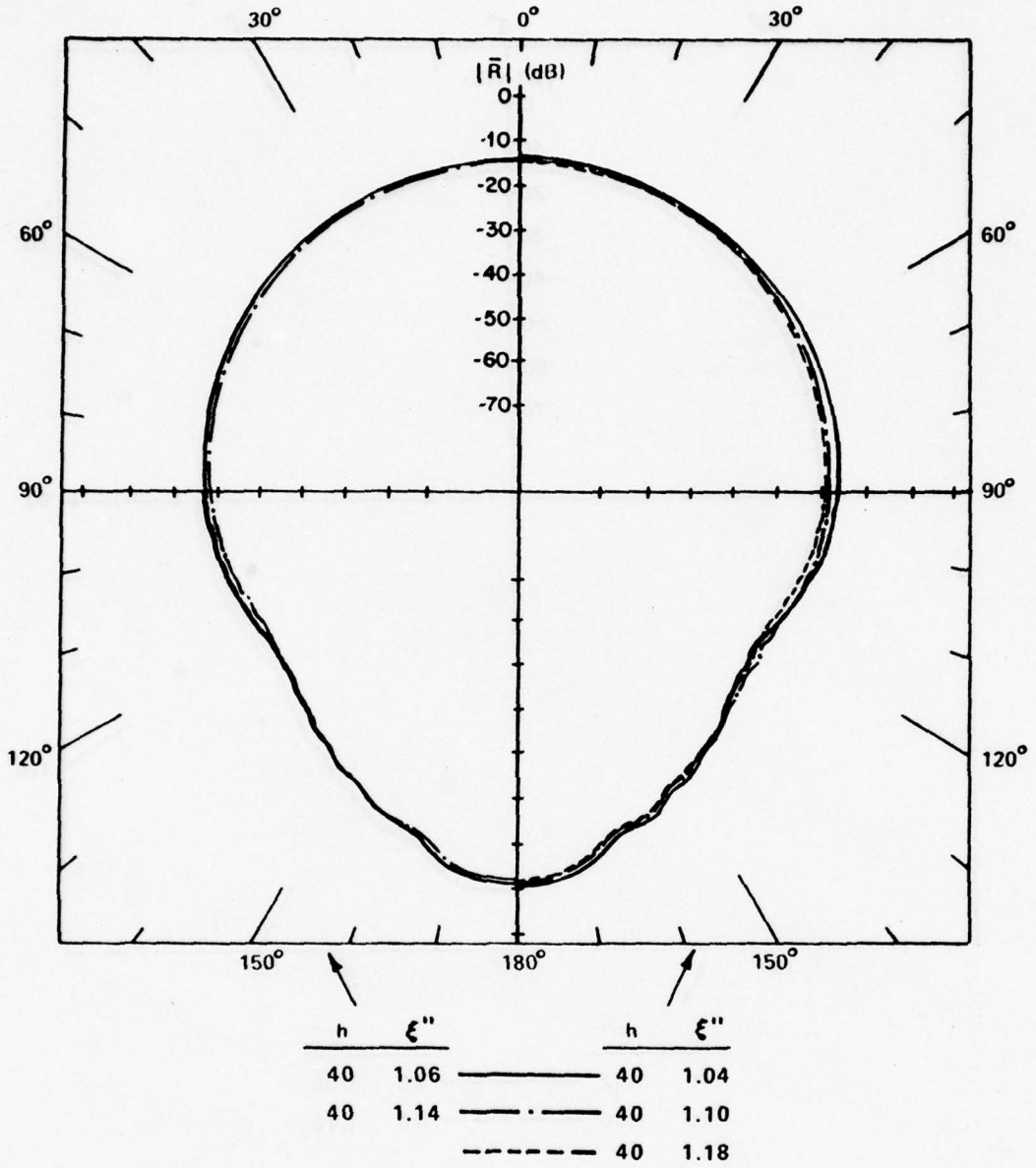

Figure 19. Directivity Patterns, Rigid Case, Two Incoherent Sources; $\xi' = 1.02$; $h = 40$; $\xi'' = 1.04$, 1.06, 1.10, 1.14, and 1.18

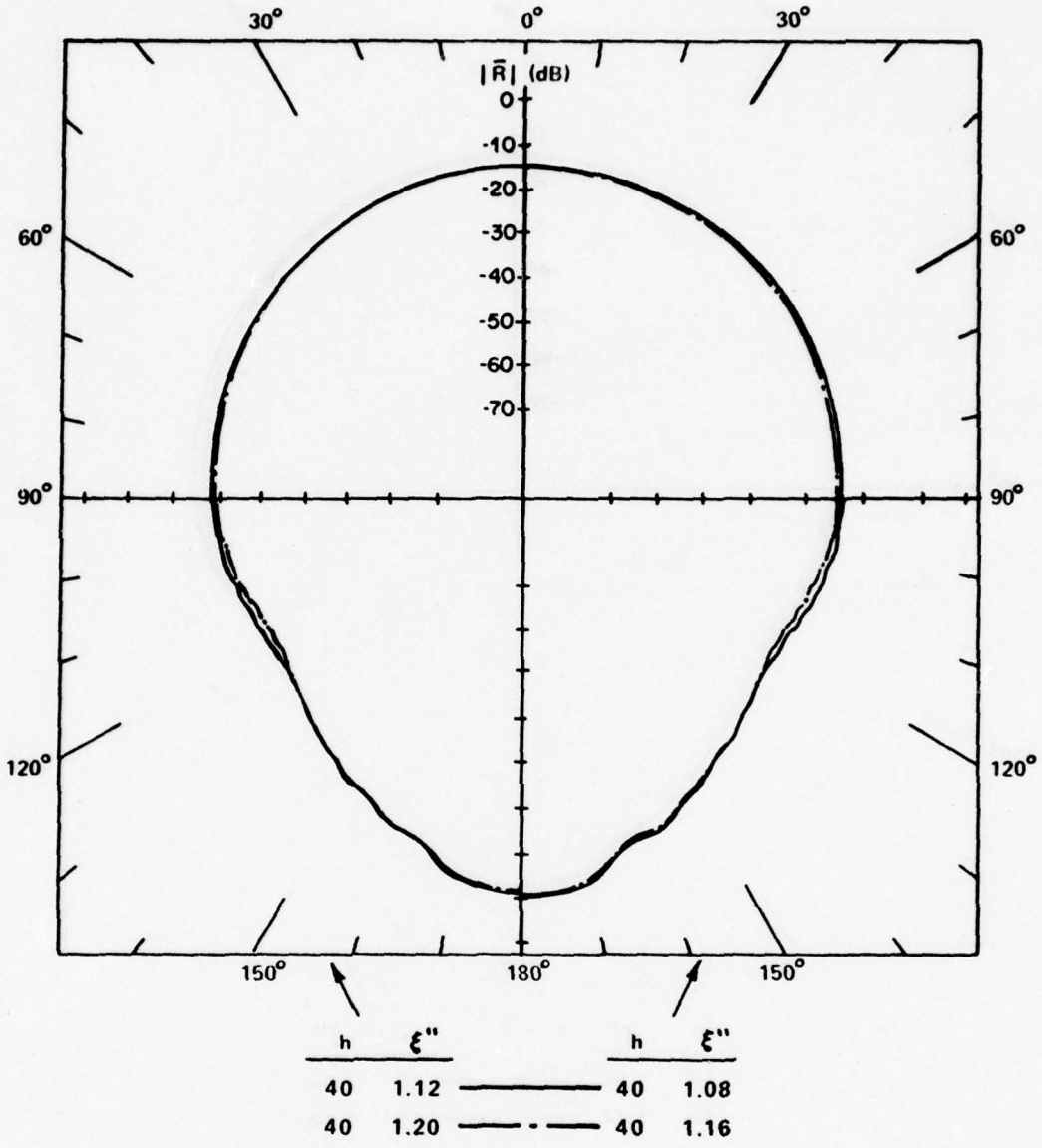

Figure 20. Directivity Patterns, Rigid Case, Two Incoherent Sources; ξ' = 1.02; h = 40; ξ'' = 1.08. 1.12, 1.16, and 1.20

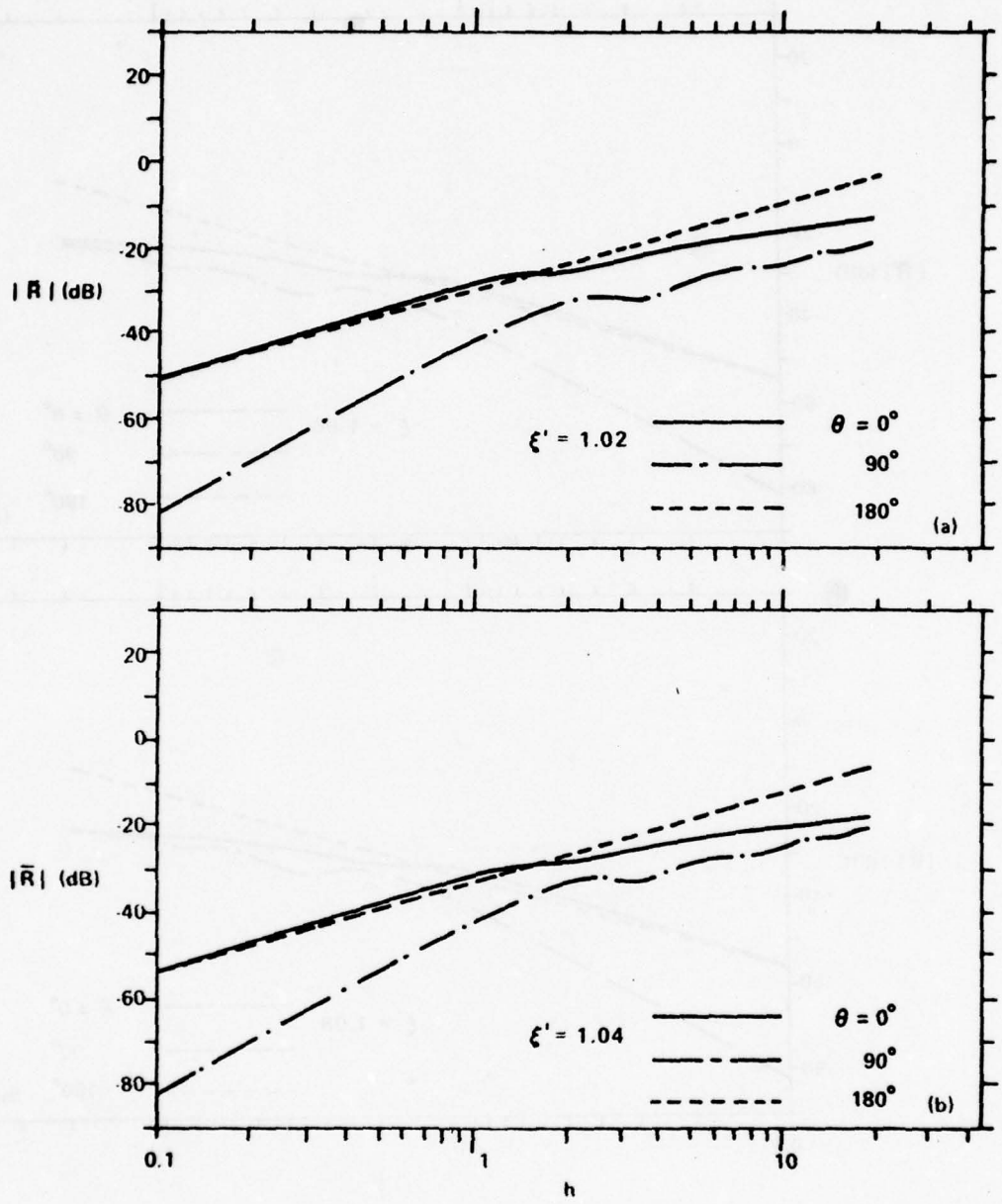

Figure 21. Frequency Response Curves, Rigid Case, One Source; (a) $\xi' = 1.02$, (b) $\xi' = 1.04$

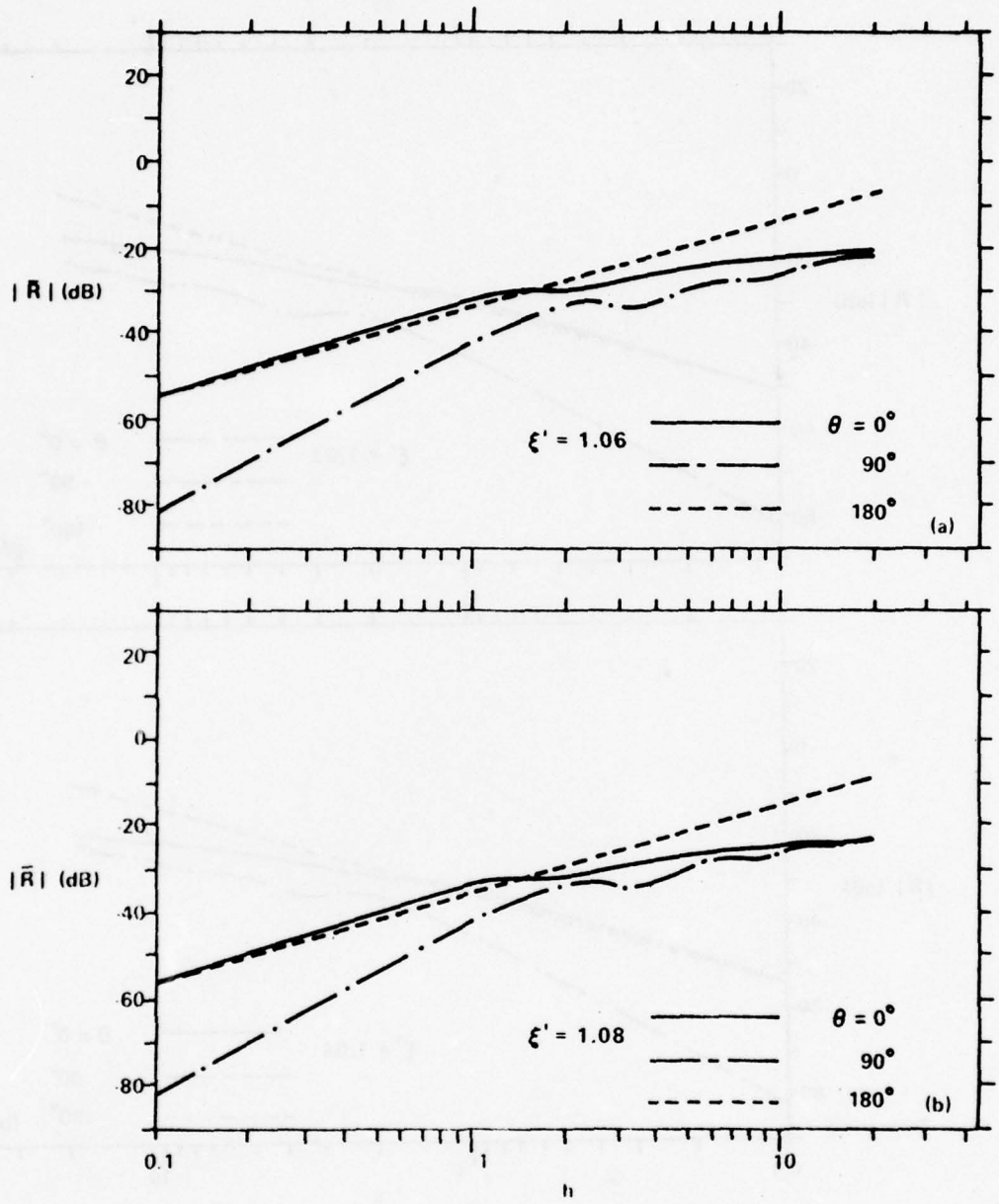

Figure 22. Frequency Response Curves, Rigid Case, One Source; (a) $\xi' = 1.06$; (b) $\xi' = 1.08$

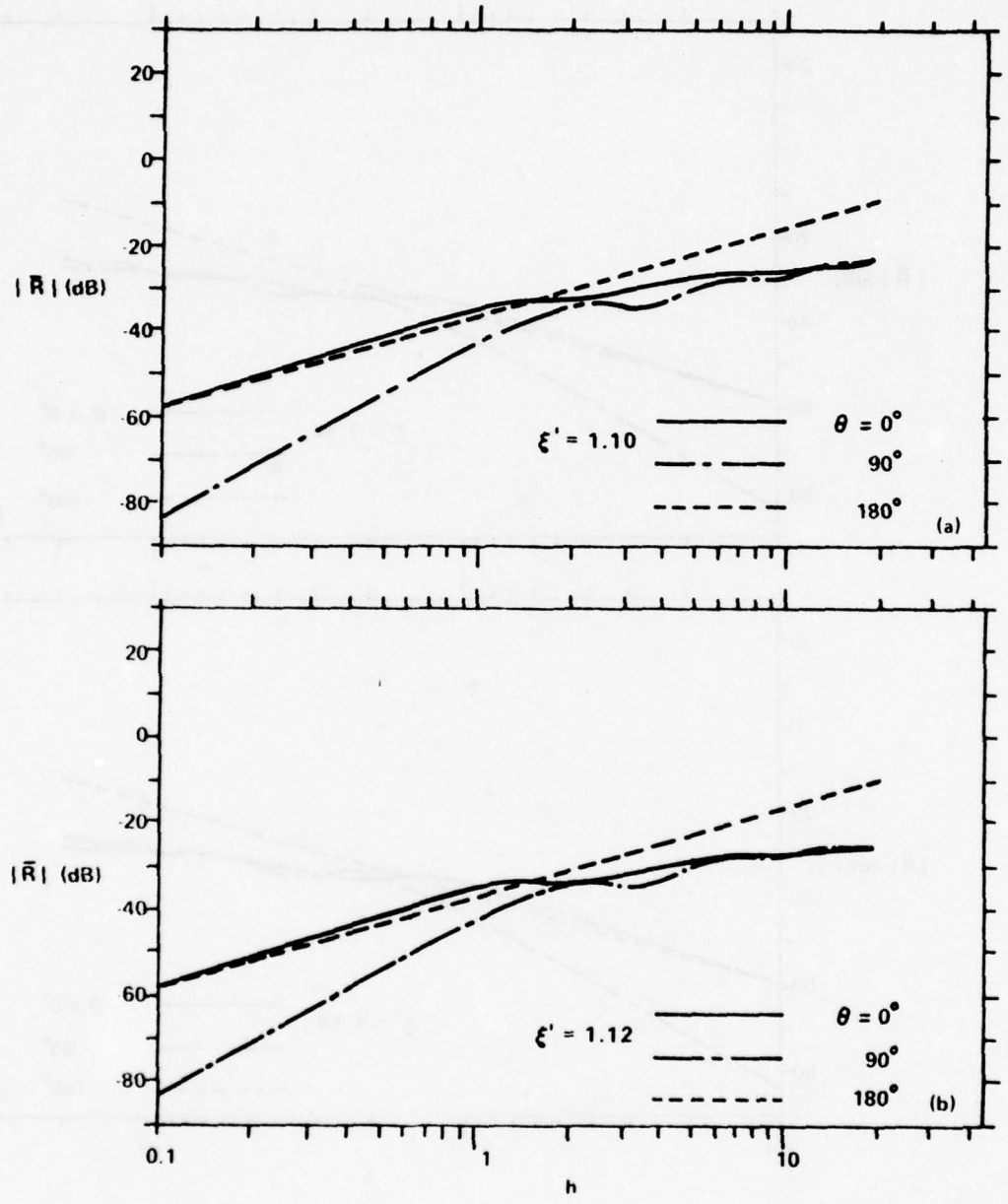

Figure 23. Frequency Response Curves, Rigid Case, One Source; (a) $\xi' = 1.10$; (b) $\xi' = 1.12$

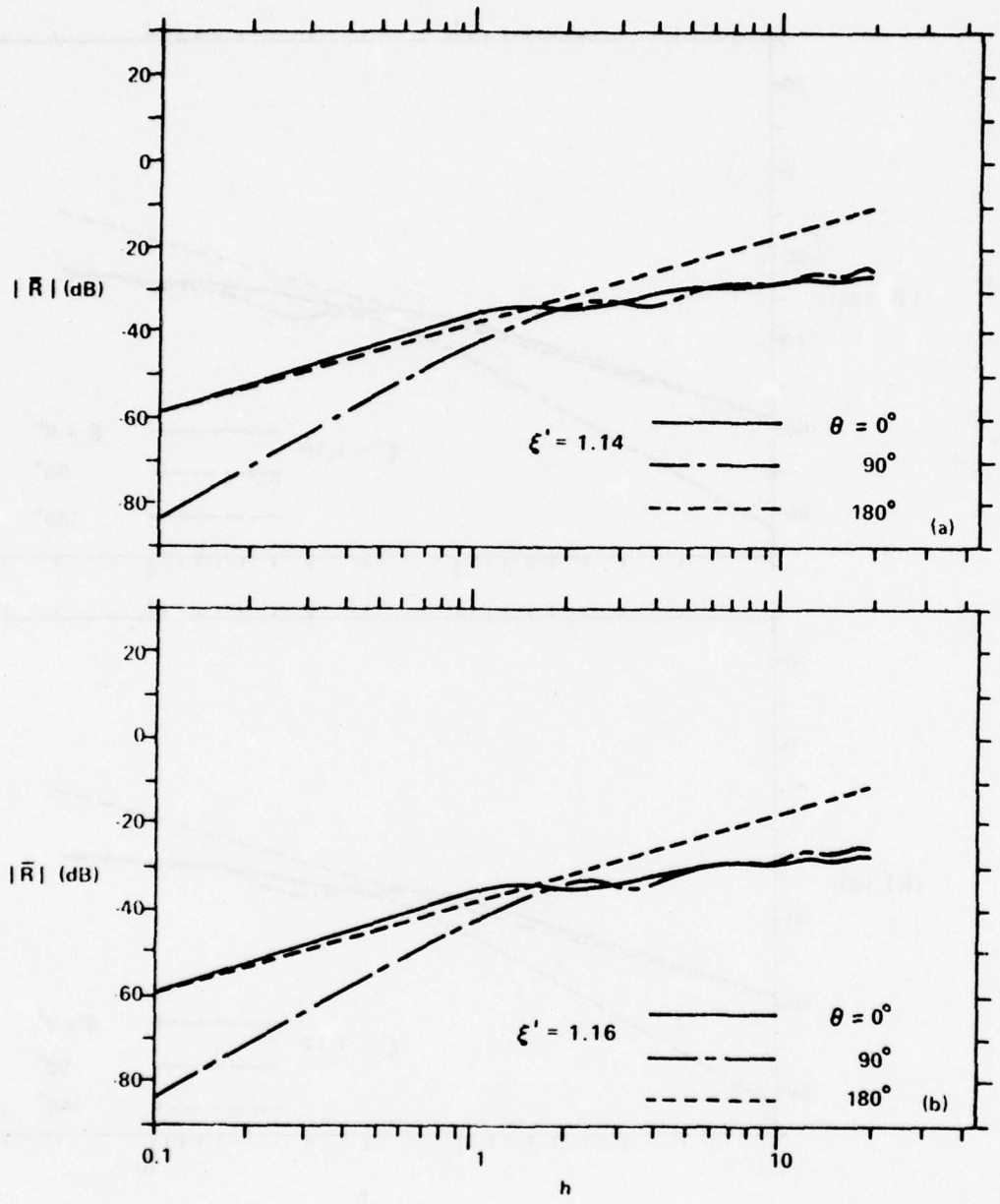

Figure 24. Frequency Response Curves, Rigid Case, One Source; (a) $\xi' = 1.14$; (b) $\xi' = 1.16$

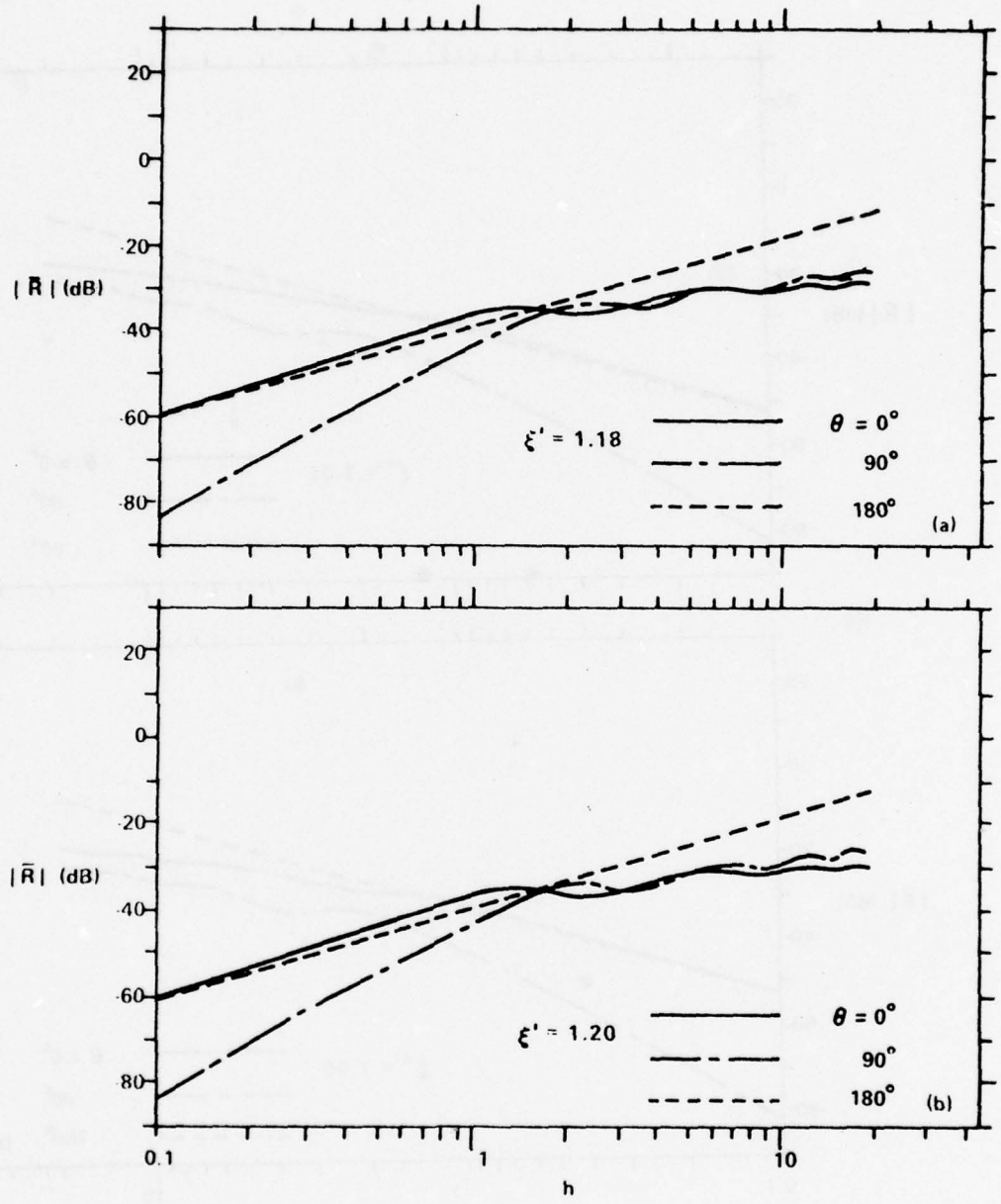

Figure 25. Frequency Response Curves, Rigid Case, One Source; (a) $\xi' = 1.18$; (b) $\xi' = 1.20$

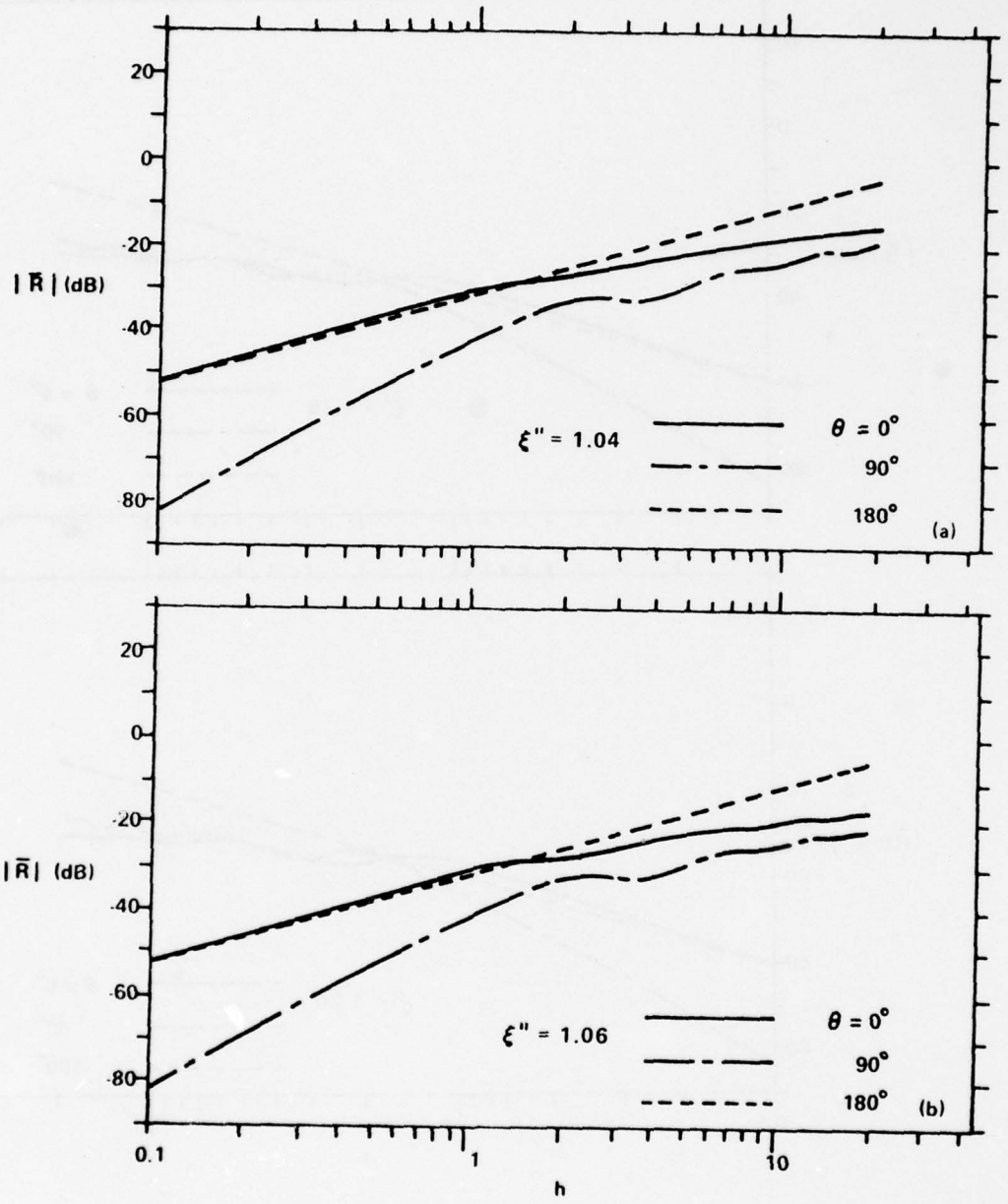

Figure 26. Frequency Response Curves, Rigid Case, Two Sources in Phase; $\xi' = 1.02$; (a) $\xi'' = 1.04$; (b) $\xi'' = 1.06$

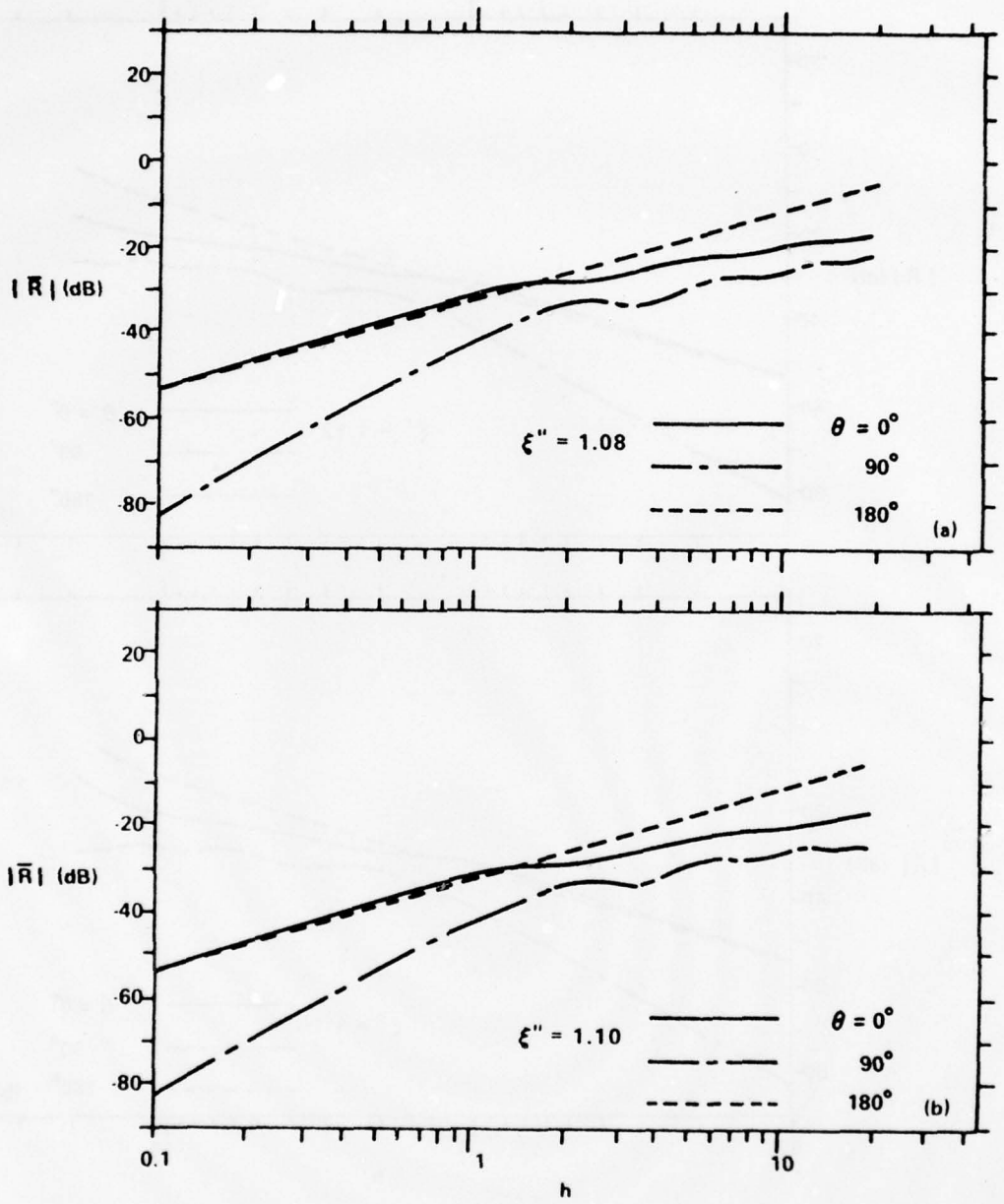

Figure 27. Frequency Response Curves, Rigid Case, Two Sources in Phase; $\xi' = 1.02$; (a) $\xi'' = 1.08$; (b) $\xi'' = 1.10$

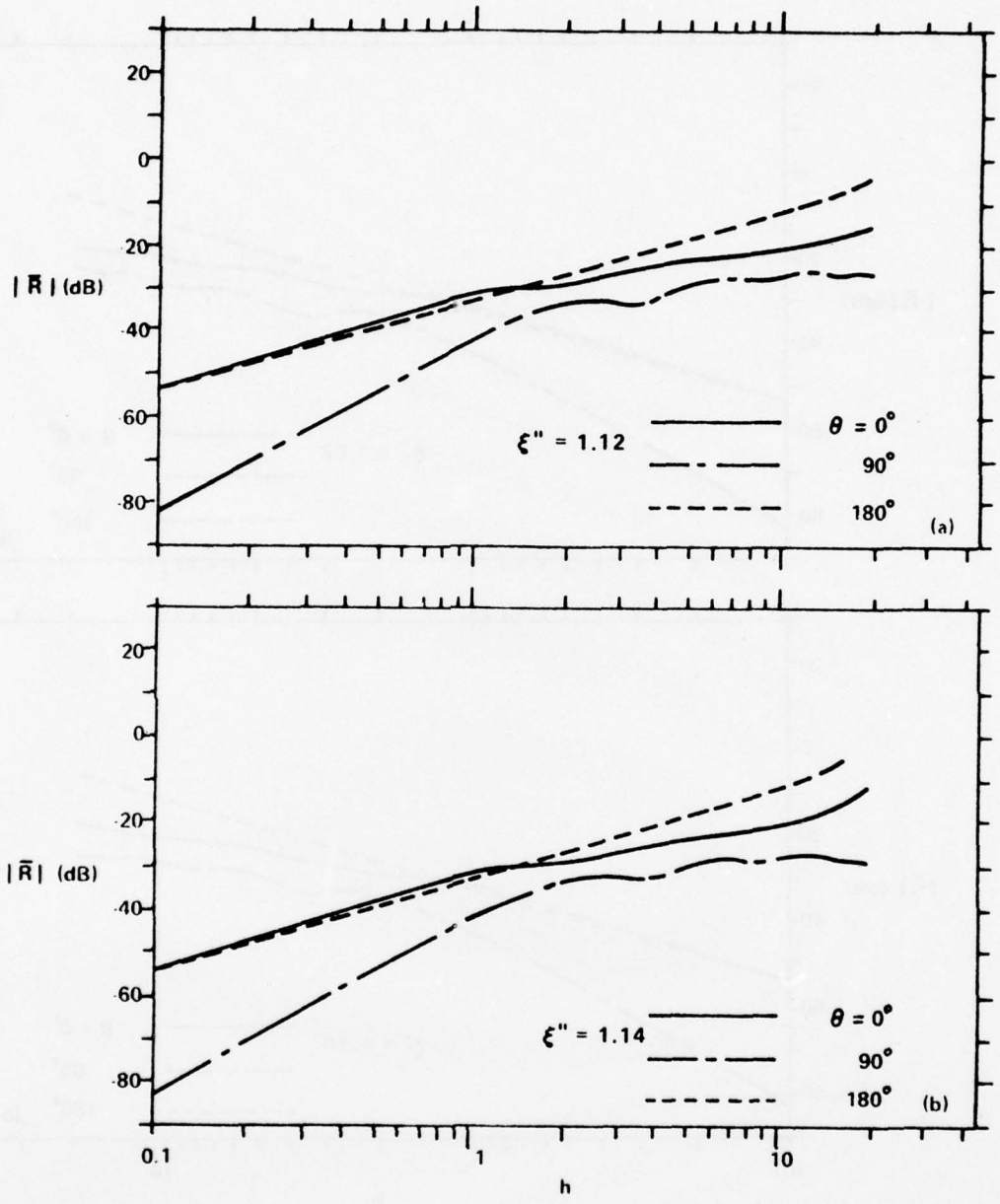

Figure 28. Frequency Response Curves, Rigid Case, Two Sources in Phase; $\xi' = 1.02$; $\xi'' = 1.12$; (b) $\xi'' = 1.14$

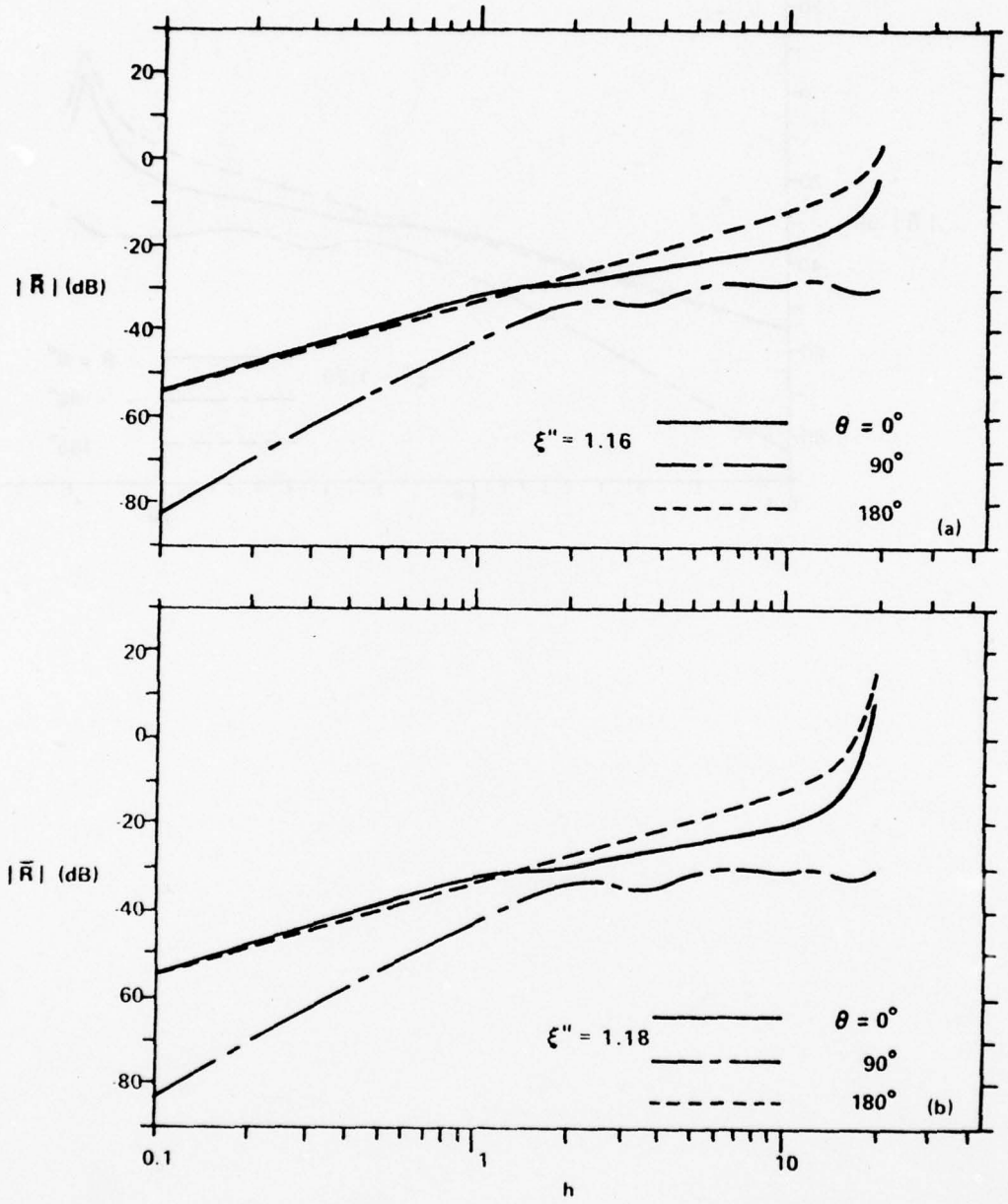

Figure 29. Frequency Response Curves, Rigid Case, Two Sources in Phase; $\xi' = 1.02$; (a) $\xi'' = 1.16$; (b) $\xi'' = 1.18$

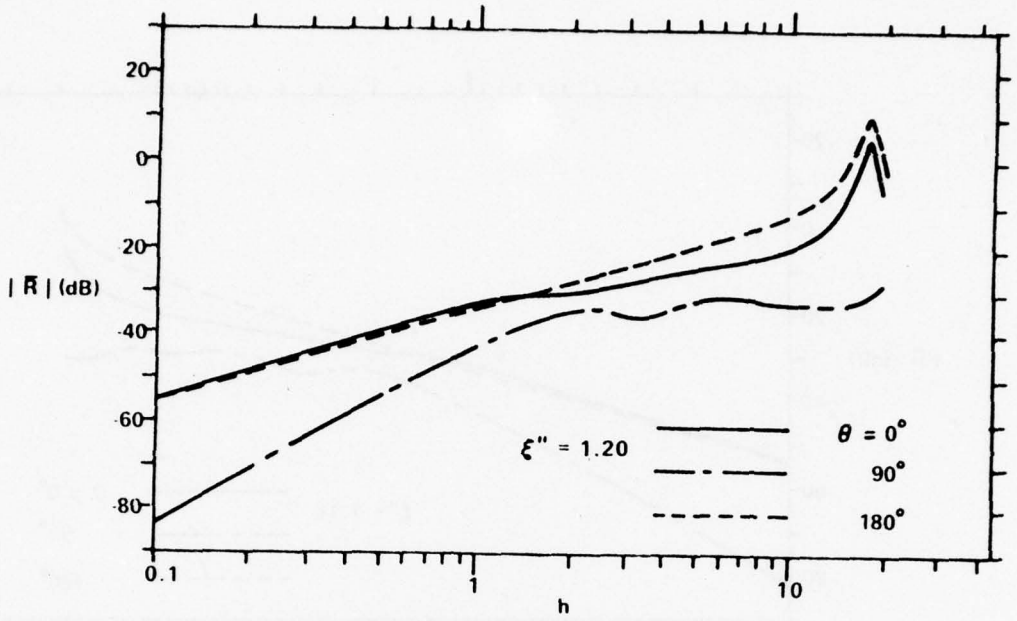

Figure 30. Frequency Response Curves, Rigid Case, Two Sources in Phase; $\xi' = 1.02$; $\xi'' = 1.20$

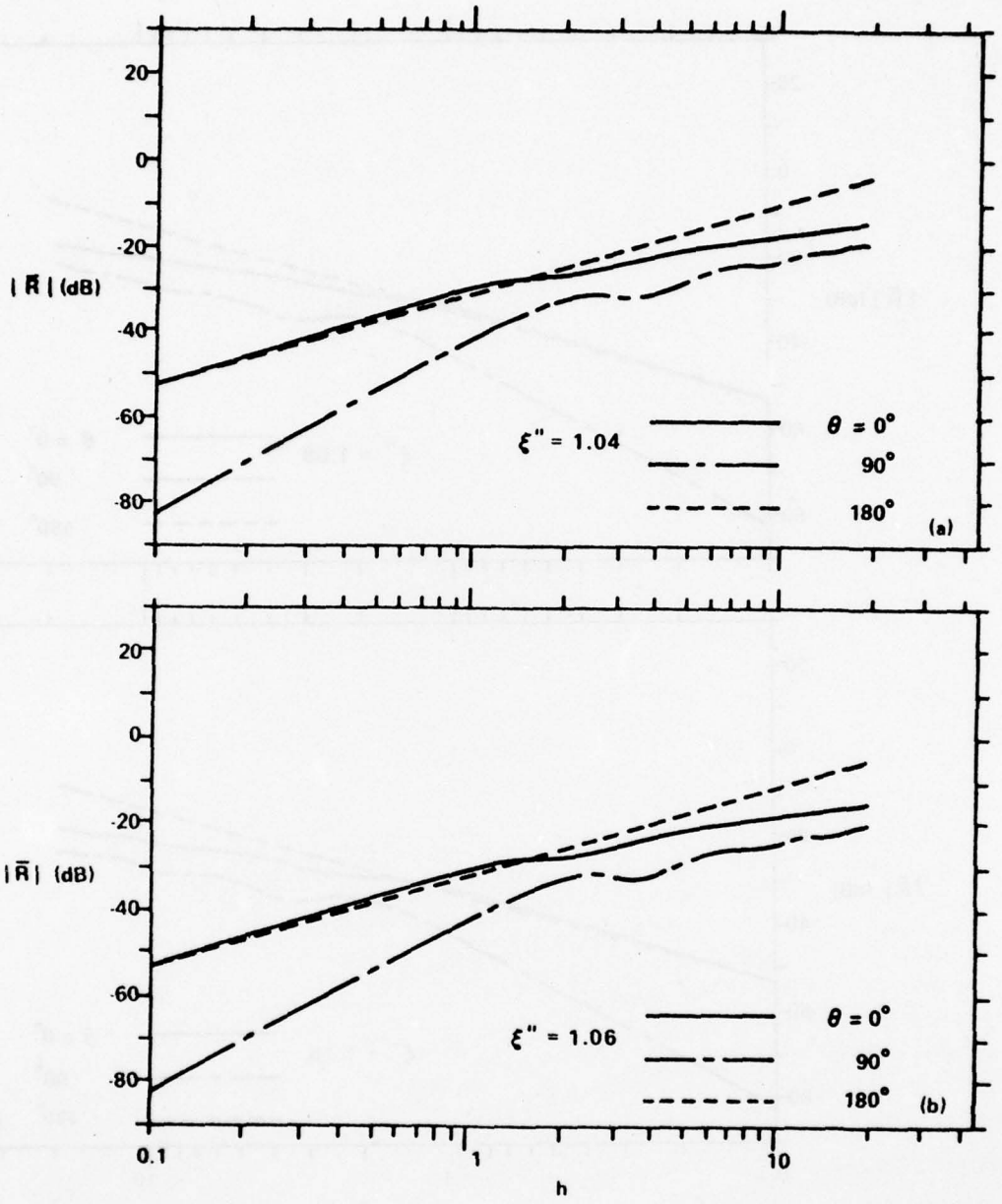

Figure 31. Frequency Response Curves, Rigid Case, Two Incoherent Sources; $\xi' = 1.02$; (a) $\xi'' = 1.04$; (b) $\xi'' = 1.06$

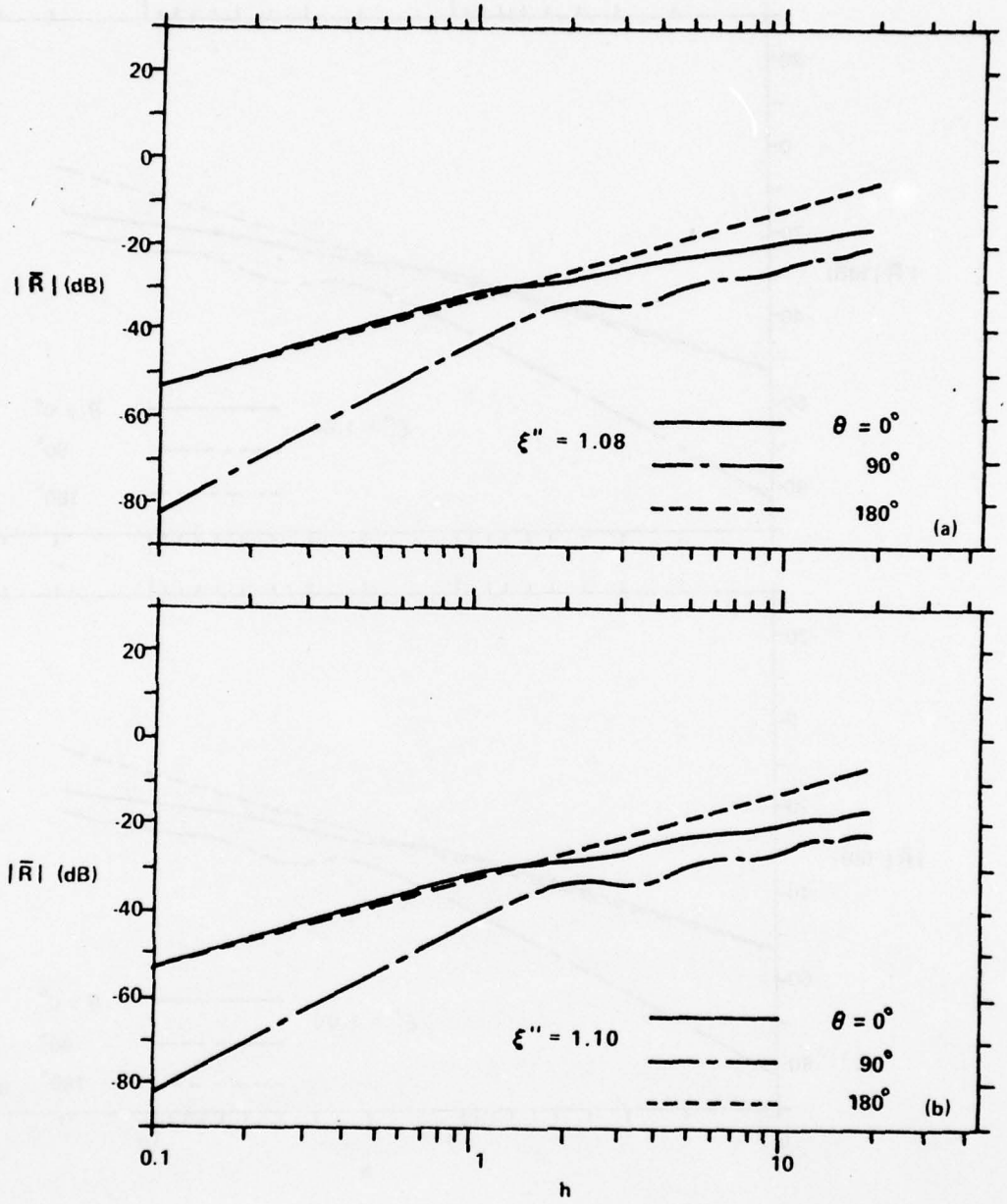

Figure 32. Frequency Response Curves, Rigid Case, Two Incoherent Sources; $\xi' = 1.02$; (a) $\xi'' = 1.08$; (b) $\xi'' = 1.10$

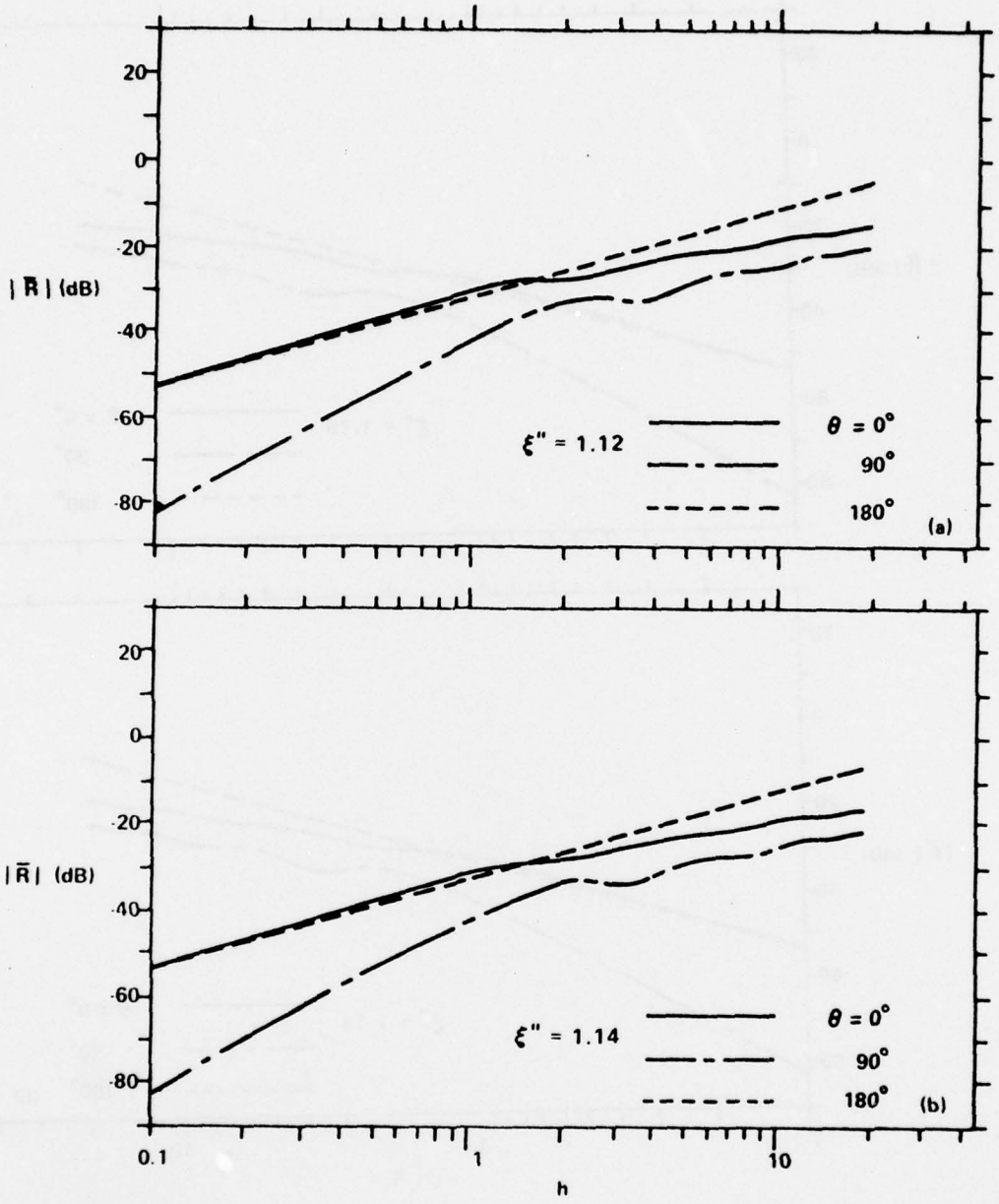

Figure 33. Frequency Response Curves, Rigid Case, Two Incoherent Sources; $\xi' = 1.02$; (a) $\xi'' = 1.12$; (b) $\xi'' = 1.14$

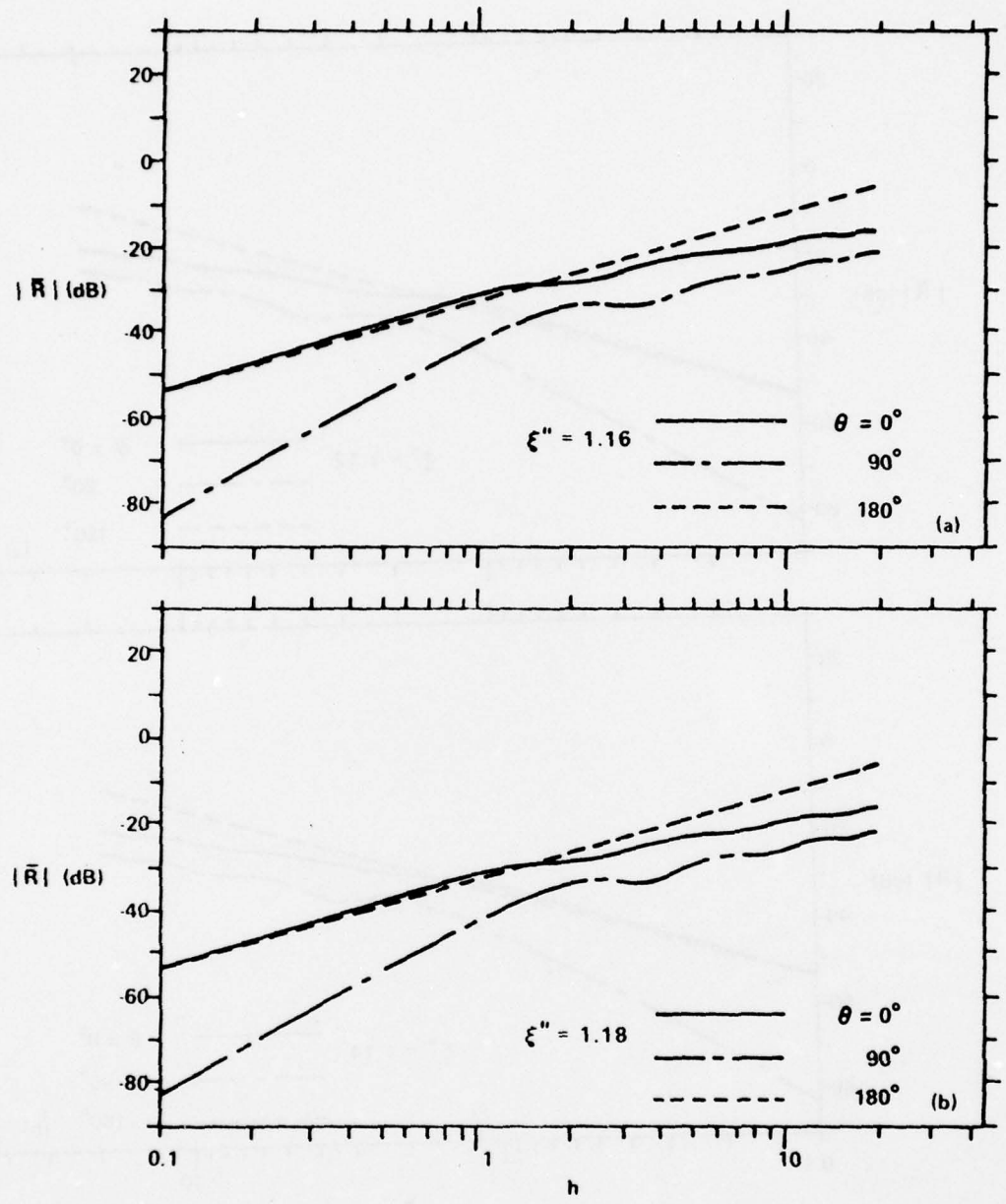

Figure 34. Frequency Response Curves, Rigid Case, Two Incoherent Sources; $\xi' = 1.02$; (a) $\xi'' = 1.16$; (b) $\xi'' = 1.18$

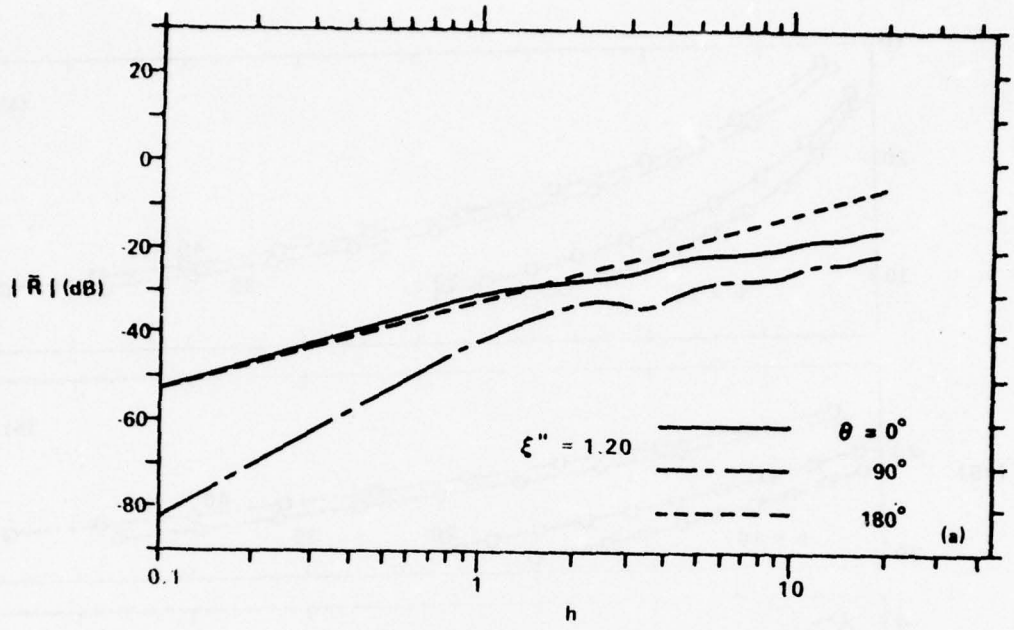

Figure 35. Frequency Response Curves, Rigid Case, Two Incoherent Sources; $\xi' = 1.02$; $\xi'' = 1.20$

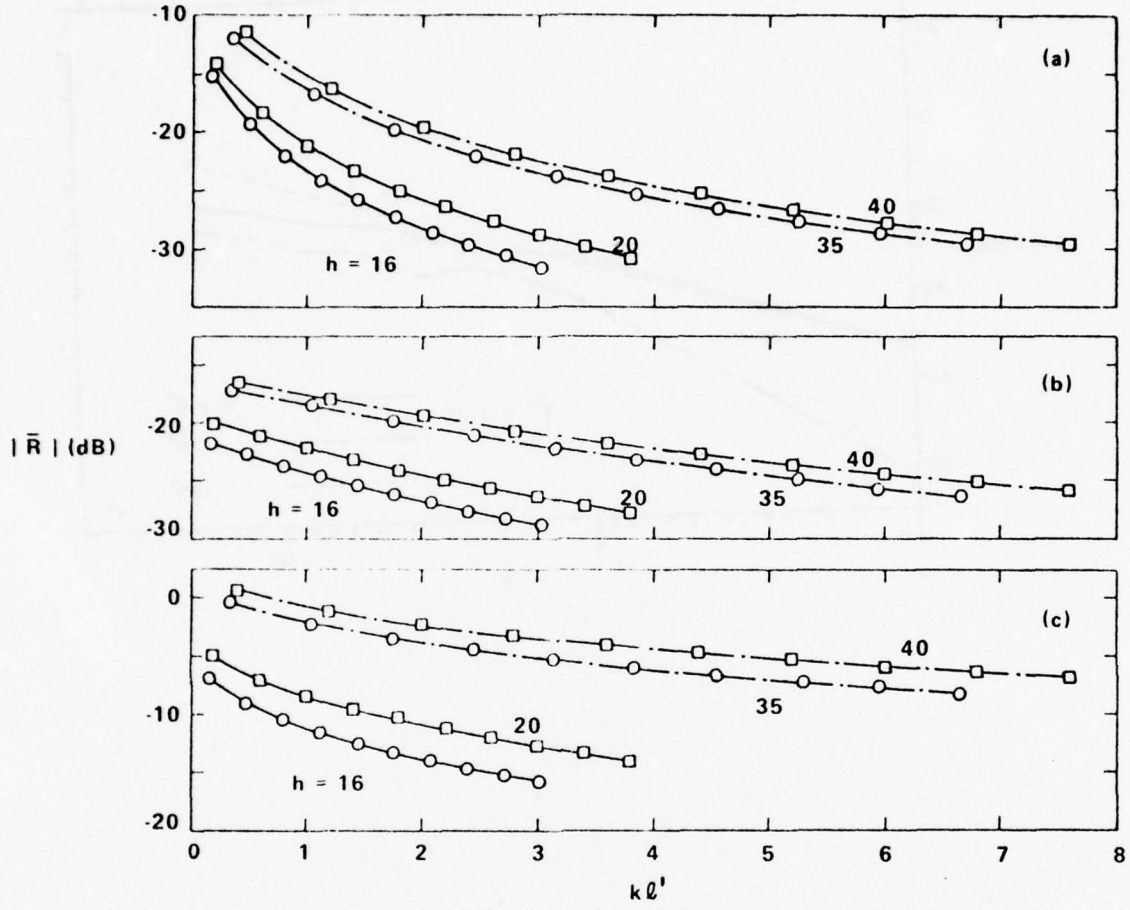

Figure 36. Reflection Factor as a Function of kℓ', Rigid Case, One Source; (a) θ = 0°; (b) θ = 90°; (c) θ = 180°

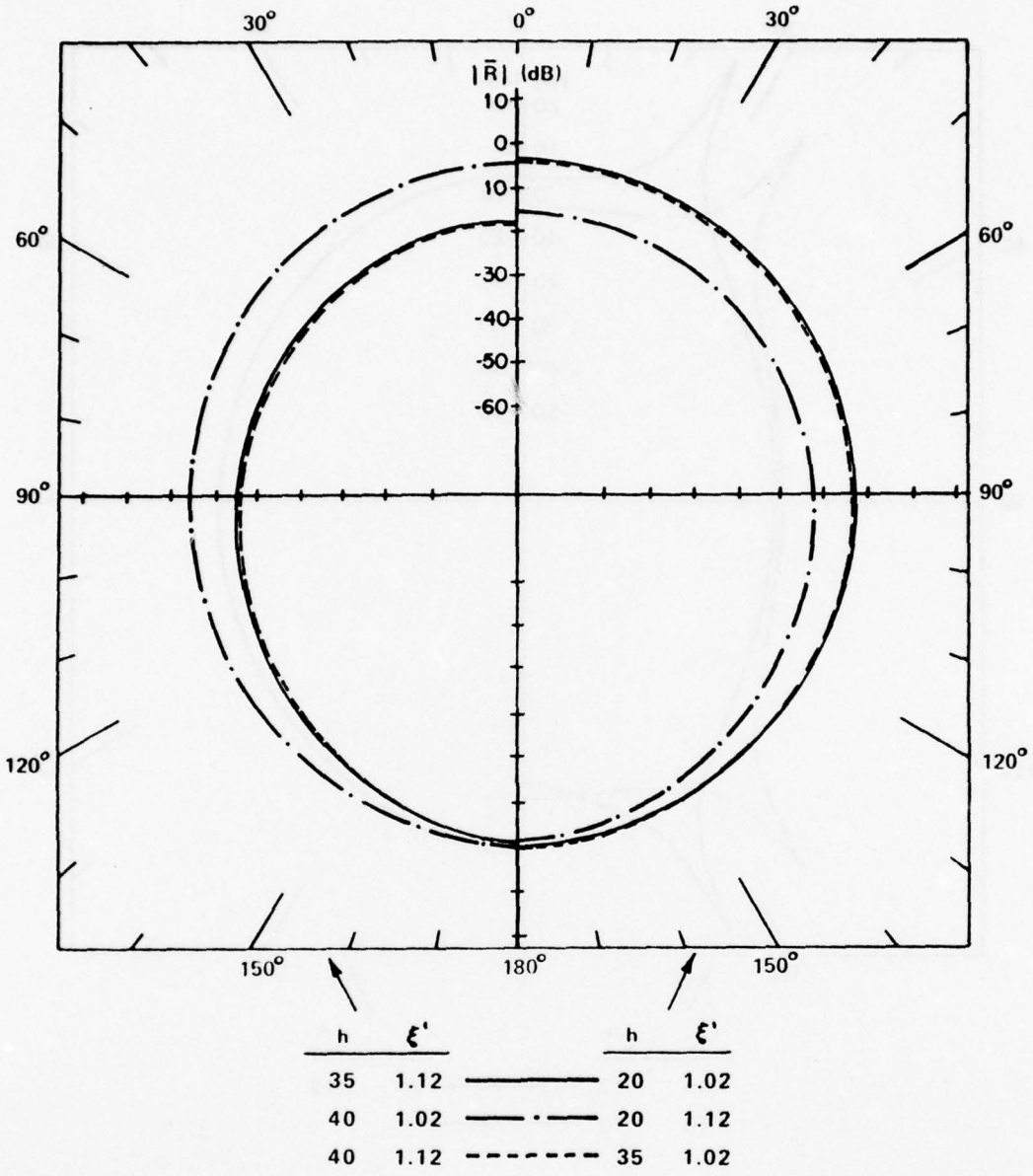

Figure 37. Directivity Patterns, Pressure Release Case, One Source; h = 20, 35, and 40; ξ' = 1.02 and 1.12

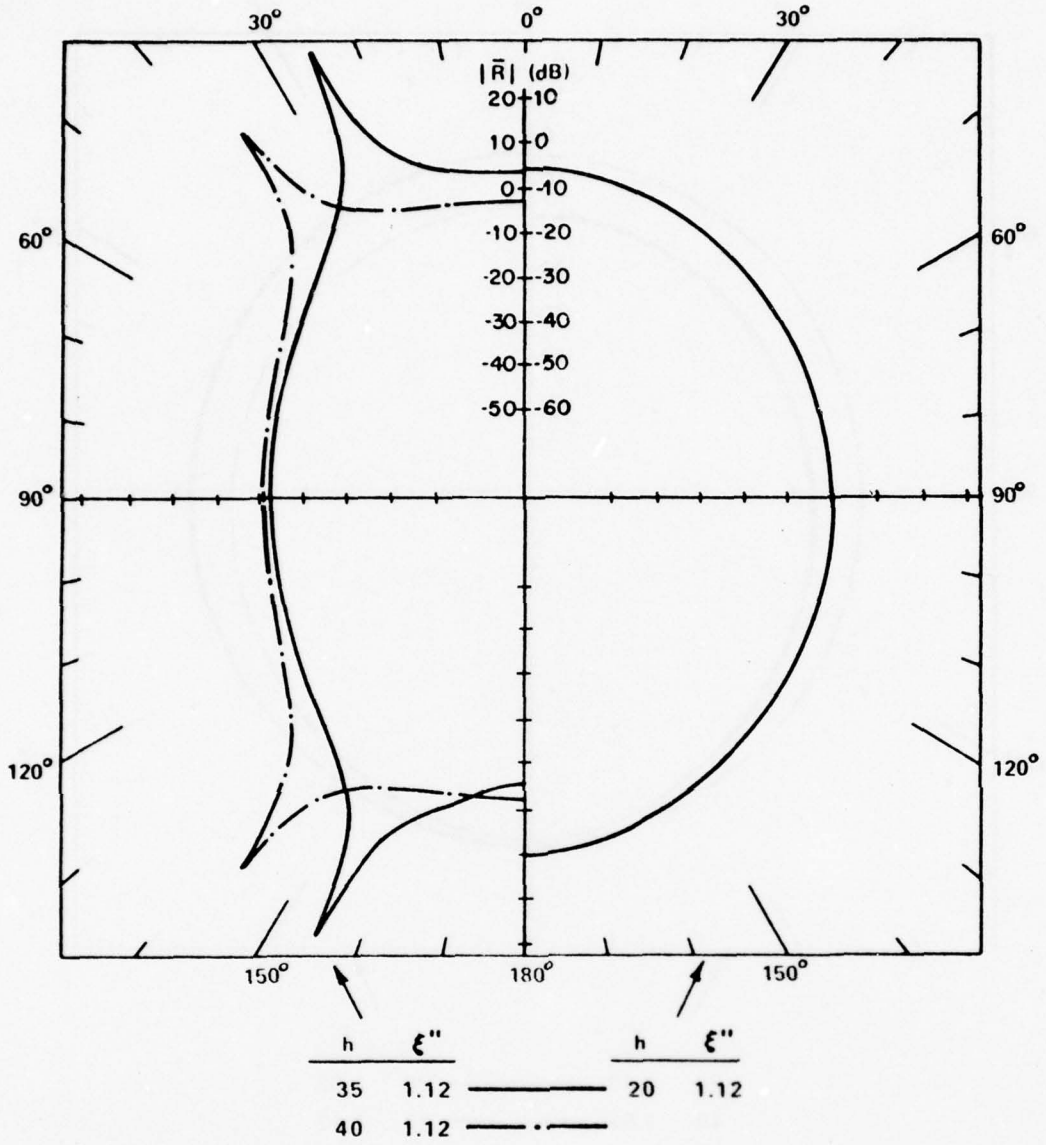

Figure 38. Directivity Patterns, Pressure Release Case, Two Sources in Phase; $\xi' = 1.02$; h = 20, 25, and 40; $\xi'' = 1.12$

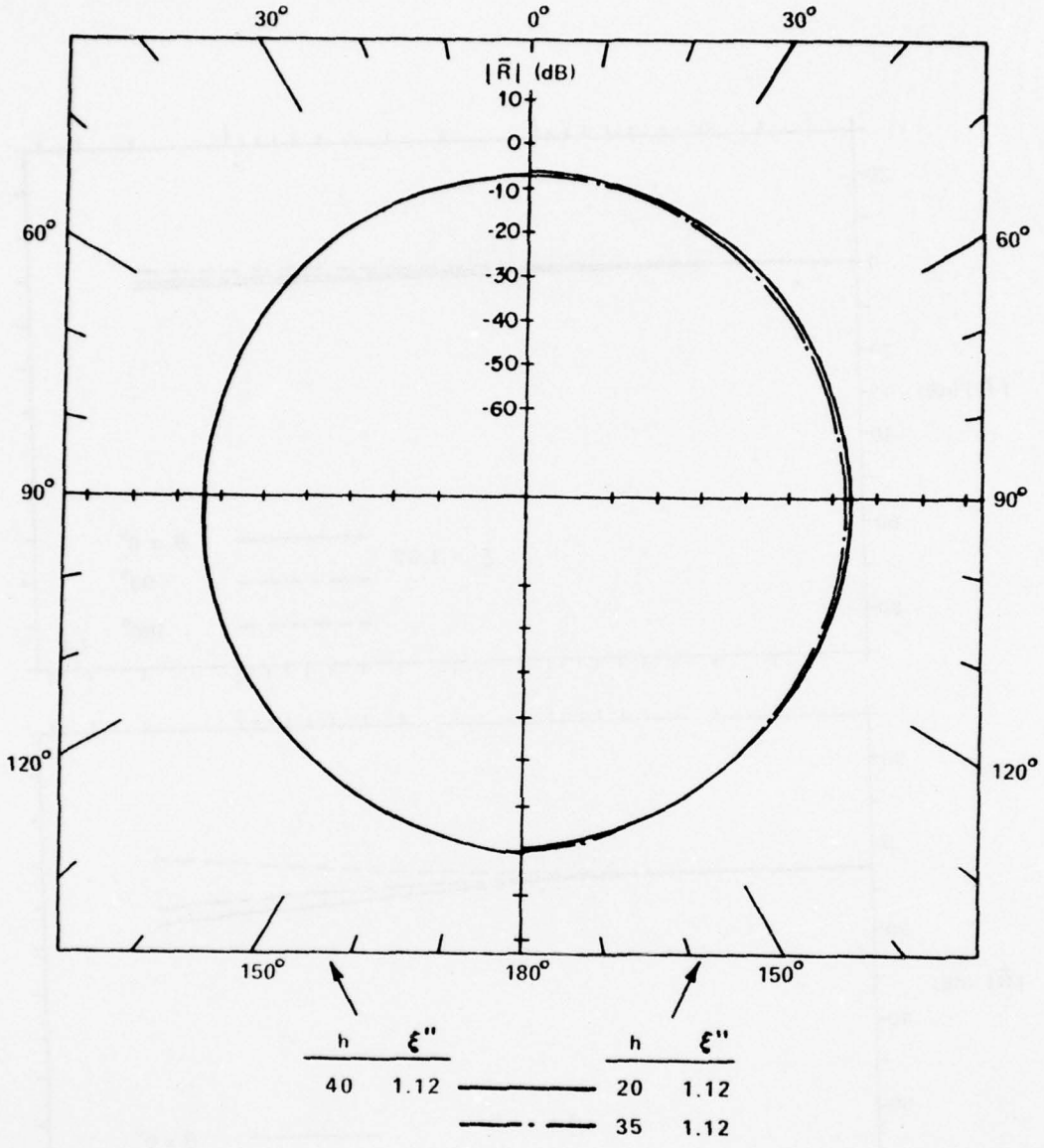

Figure 39. Directivity Patterns, Pressure Release Case, Two Incoherent Sources; $\xi' = 1.02$; h = 20, 35, and 40; $\xi'' = 1.12$

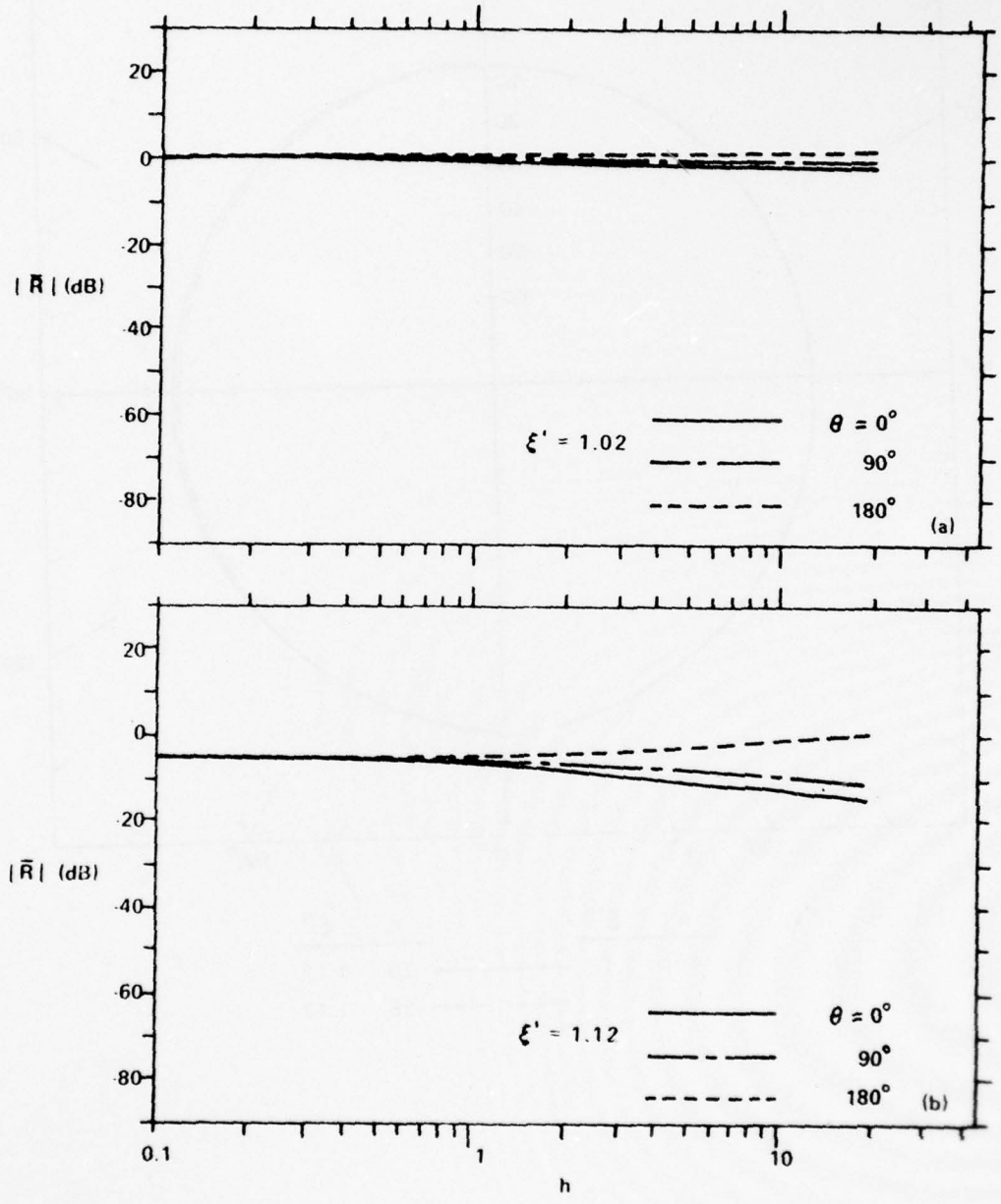

Figure 40. Frequency Response Curves, Pressure Release Case, One Source: (a) $\xi' = 1.02$; (b) $\xi' = 1.12$

AD-A062 989 PENNSYLVANIA STATE UNIV UNIVERSITY PARK APPLIED RESE--ETC F/G 20/1
AXISYMMETRIC SCATTERING OF A SPHERICAL WAVE BY A PROLATE SPHERO--ETC(U)
MAY 78 A GERMON N00017-73-C-1418

UNCLASSIFIED ARL/PSU/TM-78-174 NL

2 OF 3
AD
AD 62989

END
DATE FILMED
3-79
DDC

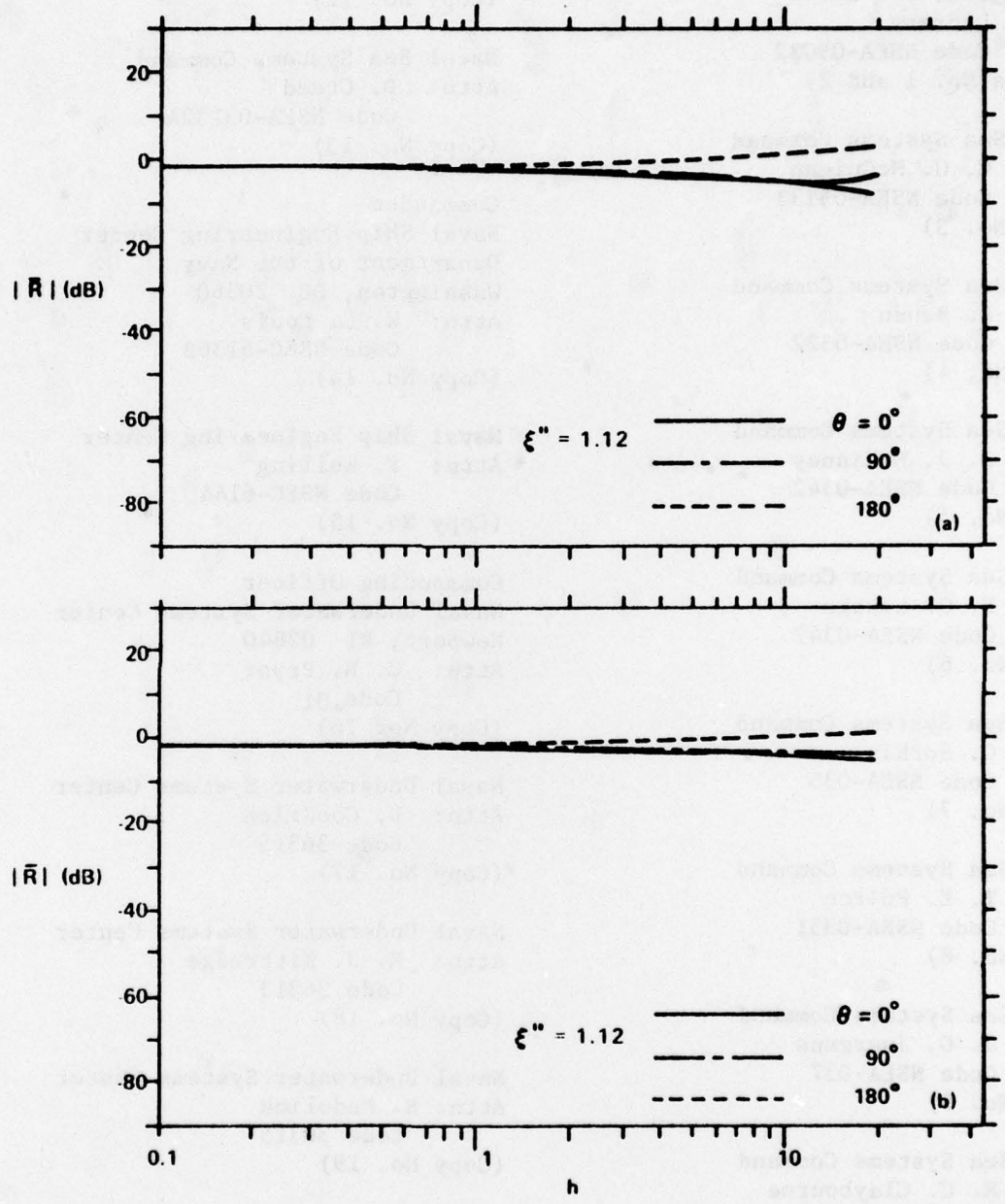

Figure 41. Frequency Response Curves, Pressure Release Case, Two Sources; $\xi' = 1.02$; $\xi'' = 1.12$; (a) in Phase; (b) Incoherent

DISTRIBUTION LIST FOR UNCLASSIFIED TM 78-174 by A. Germon, dated May 15, 1978

Commander
Naval Sea Systems Command
Department of the Navy
Washington, DC 20362
Attn: Library
Code NSEA-09G32
(Copies No. 1 and 2)

Naval Sea Systems Command
Attn: C. G. McGuigan
Code NSEA-03133
(Copy No. 3)

Naval Sea Systems Command
Attn: L. Benen
Code NSEA-0322
(Copy No. 4)

Naval Sea Systems Command
Attn: E. J. McKinney
Code NSEA-0342
(Copy No. 5)

Naval Sea Systems Command
Attn: E. G. Liszka
Code NSEA-0342
(Copy No. 6)

Naval Sea Systems Command
Attn: G. Sorkin
Code NSEA-035
(Copy No. 7)

Naval Sea Systems Command
Attn: T. E. Peirce
Code NSEA-0351
(Copy No. 8)

Naval Sea Systems Command
Attn: J. G. Juergens
Code NSEA-037
(Copy No. 9)

Naval Sea Systems Command
Attn: H. C. Claybourne
Code NSEA-0371
(Copy No. 10)

Naval Sea Systems Command
Attn: A. R. Paladino
Code NSEA-0372
(Copy No. 11)

Naval Sea Systems Command
Attn: C. C. Taylor
Code NSEA-037
(Copy No. 12)

Naval Sea Systems Command
Attn: D. Creed
Code NSEA-03132A
(Copy No. 13)

Commander
Naval Ship Engineering Center
Department of the Navy
Washington, DC 20360
Attn: W. L. Louis
Code NSEC-6136B
(Copy No. 14)

Naval Ship Engineering Center
Attn: F. Welling
Code NSEC-6144
(Copy No. 15)

Commanding Officer
Naval Underwater Systems Center
Newport, RI 02840
Attn: C. N. Pryor
Code 01
(Copy No. 16)

Naval Underwater Systems Center
Attn: D. Goodrich
Code 36315
(Copy No. 17)

Naval Underwater Systems Center
Attn: R. J. Kittredge
Code 36313
(Copy No. 18)

Naval Underwater Systems Center
Attn: R. Nadolink
Code 36315
(Copy No. 19)

Naval Underwater Systems Center
Attn: D. A. Quadrini
Code 36314
(Copy No. 20)

Naval Underwater Systems Center
Attn: E. J. Sullivan
Code 36311
(Copy No. 21)

DISTRIBUTION LIST FOR UNCLASSIFIED TM 78-174 by A. Germon, dated May 15, 1978

Naval Underwater Systems Center
Attn: R. Trainor
Code 36314
(Copy No. 22)

Naval Underwater Systems Center
Attn: F. White
Code 36301
(Copy No. 23)

Naval Underwater Systems Center
Attn: Library
Code 54
(Copy No. 24)

Commanding Officer
Naval Ocean Systems Center
San Diego, CA 92152
Attn: J. W. Hoyt
Code 2501
(Copy No. 25)

Naval Ocean Systems Center
Attn: M. M. Reischman
Code 2542
(Copy No. 26)

Naval Ocean Systems Center
Attn: G. L. Donohue
Code 2542
(Copy No. 27)

Commanding Officer and Director
David W. Taylor Naval Ship R&D Center
Department of the Navy
Bethesda, MD 20084
Attn: S. F. Crump
Code 1505
(Copy No. 28)

David W. Taylor Naval Ship R&D Center
Attn: W. B. Morgan
Code 154
(Copy No. 29)

David W. Taylor Naval Ship R&D Center
Attn: R. Cumming
Code 1544
(Copy No. 30)

David W. Taylor Naval Ship R&D Center
Attn: J. McCarthy
Code 1552
(Copy No. 31)

David W. Taylor Naval Ship R&D Center
Attn: T. Brockett
Code 1544
(Copy No. 32)

David W. Taylor Naval Ship R&D Center
Attn: Y. T. Shen
Code 1524
(Copy No. 33)

David W. Taylor Naval Ship R&D Center
Attn: M. Sevik
Code 19
(Copy No. 34)

David W. Taylor Naval Ship R&D Center
Attn: W. K. Blake
Code 1942
(Copy No. 35)

Commanding Officer and Director
David W. Taylor Naval Ship R&D Center
Department of the Navy
Annapolis Laboratory
Annapolis, MD 21402
Attn: J. G. Stricker
Code 2721
(Copy No. 36)

Commander
Naval Surface Weapon Center
Silver Spring, MD 20910
Attn: G. C. Gaunaurd
Code R-31
(Copy No. 37)

Naval Surface Weapon Center
Attn: Library
(Copy No. 38)

Office of Naval Research
Department of the Navy
800 N. Quincy Street
Arlington, VA 22217
Attn: H. Fitzpatrick
Code 438
(Copy No. 39)

DISTRIBUTION LIST FOR UNCLASSIFIED TM 78-174 by A. Germon, dated May 15, 1978

Office of Naval Research
Attn: R. Cooper
Code 438
(Copy No. 40)

Naval Research Laboratory
Washington, DC 20390
Attn: R. J. Hansen
(Copy No. 41)

Naval Research Laboratory
Attn: R. V. Baier
(Copy No. 42)

Naval Research Laboratory
Attn: S. Hanish
(Copy No. 43)

Naval Research Laboratory
Attn: B. J. King
(Copy No. 44)

Naval Research Laboratory
Attn: A. L. Van Buren
(Copy No. 45)

Defense Documentation Center
5010 Duke Street
Cameron Station
Alexandria, VA 22314
(Copies 46 to and including 57)

National Bureau of Standards
Aerodynamics Section
Washington, DC 20234
Attn: P. S. Klebanoff
(Copy No. 58)

Rand Corporation
1700 Main Street
Santa Monica, CA 90406
Attn: R. King
(Copy No. 59)

Rand Corporation
Attn: C. Gazley
(Copy No. 60)

Dyanmics Technology, Inc.
3838 Carson Street, Suite 110
Torrance, CA 90503
Attn: W. Haigh
(Copy No. 61)

Bolt Beranek and Newman
50 Moulton Street
Cambridge, MA 20136
Attn: N. Brown
(Copy No. 62)

Dr. J. L. Lumley
Sibley School of Mechanical and
Aeronautical Engineering
Upson Hall
Cornell University
Ithaca, NY 14850
(Copy No. 63)

Dr. D. G. Crighton
University of Leeds
Department of Applied Mathematical Studies
Leeds LS29JT
England
(Copy No. 64)

Applied Research Laboratory
The Pennsylvania State University
Post Office Box 30
State College, PA 16801
Attn: W. Thompson, Jr.
(Copy No. 65)

Applied Research Laboratory
Attn: R. E. Henderson
(Copy No. 66)

Applied Research Laboratory
Attn: E. J. Skudrzky
(Copy No. 67)

Applied Research Laboratory
Attn: F. H. Fenlon
(Copy No. 68)

Applied Research Laboratory
Attn: G. C. Lauchle
(Copy No. 69)

Applied Research Laboratory
Garfield Thomas Water Tunnel File
(Copy No. 70)